A Human Motor Control Framework based on Muscle Synergies

by

Reza Sharif Razavian

A thesis
presented to the University of Waterloo
in fulfilment of the
thesis requirement for the degree of
Doctorate of Philosophy
in
Systems Design Engineering

Waterloo, Ontario, Canada, 2017

Examining Committee Membership

The following served on the Examining Committee for this thesis. The decision of the Examining Committee is by majority vote.

External Examiner	Dr. Benjamin Fregly Professor
Supervisor	Dr. John McPhee Professor
Internal Members	Dr. Bryan Tripp Assistant Professor
	Dr. Ning Jiang Assistant Professor
Internal-external Member	Dr. Clark Dickerson Associate Professor

This thesis consists of material all of which I authored or co-authored: see Statement of Contributions included in the thesis. This is a true copy of the thesis, including any required final revisions, as accepted by my examiners.

I understand that my thesis may be made electronically available to the public.

Statement of Contributions

I declare that the entire human motor control framework presented in this thesis is developed by me. The experimental trials were also designed and conducted by me.

This thesis contains the materials that are taken from multi-author papers. These papers include:

- Sharif Razavian, R., Ghannadi, B., and McPhee, J. (2017). How do muscle synergies affect redundant degrees of freedom in musculoskeletal systems? Journal of Biomechanics (Under Review).

- Sharif Razavian, R., Ghannadi, B., and McPhee, J. (2017). A synergy-based motor control framework for the feedback control of musculoskeletal systems. Journal of Biomchanics (Under Review).

  Contributions of B. Ghannadi: technical support with the rehab robot as the measurement device in the experiments.

- Sharif Razavian, R., Mehrabi, N., and McPhee, J. (2015). A model-based approach to predict muscle synergies using optimization: application to feedback control. Frontiers in Computational Neuroscience, 9(October), 113.

  Contributions of N. Mehrabi: collaboration on the development of the 3D driver model

The planar musculoskeletal model (the example in section 4.2 to which I applied my motor control model) is taken from the following paper:

- Ghannadi, B., Mehrabi, N., and McPhee, J. (2015). Development of a Human-Robot Dynamic Model to Support Model-Based Control Design of an Upper Limb Rehabilitation Robot. In ECCOMAS Thematic Conference on Multibody Dynamics. Barcelona, Spain.

Abstract

In spite of the complexities of the human musculoskeletal system, the central nervous system has the ability to orchestrate difficult motor tasks. Many researchers have tried to understand how the human nervous system works. Yet, our knowledge about the integration of sensory information and motor control is incomplete.

This thesis presents a mathematical motor control framework that is developed to give the scientific community a **biologically-plausible** feedback controller for **fast** and **efficient** control of musculoskeletal systems. This motor control framework can be applied to musculoskeletal systems of various complexities, which makes it a viable tool for many predictive musculoskeletal simulations, assistive device design and control, and general motor control studies.

The most important feature of this real-time motor control framework is its emphasis on the *intended task*. In this framework, a task is distinguished by the kinematic variables that need to be controlled. For example, in a reaching task, the task variables are the position of the hand (individual joint angles are irrelevant to the reaching task). Consequently, the *task space* is defined as the subspace that is formed by all the controlled variables.

This motor control framework employs a *hierarchical structure* to speed up the calculations while maintaining high control efficiency. In this framework, there is a high-level controller, which deals with path planning and error compensation in the task space. The output of this task space controller is the acceleration vector in the task space, which needs to be fulfilled by muscle activities.

The fast and efficient transformation of the task space accelerations to muscle activities in *real-time* is a main contribution of this research. Instead of using optimization to solve for the muscle activations (the usual practice in the past), this acceleration-to-activation (A2A) mapping uses muscle synergies to keep the computations simple enough to be real-time implementable. This A2A mapping takes advantage of the known effect of muscle synergies in the task space, thereby *reducing the optimization problem to a vector decomposition problem*. To make the result of the A2A mapping more efficient, the novel concept of posture-dependent synergies is introduced.

The validity of the assumptions and the performance of the motor control framework are assessed using experimental trials. The experimental results show that the motor control framework can reconstruct the measured muscle activities only using the task-related kinematic/dynamic information.

The application of the motor control framework to feedback motion control of musculoskeletal systems is also presented in this thesis. The framework is applied to musculoskeletal systems of various complexities (up to four-degree-of-freedom systems with 15 muscles) to show its effectiveness and generalizability to different dimensions.

The control of functional electrical stimulation (FES) is another important application of my motor control framework. In FES, the muscles are activated by external electrical pulses to generate force, and consequently motion in paralysed limbs. There exists no feedback FES controller of upper extremity movements in the literature. The proposed motor control model is the first feedback FES controller that can be used for the control of reaching movements to arbitrary targets. Experimental results show that the motor control model is fast enough and accurate enough to be used as a practical motion controller for FES systems. Using such a biologically-plausible motor control model, it is possible to control the motion of a patient's arm (for example a stroke survivor) in a natural way, to accelerate recovery and improve the patient's quality of life.

Acknowledgements

I would like to thank my supervisor, Professor John McPhee, who guided me throughout this work.

I am also grateful of my friends, Mr. Borna Ghannadi, Dr. Naser Mehrabi and Dr. Mohammad Sharif Shourijeh, who helped me push my research ahead whenever it was stuck.

I would also like to thank the Natural Sciences and Engineering Research Council of Canada, Canada Research Chairs Program, and Ontario Graduate Scholarship Program for funding my research.

Table of Contents

List of Tables

List of Figures

Nomenclature

α	Muscle pennation angle
$\bar{\mathbf{a}}$	The acceleration vector in the redundant space
$\bar{\mathbf{B}}$	The basis set that spans the redundant space
$\bar{\mathbf{S}}$	The synergy matrix for the redundant space
δ	The slack variable in optimization
$\hat{J}$	The cost function augmented with constraints
$\hat{\mathbf{a}}$	The augmented acceleration vector
$\hat{\mathbf{B}}$	The augmented basis set that contains orthogonal bases in the task and redundant spaces
$\hat{\mathbf{S}}$	The augmented synergy matrix
$\hat{\mathbf{u}}_F$	The unit vector in the direction of the force F
$\hat{\mathcal{T}_N}$	The full-dimensional task space in a previously redundant system
λ	Lagrange multiplier in optimization
$\mathbf{a}$	The acceleration vector in the task space

$\mathbf{B}$ The basis set that spans the task space

$\mathbf{b}$ The non-linear velocity-dependent acceleration terms in musculoskeletal system dynamics

$\mathbf{C}$ The coefficient matrix

$\mathbf{F}$ The task space forces vector

$\mathbf{f}(\mathbf{u})$ The non-linear contributions of muscle activations to joint moments

$\mathbf{g}$ The gravitational acceleration term in musculoskeletal system dynamics

$\mathbf{J}$ The Jacobian matrix for the musculoskeletal system

$\mathbf{M}$ The mass matrix in musculoskeletal system dynamics

$\mathbf{q}, \dot{\mathbf{q}}, \ddot{\mathbf{q}}$ The vectors of joint angles, angular velocities, and angular accelerations, respectively

$\mathbf{S}$ The synergy matrix

$\mathbf{u}$ The vector of muscle activations

$\mathbf{X}$ The state vector in the control-oriented model

$\mathbf{Y}$ The measurement (output) vector in the control-oriented model

$\mathcal{R}_q$ The q-dimensional redundant space

$\mathcal{T}_p$ The p-dimensional task space

ϕ The redundant degree of freedom

θ The angle in the task space for 1-DoF systems

$\tilde{\ddot{\mathbf{q}}}$ The joint-space acceleration vector that is corrected using systems dynamics

A	The data matrix for NNMF
a	The muscle activation mapping as a function of stimulation pw
B	A basis vector (a column of the basis matrix)
c	The coefficient of a synergy/basis vector
d	The distance from elbow to the axis of rotation
e	Factorization error in NNMF
F	The scalar force value in a 1D task space
f	Muscle force from the Hill muscle model
f_l	Muscle force-length relation in the Hill muscle model
f_v	Muscle force-velocity relation in the Hill muscle model
$F_{0_{max}}$	Maximum isometric muscle force
F_{max}	The maximum hand force measured at the maximum muscle stimulation
h	Non-linear transformation from muscle activity to operational space torque
J	The objective function in the optimization problem
k	The number of synergies
l	The number of synergies in the redundant space
m	The number of muscles in the musculoskeletal system
N	The number of degrees of freedom in the musculoskeletal system
n	The number of samples in the data matrix

P	The number of postures used in CNNMF method
p	The number of dimensions of the task space
pw	The Electrical stimulations pulse width
q	The number of dimensions of the redundant space
r	Muscle moment arm
S	A single synergy vector, a column of the synergy matrix
s	The synergy ratios, or an element of the synergy matrix
T	Torque in the task or redundant space
u	Muscle activation
u^*	The optimal muscle activation
u_x	The x component of the unit vector $\hat{\mathbf{u}}_F$
u_y	The y component of the unit vector $\hat{\mathbf{u}}_F$
v	The velocity in the task space
w	The weighting factors in the objective functions
x, y, z	Positions in the task space

Chapter 1

Introduction

The human nervous system is one of the most complex systems known to mankind. This relatively small biological tissue is responsible for all the thoughts, imaginations, personalities and everything that make us human. All such aspects originate from a small portion (supposedly the frontal lobe) of the brain. The greater part of the nervous system is dedicated to sensory and motor functions. This fact alone is sufficient to realize how complex is the human sensory-motor system. The integration of sensory feedback with body motion is an extremely complicated process, and our understanding of such an integration is far from complete.

The human motor control system manages to perform tasks, be it voluntary or involuntary, in a remarkably fast, efficient, and robust way. Modelling of such a complex system is, therefore, a very challenging task—challenging enough that it is not done yet, nor does it look possible in the near future.

Experimentation is an approach that can be used in the analysis of the human central nervous system (CNS); however, doing experimental trials is usually time-consuming and very expensive. Besides, performing many experiments may be unethical, infeasible with the available tools, or impossible altogether (e.g. isolate one specific part of the brain to study its function).

Modelling is another possible direction in studying the human motor control system. Models can be used when experimentation is not possible. It is much easier to perform what-if studies *in silico* than *in vivo*. Furthermore, modelling is the low-cost alternative for many experiments. Additionally, by developing models for the human motor control system, we may be able to extract the human control mechanism and employ a similar controller in the control of other machinery.

1.1 Human motor control modelling

The goal of this research is to develop a working model of the human motor control system. However, developing a motor control model is very a challenging problem. Some of the difficulties are:

- Degrees of freedom: The human body is a complex mechanical system, with more degrees of freedom than are needed to perform a task. The complex dynamical interaction between body segments in a known movement is difficult to study, let alone understanding how the CNS plans and executes the actions in the unpredictable environments that we live in.

- Dimensionality: For every degree of freedom in the human body, there are multiple muscles, and within each muscle, there are hundreds to thousands of motor units that can be activated. The control of this large number of inputs (likely in an optimal manner) requires a complex plan.

- Pool of sensory information: A huge amount of sensory information is sent to the nervous system. Depending on the situation, some sensory information may give inaccurate/contradicting representations of the body to the CNS. Integration of sensory information in the CNS is a very challenging process to model.

- Complex dynamics: Besides the non-linearities of the skeletal dynamics, muscles and tendons have very difficult-to-predict behaviour. Thus, building a controller that can reliably control such a system is not trivial.
- Subject-specific: Every person has a different body; the skeleton, muscles, attachment points, responses, and basically every feature of human bodies is different. Therefore, the motor control model has to be tuned for every person. Making the motor control model easily tunable is challenging.
- Coupled responses: There are multiple pathways in the neural circuitries (e.g. reflex loops in the spinal cord), which add to the complexity of the reposes we observe during task executions.

1.2 Applications of the research

A realistic model of the human motor control system can be used in a variety of applications. First and foremost, such a model can help researchers better understand the mechanisms underlying the control of human movements. A model allows for *virtual experiments* that may be difficult or impossible to do otherwise. For example, one can alter the parameters of the system (e.g. transmission delay of the sensory information) to investigate their effects on the movement control. Furthermore, certain features of a motor control model (e.g. reflexes) can be isolated for more detailed studies.

Having a motor control model, we can also run predictive simulations; for instance, it is possible to couple the motor control model to a human musculoskeletal model, and then perform virtual experiments on a new design of a prosthesis. In such a scenario, where no previous motion analysis is available, one cannot use inverse dynamics methods to solve for the muscle loads. Therefore, only with the presence of a realistic motor control model, is it possible to run such a simulation.

On a similar note, knowing how humans interact with their environment is essential to developing controllers for the machines that interact with humans. Examples of such systems include exoskeletons, rehabilitation robots, and many common devices that we use daily such as cars. Reliable prediction of the human behaviour during interaction with an external device is required to make the device safe and comfortable to use.

Lastly, a motor control model can be used to re-produce the movements in paralysed limbs by artificially stimulating the muscles—a process called functional electrical stimulation (FES). In FES, the muscles are stimulated by electrical pulses to generate force and motion. There exists no feedback controller that can handle the complexities of the human musculoskeletal system. Only a controller as complex as the human nervous system seems able to control it.

1.3 Problem statement

The goal of the proposed research is to develop a *biologically plausible* model of the human motor control system. In this context, the term biologically plausible refers to a model that could be considered as a possible way of movement control by the CNS. For instance, a computationally-heavy off-line optimization solution to the muscle force sharing problem is not biologically plausible, as it cannot be run concurrent to the movement. Therefore, the developed biologically plausible motor control model should have the following properties:

1. Bio-fidelity: be based on biological observations, and provide close to normal response.
2. Real-time: so that it can be used to control the actions.
3. Flexible: so that it can be utilized for subject-specific applications.

As mentioned earlier, our knowledge of the mechanism used by the human CNS in motion control is incomplete. Therefore, it is hard to guarantee that the developed motor

control model will faithfully replicate the exact mechanism of the CNS.

Muscle synergy is a popular topic among motor control theories. This theory suggests that the central nervous system activates the muscle not individually, but in groups called a synergy or a primitive of motor control. By combining these synergies, the nervous system builds the muscle excitation levels required to perform a task. To develop a biologically plausible motor control model, the muscle synergy theory will be used. In other words, the developed motor control model will use a number of synergies and combine them to build the required muscle excitations.

1.4 Document outline

In the next chapter, the existing knowledge in the fields of motor control modelling and FES control will be reviewed. Chapter 3 will present the basics of the proposed motor control framework. The next two chapters include the application of this framework to the control of the motions in musculoskeletal simulation and FES devices. The document will close by presenting the concluding remarks and a list of contributions in chapter 6. The list of references and appendices are provided at the end of the thesis.

Chapter 2

Background

This chapter presents a review of the existing theories and models of the human motor control system, as well as the available methods for the control of functional electrical stimulation systems.

2.1 What is the challenge?

The number of degrees-of-freedom (DoF) and the number of actuators (muscles) in the human body exceed the minimum number required to perform various tasks. Therefore, a task can be carried out in a multitude of ways (the *degree of freedom problem*, Bernstein, 1967), and a certain movement can be produced by an infinite number of muscle activation levels (the *muscle redundancy problem*). The first issue is known as kinematic redundancy, and the second is the dynamic redundancy.

Because of muscle redundancy, no unique solution for muscle activities can be found for a given movement. Thus, optimization has gained significant attention in musculoskeletal modelling. Generally, in the optimization setting, the goal is to find the set of muscle activity levels that minimizes a physiological cost. It is generally accepted that the solution

to the optimization problem is close to normal human behaviour (for a review see Valero-Cuevas et al., 2009a). A simple optimization problem, however, does not provide significant insight into the actual mechanism of motor control in humans. More theories and models have been proposed in the literature to study the human motor control system.

2.2 Motor control theories

Many efforts have been made to understand movement control mechanisms of the central nervous system (CNS), yet the clear answer remains unknown. Although many researchers have investigated various aspects of motor control (such as cortical areas related to motor control, the role of the basal ganglia and cerebellum, structure of reflex loops, and so on), the full integration of such pieces of information is not yet done. Thus, no complete understanding of human motor control mechanisms is available.

In the following, an overview of the studies regarding the mechanisms of motor control are presented. In particular, the focus is on the studies that try to gain insight into motor control through mathematical modelling.

2.2.1 Motor planning

Before hypothesizing about the *mechanisms* employed by the CNS in motor control, one has to figure out what aspects of motion are controlled, i.e. what are the *desired variables* that the CNS is controlling.

The well-supported hypothesis regarding the desired variables in motor control was pioneered by Morasso (1981). Morasso showed that in reaching actions, the joint angle and velocity trajectories have no consistent pattern among different reach trials, whereas, the end-effector (hand) moves in a straight line from the origin to the targets, with bell-shaped velocity trajectories. This observation led Morasso to suggest that the movement trajectories are not planned in the joint angle space, but rather in the *task space*.

Furthermore, the strong correlation between the task-related variables (both kinematic and dynamic variables) and neuronal activities in motor cortex (Georgopoulos et al., 1986, 1988; Schwartz et al., 1988; Kettner et al., 1988; Ashe and Georgopoulos, 1994; Moran and Schwartz, 1999; Boline and Ashe, 2005; Lillicrap and Scott, 2013) supports the importance of task-related variables in motion control.

To quantify the classification of controlled/uncontrolled variables, Scholz and Schöner (1999) and Latash et al. (2010) presented the method of *uncontrolled manifold* (UCM). According to this theory, for every kinematic variable (e.g. hand position), the degrees of freedom (the joint angles) can be separated into two groups: the ones whose variation result in a change in the kinematic variable of interest, and the ones whose variation does not affect it. The latter is referred to as the *uncontrolled manifold* because the variations in this manifold do not affect the *task variable*, thus do not need to be precisely controlled to finish a task. As a result, the joint angles in the UCM show higher trial-to-trial variability.

The UCM approach can, therefore, provide a quantitative measure to rank the importance of different kinematic variables in the control of complex motions by analysing the joint angle variability in the corresponding UCMs. If the variability in a variable's UCM is significantly higher than the variability in the subspace orthogonal to it, then we can conclude that the kinematic variable is actively stabilized (controlled) by the nervous system. Conversely, if the variabilities in UCM and non-UCM spaces are the same, the kinematic variable is not controlled. As an example, Scholz and Schöner (1999) used this approach in the analysis of sit-to-stand motion, and argued that the centre of mass (COM) position (in both horizontal and vertical directions) is tightly controlled by the CNS, while the positions of head and hand are less controlled.

As will be discussed later, the knowledge of the controlled variable (the task space) is the key information in constructing the proposed motor control model.

2.2.2 Motor command execution

How the muscles contribute to the control of the task variables (whatever they might be) is not well understood either. Optimization-based approaches have been proposed as a possible method to find muscle activations that produce a certain movement (for a review see Erdemir et al., 2007). Although these optimization-based models can estimate the muscle activations reasonably well (e.g. Meyer et al., 2016; Sharif Shourijeh et al., 2016; Walter et al., 2014), their usefulness as a feedback motor control model is questionable. The optimization framework may work well in the context of well-practised motions, where the control can be viewed as feed-forward (Shourijeh et al., 2017; Sharif Razavian et al., 2015; Neptune et al., 2009; Berniker et al., 2009; Anderson and Pandy, 2001); however, it is not clear whether the nervous system is capable of continuously solving for the optimal muscle activations during the course of an action. The high computation cost of the optimization process renders it inapplicable for real-time control. Another major question in this regard is the availability of an instantaneous cost value to the CNS.

Two important control strategies presented in the literature that try to replace optimization are the threshold control theory and muscle synergy theory, which are briefly discussed here.

Threshold control theory

Feldman and Levin (2009) have proposed the equilibrium point (or the threshold control theory) as a possible motor control strategy. According to this hypothesis, the CNS controls a motion, not by modulating the muscle activities directly, but by adjusting some *muscle length thresholds*, beyond which the muscles automatically start to generate force. The interaction between the external loads and the defined thresholds will result in a posture at which the dynamical system reaches an equilibrium. Equilibrium point theory suggests that the synergistic activation of the muscles is not the control mechanism by itself—it is a result of the dynamical interaction between the defined thresholds and the external loads.

Another advantage of the equilibrium point theory is that it does not rely on the interpretation of an *internal model*. Additionally, this way of thinking about the motor control readily solves the redundancy problem, as the CNS is no longer concerned about the individual joint angle or muscle activity. This approach is also very useful to explain involuntary reflexes.

Muscle synergy theory

Muscle synergy theory has gained considerable attention in motor control research (Tresch and Jarc, 2009) as a biologically-plausible approach to simplify the muscle redundancy problem. According to this theory, the nervous system activates the muscles by combining a few *bundles of activations* (known as modules, synergies, or motor primitives). This theory has been proposed as a way to simplify computations, by reducing the number of signals that the nervous system has to control (Bizzi et al., 2008).

Muscle synergy has mostly been studied in an inverse manner (i.e. finding the synergies by looking at the measured muscle activities). The literature is rich with studies that aim to extract these building blocks from the measured muscle activations. A few examples include studies on healthy human movements (Kutch et al., 2008; Smale et al., 2016; Shourijeh et al., 2016), spinal cord injury (Zariffa et al., 2012) and cerebral palsy patients (Steele et al., 2015), frogs (Bizzi et al., 2008; Cheung et al., 2005), and cats (Ting and McKay, 2007; Sohn and Ting, 2016).

Despite being used extensively in the literature, muscle synergy theory carries many uncertainties that need to discussed.

Structure and number of synergies The structure of the dimension reduction in the nervous system via muscle synergies is not properly understood. *Muscle synergies* are often defined as fixed relations between instantaneous activation levels of multiple muscles (Zelik et al., 2014; Steele et al., 2013; Ting, 2007; McKay and Ting, 2008; Berniker et al., 2009; Roh et al., 2011; Safavynia et al., 2011; Kutch and Valero-Cuevas, 2012). Alternatively,

time-varying patterns (also called the *motor primitives*) are proposed as the building blocks of muscle activations (Meyer et al., 2016; Sartori et al., 2013; D'Avella and Tresch, 2001; Ivanenko et al., 2006; Bizzi et al., 2008; D'Avella et al., 2008). A mixture of both approaches has also been investigated by Delis et al. (2014).

The identification of the synergies is an important part of the theory. Various methods have been proposed in the literature to decompose muscle activities into a number of synergies. In the majority of research articles, the goal has been to reconstruct the measured muscle activities as closely as possible, using a low-dimensional basis set (the synergies). Non-negative matrix factorization (NNMF, Lee and Seung, 2000) is a widely-used method in this application (Berger and D'Avella, 2014; Berniker et al., 2009; McKay and Ting, 2008; Kargo et al., 2010; D'Avella et al., 2008). This approach, however, is unable to determine whether the synergies result from neural origins (as claimed by the synergy theory), or are by-products of other processes (e.g. biomechanical constraints (Kutch and Valero-Cuevas, 2012; Kutch et al., 2008), or optimization (de Rugy et al., 2013)).

There is also uncertainty about the number of synergies. The usual practice is to examine the variance accounted for (VAF) of the experimental EMG after synergy decomposition (Delis et al., 2014; Steele et al., 2013; Sartori et al., 2013; de Rugy et al., 2013; Moghadam et al., 2013; Lockhart and Ting, 2007; Roh et al., 2011). In general, a fewer number of synergies produce a lower VAF, and as the number of synergies increase, more variation in the experimental data can be captured. Therefore, the number of synergies beyond which no further improvement in VAF is observed is usually chosen. Unfortunately, this approach is purely statistical and does not provide significant insight into biomechanical aspects of muscle synergy theory.

Relation with the task and posture The dependency of synergies on the task and posture has not been extensively investigated. Efforts have been made to find *shared* synergies that can reconstruct EMG data in a variety of tasks (e.g. Zelik et al. (2014); Sartori et al. (2013); Bizzi et al. (2008)). In the majority of the articles, however, synergies

from a single task are studied, without explicit investigation as to if the synergies vary from one task to another. The relationship between the task and the synergies seems to be left unattended. The exceptions are (D'Avella et al., 2008) where proposed posture- and speed-dependent synergies are proposed (for opposing gravity, and acceleration, respectively), and (de Rugy et al., 2013; Moghadam et al., 2013) where the synergies are identified while also trying to reconstruct the task forces.

de Rugy (2010) has shown that visuomotor adaptation occurs at the muscle synergy level, suggesting the necessity of task-dependent synergies. It is, therefore, reasonable to argue that the recruited set of synergies may depend on the intended action. For example, the set of synergies used during a hand-writing action is perhaps different from the set recruited during a simple grasp motion, though the same muscles are activated. One possibility is that different sets of synergies are known to the CNS, and the CNS chooses the appropriate set to manipulate and perform the tasks.

Therefore, information about the intended task seems to be essential in the identification of the synergies. For this purpose, a quantifiable criterion is needed to distinguish between tasks. I hypothesize that the desired controlled variable (equivalently the task space) could provide such information. In this regard, the uncontrolled manifold theory (UCM, Scholz and Schöner, 1999) can be used to identify the controlled variable in various tasks. Furthermore, the concept of task-dependent synergies aligns well with the *minimal intervention theory*, which states that the CNS activates muscles to control only the task-relevant variable (Valero-Cuevas et al., 2009b).

The possible dependency of the synergies on body posture also needs to be studied. D'Avella et al. (2008) used cosine tuning curves to estimate the activation coefficient of their proposed *tonic* and *phasic* synergies based on the final posture and the motion velocity, respectively. Furthermore, the changing force production capacity and function of the muscles with posture also highlights the importance of body state on the structure of the synergies.

Synergies for motion control Muscle synergies are used to control the motion in (Lockhart and Ting, 2007; Ting and McKay, 2007; McKay and Ting, 2008; Neptune et al., 2009; Berniker et al., 2009; Kargo et al., 2010; Allen and Neptune, 2012). However, they all reported that a fine tuning of the synergies (by an optimization algorithm) is required in the control of the motion. One possible reason for such fine tuning is the feed-forward nature of the controllers in all these articles. Furthermore, despite the reduction in the number of control inputs, the problem is still redundant, requiring an optimization routine to solve for the best combination of the synergies.

A feedback control scheme can be used for the modulation of the synergies, thus improving motion control performance. Unfortunately, despite the appealing concept of using synergies-based controllers that act on task space variables, the literature is very limited; only Lockhart and Ting (2007) and Ting (2007) have used the centre of mass position as the feedback to construct a balance controller. No other article seems to be available that employed muscle synergies for motion control using a task space representation.

Relation to optimal control It should be noted that it is still not clear whether the synergies are the tools used by the CNS in motion control, or they are by-products of other motor control processes. de Rugy et al. (2013) argue that the muscle activation obtained from the solution of an optimization problem (e.g. Todorov et al., 2005) can also be decomposed into a few synergies. In other words, an optimal pattern of muscle activities is inherently synergistic (de Rugy et al., 2013; Steele et al., 2013). Therefore, if one assumes that the CNS performs some form of optimization, the synergies will naturally come out of the optimization as an inherent property of optimal solutions.

Relation to kinematic redundancy It was mentioned earlier that many observations support the existence of a control mechanism in the task space. In this regard, it is important to note that the dimensions of the task space is usually smaller than the number of available degrees of freedom (the degree of freedom problem). This raises the question of how the synergies are employed to control only a subset of degrees of freedom, and leave

the rest uncontrolled. Furthermore, there are situations when not just the task-related variables, but all the degrees of freedom need to be tightly controlled (e.g. reach to a target while avoiding an obstacle). How do these situations fit in the "task space control" theme?

There is no published study that has investigated the separation of the task and redundant variables control. The only exception is the *minimal intervention principle* (Todorov and Jordan, 2002a), which uses optimal control theories to show that the optimal control is the one that puts less effort on the control of redundant variables. Nonetheless, it is still an optimization-based model, and therefore is computationally costly. Other feedback motion controllers for musculoskeletal systems (Todorov et al., 2005; Liu and Todorov, 2009; Mehrabi et al., 2015a,b) are optimization-based models that inherently control all the degrees of freedom at all times, and as a result are computationally costly. The models developed by Park and Durand (2008); Blana et al. (2009); Jagodnik and van den Bogert (2010) are joint space controllers. Lockhart and Ting (2007) have developed feedback controllers based on muscle synergies, but for systems without kinematic redundancy. Lastly, Fu et al. (2015) have developed a controller for a kinematically redundant system; however, only the control of the task variables are reported.

The relation between muscle synergies and task/redundant variables is not well-studied either. The correlation between the synergies and the endpoint force has been shown in (Bizzi et al., 1991; Ting and Macpherson, 2005). Berger and D'Avella (2014) have used a mapping to estimate the end-point force from the measured muscle activities. Conversely, Lockhart and Ting (2007) have used center of mass kinematics (task variable) to estimate muscle activations in a balancing task. The missing point in all these articles is: how do the synergies affect the redundant degrees of freedom, besides the task space?

2.3 Motor control models

So far in this chapter, the existing knowledge about two important motor control theories was presented (with more emphasis on muscle synergy theory). The following sections give a review of the *motor control models* that are implemented based on a variety of methods, ranging from artificial neural networks to optimization.

2.3.1 Feed-forward versus feedback controllers

Both feedback and feed-forward aspects of control are present in the human motor control. Compensating for error and uncertainties is the important evidence for feedback control strategy. However, in the absence of some or all sensory feedback, the CNS is still able to perform tasks, which proves the presence of a feed-forward pathway in the motor control mechanism. The motor control models in the literature are based on different observations, and therefore, both feedback and feed-forward models are available.

Due to the complexity of the system, a majority of motor control models are based on the feed-forward strategy; i.e. a set of predefined control inputs are used to drive the system. Among these models are MOSAIC (Gomi and Kawato, 1993; Haruno et al., 2001, 2003) and MODEM (Emadi Andani et al., 2009). A common feature of these motor control models is their modular architecture. In these models, a control module (a trained artificial neural network) is used to generate the control signal in a certain condition. Multiple modules are then used to cover the range of different conditions.

Trained networks are not the only models to operate in a feed-forward manner. Most of the optimization-based motion control models are also feed-forward (for example see Shourijeh et al., 2017; Anderson and Pandy, 2001; Neptune et al., 2009; Sharif Shourijeh and McPhee, 2013, 2014; Sharif Razavian et al., 2015; Sharif Razavian and McPhee, 2015). Only a few feedback motor control models are available. Most of the feedback control models employ a hierarchical structure (Todorov et al., 2005; Liu and Todorov, 2009; DeWolf and Eliasmith, 2011; Mehrabi et al., 2013, 2015a,b). In these motor control models, the

first level of the controller deals with the task-related dynamics (e.g. center of mass), disregarding the muscle redundancy, while the second layer solves for the optimal muscle forces. There also exist a few non-hierarchical optimal feedback controllers (Mehrabi et al., 2017; Sharif Shourijeh et al., 2017). In (Jagodnik et al., 2015) acceptable controller performance is achieved, using well-tuned Proportional-Integral-Derivative (PID) feedback controllers to control the muscle activities (the body representation in this work is in the joint space).

A combination of feedback and feed-forward control structures is developed by Park and Durand (2008) and also by Blana et al. (2009). The feedback/feed-forward models have some of the advantages of both feedback and feed-forward control methods. In (Park and Durand, 2008; Blana et al., 2009), artificial neural networks are trained to approximate the steady-state inverse model of the system to provide fast control, while proportional-integral-derivative (PID) controllers are used to compensate for errors, and to reject disturbances to the system.

2.3.2 Model-based versus trained controllers

In another classification, the motor control models, regardless of their feedback or feed-forward structure, can be grouped into *model-based* and *trained* controllers. The model-based controllers are the ones that explicitly take into account the dynamics of the system to generate the control signal. On the other hand, the trained controllers look at the system as an input-output relation, and learn the control signal over a training period.

The advantage of the model-based controllers is their ability to perceive the change in the dynamics of the system and act accordingly. The trained systems, on the other hand, can only behave reliably within the ranges for which they are trained.

Many models of motor control use trained networks (some examples are Gomi and Kawato, 1993; Haruno et al., 2001, 2003; Emadi Andani et al., 2009; Park and Durand, 2008; Blana et al., 2009). These models usually use multiple trained modules, because of the complexity of the control problem, and the fact that only one trained network cannot

control the system under all circumstances. The fact that the nervous system can learn new moves and adapt to a new condition is a strong motivation for the development of motor control models that employ trained networks.

On the other hand, some motor control models use control theory techniques to calculate the proper control command. The model-based controllers also have roots in the physiological aspects of motor control. It is thought that the cerebellum hosts internal representations of the body, which are used in the coordination of body movements. A great deal of attention is paid to optimal control theories and their application in control of neuromusculoskeletal systems (Todorov et al., 2005; Liu and Todorov, 2009; DeWolf and Eliasmith, 2011; Mehrabi et al., 2013; Anderson and Pandy, 2001; Neptune et al., 2009; Sharif Shourijeh and McPhee, 2013, 2014). There are two issues with the optimization-based models. One is, optimization is, in general, a very slow process, rendering it inapplicable for real-time control. The second issue is in the nature of the solution. Most of the optimization-based methods in the literature deal with inverse-dynamics simulations, where the motion is known. The few models that deal with forward dynamics simulations only use optimization to find signals to drive the musculoskeletal system in a feed-forward manner (Sharif Shourijeh and McPhee, 2014; Neptune et al., 2009; Anderson and Pandy, 2001; Berniker et al., 2009). Optimal feedback controllers are more scarce (Todorov et al., 2005; Todorov and Jordan, 2002b; Sharif Shourijeh et al., 2017; Mehrabi et al., 2013, 2015a,b, 2017).

The choice of the cost function in optimization-based models is also worth discussing. For instance, should we use the cost function that results in less fatigue, or less energy consumption per travelled distance? The question as to which objective function gives results closer to the natural behaviour of the CNS still has no answer.

2.4 Application of the motor control model to functional electrical stimulation

Understanding how the human motor control system works can help us design better assistive technologies to improve healthy and mobility-impaired populations. One specific area that will benefit from a realistic motor control model is the restoration of body movement by artificial stimulation of muscles.

2.4.1 Functional electrical stimulation

Functional electrical stimulation (FES) is the process of applying external electrical pulses to skeletal muscles or to the attached nerves, in order to generate force in the muscle and perform actions. There are various types of electrodes to apply the stimulations, including transcutaneous (over the skin), epimysial (on the surface of the muscle), percutaneous (within the muscle), or nerve cuff (around the nerve that innervates the muscle). Each of the electrode types has advantages and disadvantages that make them suitable for different applications. The applied electric pulse also has different properties. The electric pulses are usually in the form of a high-frequency pulse train, where the frequency, amplitude and pulse width can all be modulated to change the muscle force.

To maintain a relatively constant force in the muscle, the frequency of the applied electric signals should be 20-40 Hz. This frequency is much higher than the 6-8 Hz frequency of action potentials in motor units that are generated by the CNS in a normal *tetanic contraction* (Lynch and Popovic, 2008). The CNS maintains the constant force with such a low frequency by activating the motor units in an asynchronous manner (the CNS cycles through different motor units). In artificial stimulations, however, the activation is synchronous—all the motor units activate together. The third difference between the normal and artificially activated muscles is the order of motor unit recruitments. The CNS activates smaller fast-twitch, fibres first for lower forces. The larger motor units activate

for higher force levels. By the external stimulation, the order is reversed. The larger units that fatigue faster are activated first. All these reasons (high stimulation frequency, synchronous activation, and reverse order of recruitment) cause the rapid occurrence of muscle fatigue when stimulated by FES.

2.4.2 FES in rehabilitation

The application of functional electrical stimulation in rehabilitation programs is relatively new. It is shown in recent studies (Kapadia et al., 2014; Thrasher et al., 2008) that FES can improve reach and grasping functionality of chronic and severe stroke patients. The improvements in a variety of indices of severe patients are more significant than conventional therapies. Additionally, in the chronic patients whose recovery has plateaued, FES can still improve the hand functionality.

The results are promising that FES rehabilitation can be used for the recovery of patients, even the severe and chronic stroke patients. The current FES control approach is manual, and a feedback control scheme might improve the recovery even more (Lynch and Popovic, 2008). Furthermore, the integration of FES and robotic rehabilitation programs, in an intelligent and self-contained system, is another open area to explore.

2.4.3 Motion control with FES

Artificially stimulating the muscles to produce movements in individuals with motor impairments has always been an intriguing idea; however, there are basic challenges that prevent FES from being widely used.

The biggest challenge is associated with the complexity of the human musculoskeletal system; it is a redundant, non-linear and noisy system with significant uncertainties. The actuators in the human body are the muscles, many of which are co-activated by the nervous system to produce a certain motion. We do not know how the nervous system

calculates the required muscle activities. Thus, we have yet to mimic the same process to produce naturally-looking motions with FES.

Many methods are presented in the literature for the control of FES devices; a few examples are (Piazza et al., 2012; Abbas and Chizeck, 1995; Popovic and Popovic, 2007; Bauman et al., 2011; Schearer et al., 2014). The available FES control methods vary significantly. Finite state controllers (for example Bauman et al., 2011) are able to switch between different *states* based on the measurements of the system, but during each state the controller is essentially feed-forward. Many models use artificial neural networks to generate the proper control signals (Abbas and Chizeck, 1995; Schearer et al., 2014; Park and Durand, 2008). PID and sliding-mode controllers are also used for the control of FES systems (Lynch and Popovic, 2012). However, there are few optimal feedback control methods for FES. Furthermore, the available FES controllers do not result in a behaviour that is close to the natural response of the human body.

Proof of concept studies for more advanced feedback controllers exist that report successful control of simple motions (e.g. knee extension by Previdi (2002); Ajoudani and Erfanian (2009); Kirsch et al. (2017, 2015), elbow extension by Crago et al. (1998), and two-degree-of-freedom ankle motion by Park and Durand (2008)). However, their generalizability to multi-degree-of-freedom and multi-muscle systems has not been reported.

Controlling the upper extremity movements with FES is a more challenging control problem, mostly because of the larger number of degrees of freedom and the involved muscles. Initial steps toward solving this problem include a single-muscle controller for a one-dimensional reaching task (Freeman et al., 2009), control of isometric hand force in a multi-muscle FES system (Schearer et al., 2014), estimation of FES-produced joint torques during a prescribed 3D movement (Schearer et al., 2016), and feed-forward control of the reaching tasks (Schearer et al., 2015). Popovic and Popovic (1998, 2001) have also developed controllers for elbow extension using the measured shoulder joint velocities. However, no feedback controller exists for the upper extremity reaching movements that allows reaching to arbitrarily specified targets.

The developed motion controllers in (Freeman et al., 2009; Schearer et al., 2014, 2016, 2015) have all taken a joint space approach, in which the effect of muscle activities on joint torques are calculated, and then inverse kinematics/dynamics are used to convert the information from task space (hand position, which is the controlled variable) to joint space (for which the models are developed). This added complexity can be removed by developing the formulation in the task space, and considering the effect of muscles on the task space forces, rather than the joint torques.

2.5 Chapter summary

Here is a brief summary of the reviewed literature regarding the human motor models.

- Both feedback and feed-forward control schemes exist in the human motor control system
- Human movement control behaves optimally, but it is uncertain that the CNS performs real-time optimization
- Muscle synergy and threshold control theories are proposed as possible mechanisms to simplify the control process
- It is suggested that the control of movements occurs in the task space

Motor control models of various complexities are developed trying to explain some of the aforementioned aspects of motor control. Despite all the efforts taken to understand the human motor control system, there still exist many unknowns that need to be answered.

The human motor control system is a massively complex system for which no one can tackle all of its aspects at once. For this reason, this thesis focuses on a narrow field in this area. Specifically, I only focus on **feedback aspect of the movement control in a task space**, and I use the **muscle synergy** theory as the dimension reduction method. In this narrow field of view, there are unresolved issues that need to be explored:

- How does the CNS control the movements in real-time, while performing optimally?
- How can the nervous system control some variables (task-related) while leaving the rest uncontrolled?
- Are muscle synergies actually useful *to control the movements* in complex musculoskeletal systems?
- How do the muscle synergies relate to tasks? Are they shared between all tasks, or are they task-specific?
- Where do the adaptation and motor learning fit in muscle synergy context?

In the next chapters of this thesis, a mathematical motor control framework is described that includes all of the following aspects: 1) feedback controller for the arbitrary movement of a general multi-DoF musculoskeletal system; 2) control of the movements in the task space; 3) utilization of muscle synergies to simplify control; and 4) implementation for real-time control.

This motor control framework includes a fast feedback controller in the task space for motion planning and error compensation. Furthermore, this framework is based on an explicit relationship between the muscle synergies and the task-related variables, which allows for fast estimation of the muscle activations from the task requirements without the need to solve an online optimization problem. An important advantage of this mechanistic framework is its generalizability to arbitrary dimensions and tasks. It is also proposed that for the efficient control of the movements, the number of synergies depends on the intended task. Lastly, the potential of this framework to selectively control some or all of the degrees of freedom in kinematically redundant musculoskeletal systems is explored.

Furthermore, as requested by Lynch and Popovic (2008), there is an unsatisfied need for a real-time feedback controller that can drive FES devices efficiently, and performs similarly to the motion control of a healthy person. The proposed motor control model can effectively fulfil this need.

Chapter 3

Basics of the Motor Control Framework

This chapter introduces the proposed motor control framework and the basic ideas and assumptions made in its development. The experimental trials performed to assess the validity of the framework assumptions are also presented at the end of this chapter.

3.1 The task space

According to the uncontrolled manifold theory (UCM, Scholz and Schöner, 1999), the nervous system tightly controls the task-related kinematic variables and leaves the unrelated ones uncontrolled. In this thesis, the term *task space* is used to describe the collection of the task-related variables that are actively controlled by the nervous system. For example, during a reaching task, the task variables are the (x, y, z) position of the hand, and the task space is the 3D Cartesian space. Conversely, the collection of the kinematic variables whose variations do not affect the task form the *redundant space* (Figure 3.1a). It is readily apparent that the redundant variables are functions of all the joint angles. However, it is possible to define generalized kinematic variables that are in a subspace orthogonal to the

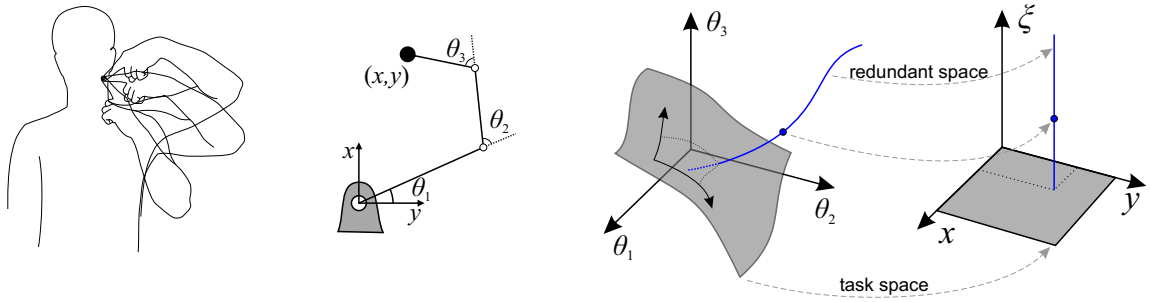

Figure 3.1: (a) Because of the kinematic redundancy in the human body, there are multiple ways to perform a certain task. The ones that are related to the task (and tightly controlled by the nervous system) form the *task space*, while the ones that do not affect the task form the *redundant space*. (b) An example of a redundant system (3-DoF with a 2D task space). There is one extra (redundant) degree of freedom besides the task-related ones. (c) The two representations of the system: the joint coordinate representation, and task/redundant representation. The task space (x, y) is visualized with the gray surface, and the redundant space is the line orthogonal to it.

task space. Figure 3.1b shows an example of a 3-degree-of-freedom (3-DoF) system, which can be described by the coordinates $(\theta_1, \theta_2, \theta_3)$ or (x, y, ξ). The former is the joint angle representation, while the latter is task/redundant variable representations. The variable ξ is any generalized coordinate lying in a subspace that is orthogonal to the task space. It can be any of the joint angles (lor a function of them) as long as its variation does not affect the task variables (x, y) (see Figure 3.1c).

3.2 The motor control framework

Various observations suggest that the nervous system controls only task-related kinematic variables. Therefore, it is hypothesized that the nervous system stores task-related rep-

resentations of the body (e.g. hand position in space, instead of joint angles). This view separates the control of the task-related and unrelated variables, without requiring the nervous system to continuously solve an inverse kinematic problem.

Muscle synergy theory holds the key to further simplify the control process. An individual muscle, specifically a bi-articular muscle (muscles that span two joints, e.g. hamstring) may have a very complex function in the task space, but the co-contraction of a number of muscles can potentially have a very clear function. Therefore, the combination of the task-related representation of the body with the task/synergy relationship has a strong potential to simplify the motion control in musculoskeletal systems.

In the following, the details of a general motor control framework are presented. Without loss of generalizability, an upper extremity reaching motion is used as an example to show the potential of this framework.

3.2.1 Overview of the motor control framework

High-level controller

The hierarchical structure of the proposed motor control framework is shown in Figure 3.2. The high-level controller is a feedback controller in the task space, which only deals with the task variables (e.g. the 3D hand position), and disregards the complexities of the musculoskeletal system. Its role is to compare the current task variables with the target and define the task space accelerations, $\mathbf{a}_{ref}$, required to achieve the goal.

In this motor control framework, this level of control is responsible for many of the properties of the human motor control system, including path planning, error compensation, anticipation/prediction, and adaptation. Identifying detailed models of the high-level controller is beyond the scope of this research, which is mostly focused on error compensation.

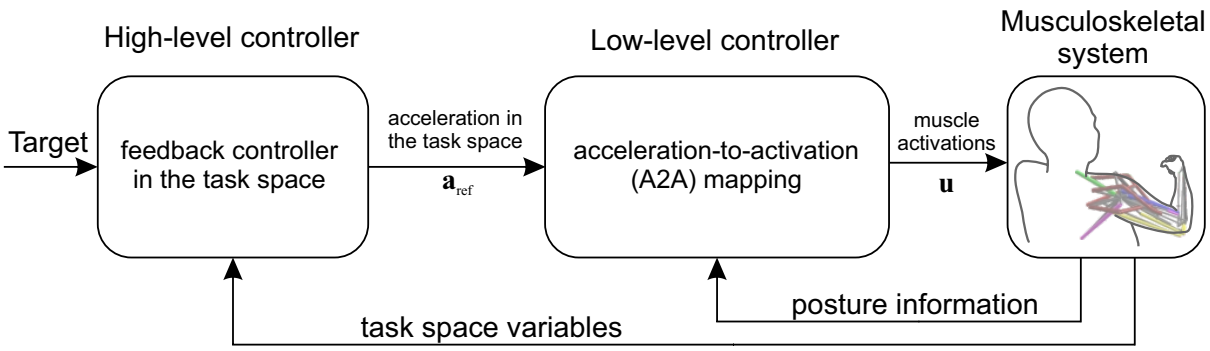

Figure 3.2: The hierarchical structure of the proposed synergy-based motor control framework. The high-level controller is responsible for task space control, and outputs the task space acceleration. The low-level controller translates this acceleration command to muscle activations.

Low-level controller

Human motions are produced by muscle contractions. Thus, the reference acceleration specified by the task space controller needs to be translated to muscle activations (see Figure 3.2). Muscle synergies have been used to simplify the calculations in this acceleration-to-activation (A2A) mapping. Essentially, muscle synergies are viewed as the pre-calculated bundles of solutions for the muscle force sharing problem (perhaps obtained through evolution or practice). The details on how to obtain these synergies will be provided later in this chapter, but for now, it is assumed that the synergies are known. The way the A2A mapping works is depicted in Figure 3.3 and described below.

Consider an N-DoF musculoskeletal system with m muscles, for which a p-dimensional task space ($\mathcal{T}_p$) is considered:

$$\mathcal{T}_p \subset \mathbb{R}^p, \qquad p \leq N \tag{3.1}$$

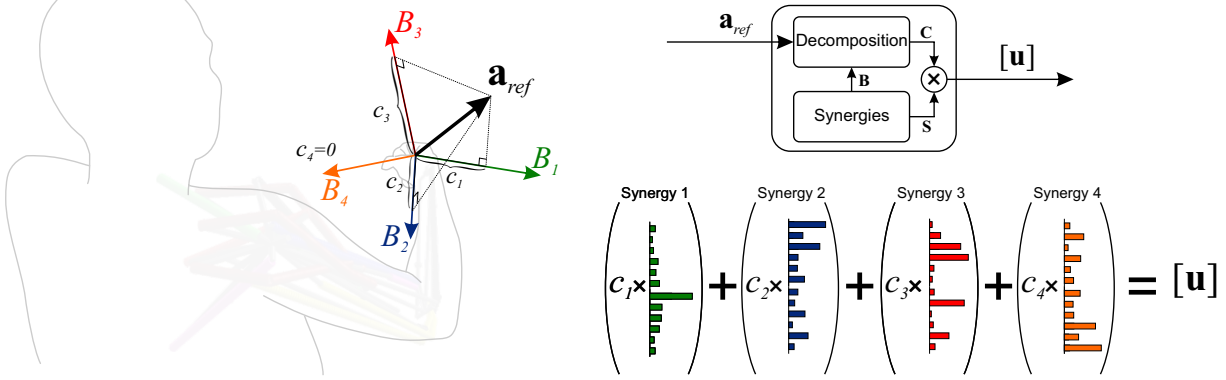

Figure 3.3: The schematic of the acceleration-to-activation (A2A) mapping. This example shows the case where the task space is 3-dimensional (hand position), $p = 3$. An arbitrary acceleration vector (black arrow, $\mathbf{a}_{ref}$) can be decomposed into the basis set (coloured vectors, B_i) to find the corresponding coefficients. The same coefficients can then be used to combine the synergies to calculate the muscle activities that result in the desired acceleration. In this example, four synergies are shown to demonstration the concept.

It is assumed that the nervous system knows k synergies, represented in this model by the matrix $\mathbf{S}_{m\times k}$, where each column of $\mathbf{S}$ contains the relative activation of the m muscles in a single synergy. It is also assumed that the nervous system knows the effect of each synergy in the task space (e.g. the resulting acceleration vectors, B_i, in Figure 3.3). The collection of these acceleration vectors can be viewed as a *basis set*, $\mathbf{B}_{p\times k}$, for the task space $\mathcal{T}_p$. It means that any arbitrary acceleration vector in the task space ($\mathbf{a} \in \mathcal{T}_p$) can be created from a linear combination of these basis vectors. Thus, the nervous system can *decompose* the reference task space acceleration vector (the output of the task space controller, $\mathbf{a}_{ref}$) onto this basis set, to calculate the coefficients (i.e. intensity) of each basis vector. This process is analogous to solving for the coefficients vector $C_{k\times 1}$ in the following equation.

$$\mathbf{a}_{ref} = \mathbf{B}_{p\times k}\mathbf{C}_{k\times 1} \tag{3.2}$$

The basis vectors combined with the coefficients c_i produce the reference acceleration. Likewise, the synergies (that generate the basis vectors) combined with the same coefficients result in the muscle activations that produce the reference acceleration; i.e.:

$$\mathbf{u}_{m\times 1} = \mathbf{S}_{m\times k}\mathbf{C}_{k\times 1} \tag{3.3}$$

is the solution of the muscle force sharing problem. The proposed A2A mapping has an important implication: *it replaces the costly and time-consuming non-linear optimization process with a linear vector decomposition problem.* As a result, it is possible to implement this method for real-time motion control. The block diagram of this process is also shown in Figure 3.3. It should be noted that, although this problem does not necessarily have a unique solution, it can easily be solved using a least-squares method as implemented in `lsqnonneg` function in Matlab.

The underlying assumptions

Positive-decomposition Muscles are pull-only actuators. Thus only a positive muscle activation level is meaningful. The same property is also assumed for a synergy; i.e. a synergy cannot have a negative coefficient. Therefore, the vector decomposition mentioned above has to be a *positive decomposition* ($c_i > 0$). This requirement implies that the basis vectors cannot all be in one half-plane. Thus, at least $p+1$ basis vectors are needed to span a p-dimensional task-space with positive coefficients. For example at least four synergies are needed to positively decompose an acceleration vector in the 3D task space.

Task-specific synergies A tight relation between the synergies and the task is assumed in this model. The term *task-specific synergies* means that, for example, the synergies

employed during a 3D reaching task (controlling the hand position) are different from the ones during elbow flexion (controlling elbow angle). The uncontrolled manifold theory (Scholz and Schöner, 1999) can help distinguish between different tasks by identifying the actively controlled variables.

Principle of superposition The proposed A2A mapping (and muscle synergy theory in general) relies on the principle of superposition. Unfortunately, the human musculoskeletal system is a non-linear system, for which superposition may not hold in general. However, musculoskeletal system dynamics equations reveal that under certain assumptions (body is stationary, and the elasticity of the muscles are neglected), the relationship between the muscle activities and the resulting task space acceleration is linear, and superposition can be applied. In other words, the effect of co-activation of multiple synergies (the total task space acceleration) is the same as the summation of the effects of individual synergies (which are the basis vectors). In such a *nominal* condition, the A2A mapping works as expected, but in real conditions, there will be errors in A2A estimations. However, it will be shown in the next chapters that, because of the presence of a feedback controller, the motion is still controllable.

3.2.2 Synergies and kinematic redundancy

There was no complication with the presented method when the number of task space dimensions was equal to the number of degrees of freedom in the system (i.e. $p = N$). In this case, there is no redundant degree of freedom. The human body, however, has usually more degrees of freedom for the intended task (usually $p < N$, e.g. at least seven degrees of freedom are involved in reaching to a point in 3D space). Therefore, the redundant space, which is defined as the collection of the kinematic variable that do not affect the task ($\mathcal{R}_q,\ q = N - p$), is non-empty.

According to the uncontrolled manifold theory, the nervous system tightly controls the task-related kinematic variables and leaves the unrelated ones uncontrolled. There is a

significant complication inherent to this theory; the task variables (e.g. hand position) are in general complex functions of all the joint angles. How does the nervous system activate the muscles (which rotate the joints) to control some of the kinematic variables and leave the others uncontrolled?

A possible solution for this issue is to restrict the task space basis vectors to have no component in the redundant space. In other words, the task space basis vectors are *orthogonal* to the redundant spaces. As a result, the activation of the task space synergies will not produce any *muscle induced* acceleration in the redundant space. Consequently, it is possible to leave the redundant variables uncontrolled, while maintaining the control over the task variables.

In redundant systems, there may be situations where the redundant DoFs are important and need to be actively controlled (for example to avoid an obstacle, or reach to a target at a particular angle). Therefore, the *new full-dimensional task space in the previously-redundant system* includes all the degrees of freedom, and is mathematically defined as:

$$\hat{\mathcal{T}}_N = \mathcal{T}_p \oplus \mathcal{R}_q \qquad (\hat{\mathcal{T}}_N \subset \mathbb{R}^N) \tag{3.4}$$

where $\hat{\mathcal{T}}_N$ is the new task space and $\oplus$ is the *direct sum* that "combines" two vector spaces.

The proposed motor control framework requires synergies that are defined for a specific task space. Thus, a new set of synergies would ideally be needed for $\hat{\mathcal{T}}_N$. However, increasing the dimensions of the problem exponentially increases its complexity. Therefore, assumptions have been made to avoid such complexities.

Instead of defining new synergies for $\mathcal{T}_N$, the original ones ($\mathbf{S}_{m\times k}$) are augmented with l new synergies ($\bar{\mathbf{S}}_{m\times l}$) that produce basis vectors orthogonal to the original ones. Mathematically, the new basis set $\hat{\mathbf{B}}$ for $\hat{\mathcal{T}}_N$ is constructed as:

$$\hat{\mathbf{B}}_{N\times(k+l)} = \mathbf{B}_{p\times k} \oplus \bar{\mathbf{B}}_{q\times l} = \begin{bmatrix} \mathbf{B}_{p\times k} & 0 \\ 0 & \bar{\mathbf{B}}_{q\times l} \end{bmatrix} \tag{3.5}$$

which is produced by the synergies:

$$\hat{\mathbf{S}}_{m\times(k+l)} = \begin{bmatrix} \mathbf{S}_{m\times k} & \bar{\mathbf{S}}_{m\times l} \end{bmatrix} \tag{3.6}$$

Here, $\hat{\mathbf{B}}$ is the augmented basis set for new task space $\hat{\mathcal{T}}_N$, and $\bar{\mathbf{B}}_{q\times l}$ is the basis set that spans the original redundant space. Therefore, $\hat{\mathcal{T}}_N$ is spanned by the collection of two basis sets that are orthogonal to each other.

To put this in the motor control framework, the high-level controller may now define an N-D reference acceleration vector $\mathbf{a}_{N\times 1}$. In an identical process to the original case, the reference acceleration vector is decomposed into the basis set:

$$\hat{\mathbf{a}}_{N\times 1} = \begin{bmatrix} \mathbf{a}_{p\times 1} \\ \bar{\mathbf{a}}_{q\times 1} \end{bmatrix}_{ref} = \hat{\mathbf{B}}_{N\times(k+l)}\hat{\mathbf{C}}_{(k+l)\times 1} \tag{3.7}$$

to find the coefficients of the synergies, $\hat{\mathbf{C}}$, which are then used as the weightings to combine the synergies as:

$$\mathbf{u}_{m\times 1} = \hat{\mathbf{S}}_{m\times(k+l)}\hat{\mathbf{C}}_{(k+l)\times 1} \tag{3.8}$$

The resulting muscle activations, $\mathbf{u}_{m\times 1}$, will produce the acceleration vectors $\mathbf{a}_{ref}$ and $\bar{\mathbf{a}}_{ref}$ in the original task and redundant spaces, respectively.

This orthogonal formulation, although being sub-optimal compared to a general N-D basis set, has the advantage of decoupling the task and redundant spaces. As a result, it is possible to switch on/off the control of the redundant DoFs by choice. The task space controller may output a non-zero reference acceleration in the redundant space ($\bar{\mathbf{a}} \neq 0$) to control it, or a zero value ($\bar{\mathbf{a}} = 0$) to leave it uncontrolled ($\bar{\mathbf{u}} = 0$). Because of the architecture of the motor control framework, the condition $\bar{\mathbf{a}} = 0$ does not enforce zero acceleration—it means no acceleration produced by the muscles. Another interesting implication of this method is the possibility of implementing a less strict controller, for a loose control of the redundant DoFs.

3.2.3 Taking the system dynamics into account

It is important to note that the A2A mapping uses synergies/bases that are usually obtained for a stationary condition (see the next section on how synergies are obtained). For a better control performance, velocity-dependent accelerations, gravity, and external forces must be accounted for in the solutions for muscle activations.

The arm dynamics in the joint-space can be described as:

$$\mathbf{M}\ddot{\mathbf{q}} + \mathbf{b}(\mathbf{q}, \dot{\mathbf{q}}) + \mathbf{g}(\mathbf{q}) = \mathbf{J}^T\mathbf{F} + \mathbf{f}(\mathbf{u}, \mathbf{q}, \dot{\mathbf{q}}) \tag{3.9}$$

where $\mathbf{q}$ is the vector of the joint angles, $\mathbf{M}$ is the inertia matrix, $\mathbf{b}$ contains the velocity dependent terms, and $\mathbf{g}$ represents the effect of gravity. $\mathbf{F}$ is the vector of the external forces in the task space, which is related to the joint space dynamics via the Jacobian matrix $\mathbf{J}$. Finally, $\mathbf{f}(\mathbf{u}, \mathbf{q}, \dot{\mathbf{q}})$ represents the effects of muscle forces on the system, which are functions of muscle activations, posture (through moment arms and muscle force-length relation), and velocities (through muscle force-velocity relations).

In the nominal condition (no gravity, no external forces, no velocity), the muscle activations found from the acceleration-to-activation mapping ($\mathbf{u} = \mathscr{A}_2\mathscr{A}(\mathbf{a}_{ref})$) result in the reference acceleration. In joint space representation:

$$\ddot{\mathbf{q}}_{ref} = \mathbf{M}^{-1}\mathbf{f}(\mathscr{A}_2\mathscr{A}(\mathbf{a}_{ref}), \mathbf{q}, 0) \tag{3.10}$$

However, in a general condition where the non-linear terms exist, the resulting acceleration ($\ddot{\mathbf{q}}_{real}$) will be different from the desired one.

$$\ddot{\mathbf{q}}_{real} + \mathbf{M}^{-1}(\mathbf{b} + \mathbf{g} - \mathbf{J}^T\mathbf{F}) = \mathbf{M}^{-1}\mathbf{f}(\mathscr{A}_2\mathscr{A}(\mathbf{a}_{ref}), \mathbf{q}, \dot{\mathbf{q}}) \tag{3.11}$$

Therefore, in order to have $\ddot{\mathbf{q}}_{real} = \ddot{\mathbf{q}}_{ref}$, one should use a corrected reference acceleration ($\tilde{\ddot{\mathbf{q}}}_{ref}$) in the mapping, i.e.:

$$\tilde{\ddot{\mathbf{q}}}_{ref} = \ddot{\mathbf{q}}_{ref} + \mathbf{M}^{-1}(\mathbf{b} + \mathbf{g} - \mathbf{J}^T\mathbf{F}) \tag{3.12}$$

Since the task-space acceleration can be written as:

$$\mathbf{a} = \mathbf{J}\ddot{\mathbf{q}} + \dot{\mathbf{J}}\dot{\mathbf{q}} \tag{3.13}$$

the corrected acceleration in the task-space will be:

$$\begin{aligned}
\tilde{\mathbf{a}}_{ref} &= \mathbf{J}\tilde{\ddot{\mathbf{q}}}_{ref} + \dot{\mathbf{J}}\dot{\mathbf{q}} && (3.14)\\
&= \mathbf{J}(\ddot{\mathbf{q}}_{ref} + \mathbf{M}^{-1}(\mathbf{b} + \mathbf{g} - \mathbf{J}^T\mathbf{F})) + \dot{\mathbf{J}}\dot{\mathbf{q}} && (3.15)\\
&= \mathbf{a}_{ref} + \mathbf{J}\mathbf{M}^{-1}(\mathbf{b} + \mathbf{g} - \mathbf{J}^T\mathbf{F}) + \dot{\mathbf{J}}\dot{\mathbf{q}} && (3.16)
\end{aligned}$$

This corrected acceleration accounts for the system dynamics. However, it must be noted that this correction does not account for the force-velocity term and tendon dynamics. Therefore, the muscle activations obtained from

$$\mathbf{u} = \mathscr{A}_2\mathscr{A}(\tilde{\mathbf{a}}_{ref}) \tag{3.17}$$

may still produce inaccurate accelerations because of the neglected muscle dynamics. Furthermore, the neglected muscle excitation/activation dynamics also affects the reliability of estimations. Fortunately, most of these *uncertainties* (i.e. unmodelled dynamics) can be effectively compensated using the task space feedback controller.

3.3 Obtaining the synergies

Muscle synergies, if they exist, are probably formed either through evolution or practice. They must be structured in such a way that results in the best performance in doing a task, whether it be reducing the effort, or increasing the robustness. It is speculated that in the

case of a familiar and well-trained action (e.g. reaching to a point in space), the synergies are structured to maximize efficiency for the intended task. Therefore, physiological effort minimization is the basis of the computational methods used in this thesis for synergy extraction.

3.3.1 Synergies from factorization of data matrices

A common practice to obtain the muscle synergies is to use a computer algorithm to *unfold* a set of muscle activities to reveal the underlying building blocks. Both measured and simulated (optimal) muscle activities exhibit such modularity (Steele et al., 2013) that can be used to identify the muscle synergies.

To unravel the synergies, multiple sets of muscle activity data (either measured or simulated) are required. These multiple sets may include multiple trials of one task, or multiple tasks. Regardless, a *rich-enough* set of muscle activity data is usually gathered in a data matrix as:

$$\mathbf{A}_{m\times n} = [\mathbf{u}_1, \mathbf{u}_2, \ldots, \mathbf{u}_n] \tag{3.18}$$

where m is the number of muscles, and n is number of samples. In the simplest case, the data matrix $\mathbf{A}$ is assumed to be a linear combination of k muscle synergies, which can mathematically be presented as:

$$\mathbf{A}_{m\times n} = \mathbf{S}_{m\times k}\mathbf{C}_{k\times n} \tag{3.19}$$

where $\mathbf{S}$ is called the *synergy matrix*, with muscle synergies represented by its columns; $s_{i,j}$ contains the share of the i^{th} muscle in the j^{th} synergy. The *coefficient matrix* $\mathbf{C}$ contains the weighting of the synergies corresponding to each sample of the data matrix.

Various algorithms have been proposed to extract the synergies, including non-negative matrix factorization (NNMF), independent component analysis (ICA), principal component analysis (PCA), and matrix factorization (MF). For a review of factorization algo-

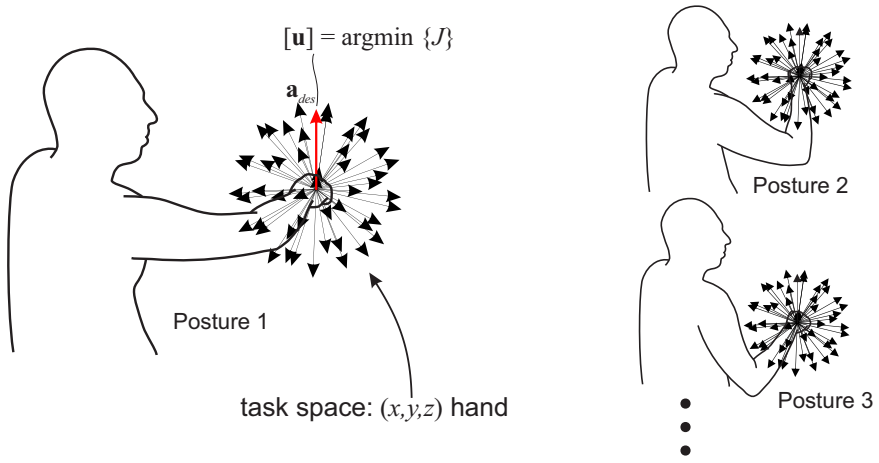

Figure 3.4: A large number of optimization problems are solved off-line to obtain the synergies. In a given posture, an optimization is solved to find the optimal muscle activations that produce each of the desired task space accelerations ($\mathbf{a}_{des}$). The same process is repeated for a variety of postures.

rithms see (Tresch et al., 2006). Among these algorithms, NNMF (initially proposed by Lee and Seung, 2000) is the most widely used one due to its non-negativity constraint.

An NNMF problem is defined as:

$$\text{minimize: } e = \text{norm}(\mathbf{A}_{m\times n} - \mathbf{S}_{m\times k}\mathbf{C}_{k\times n}) \tag{3.20}$$

such that $\mathbf{S}$ and $\mathbf{C}$ have non-negative elements.

Synergies with posture-dependent bases

To obtain and store the synergies in musculoskeletal simulations, a large number of optimization problems can be solved to mimic the human evolution/practice process. At a given posture, the best combination of muscle activities that produce a certain task space acceleration is found through an optimization process (see Figure 3.4). The optimization algorithm calculates the vector of muscle activations, $\mathbf{u}_{m\times 1}$, that minimize the following objective function:

$$\mathbf{u}_{m\times 1} = \arg\min \left\{ J = w_1 \frac{1}{|\mathbf{a}_{des}|^2} |\mathbf{a}_{des} - \mathbf{a}|^2 + w_2 \mathbf{u}^T \mathbf{u} \right\} \tag{3.21}$$

Here, J is the objective function that is minimized. $\mathbf{a}_{des}$ and $\mathbf{a}$ are the desired and actual task space acceleration vectors, respectively. w_1 and w_2 are the weighting factors that balance the importance of the tracking error and the muscular effort terms. The optimization is subjected to the constraints:

$$0 \leq u_i \leq 1 \quad , i \in \{1, .., m\} \tag{3.22}$$

The same optimization process is repeated for n different acceleration vectors in various directions (see Figure 3.4) to get the samples in the matrix $\mathbf{A}$ as:

$$\mathbf{A}_{m\times n} = [\mathbf{u}_1, \mathbf{u}_2, \ldots, \mathbf{u}_n] \tag{3.23}$$

Applying the NNMF to the solution matrix $\mathbf{A}$ gives a set of synergies at the current posture. If the entire process is repeated for all positions/orientations in the working space, a set of *posture-dependent* synergies can be defined.

These posture-dependent synergies and the corresponding task space basis vectors are assumed to be stored in the nervous system. During motion control, they are recalled and used in the A2A mapping to estimate muscle activations.

A problem with the application of the NNMF algorithm as described above is its sensitivity to its initial guesses. In other words, there are very many local minima in the solution space of (3.20), and the NNMF may hit a local minimum instead of the global minimum. Therefore, when the NNMF is run for two neighbouring postures, the resulting synergies may be substantially different. These inconsistencies adversely impact the functionality of the A2A mapping. An example of this inconsistency issue is illustrated in the top row of Figure 3.5. The data to obtain these synergies are measured EMGs in 9 different

postures in a 2D task space (the data belongs to the experiment #1 explained in section 3.4.2). It is visible in the top plots that there is no consistency between synergies of neighbouring points in the 2D task space, if NNMF is applied to the data matrices separately. Furthermore, the corresponding basis vectors seem to point in random direction.

One approach to improving the consistency of NNMF is to use the synergies of a neighbouring point as the initial guess for the next posture. In this approach, the algorithm starts from one corner of the task-space with some random initial guess (see Figure 3.6). Then the algorithm moves to the next point (posture) along the first dimension (the red line in Figure 3.6), and uses the NNMF results of the previous point as its initial guess. The algorithm continuous to the end of the line, and uses the previous point's results as the initial guess. When the first line is covered, the algorithm moves along the second dimension (the blue lines in Figure 3.6). The algorithm uses the NNMF results of the point in the previous line as its initial guess, until the first "page" (coloured in green) is covered. Finally, the algorithm moves along the last dimension, and uses the NNMF results of the points in the previous page as its initial guess, until the whole task-space is covered.

This algorithm results in more consistent synergy matrices across the postures. An example is shown in the second row of Figure 3.5. It is also visible that the basis vectors from the synergies are more clustered, which improves the A2A mapping results.

Notes on posture-dependent synergies: The synergies are essentially calculated at discrete points in space. However, during motion, the hand moves through continuous space, where synergies are not necessarily calculated. To continue the feedback control process, the synergies at every single point in the task-space has to be identified. The synergies at an intermediate point can be estimated by interpolating between the mesh points. In the nervous system, this may not be an issue, as the synergies may be confined within neural circuits that output signals as continuous functions of body posture.

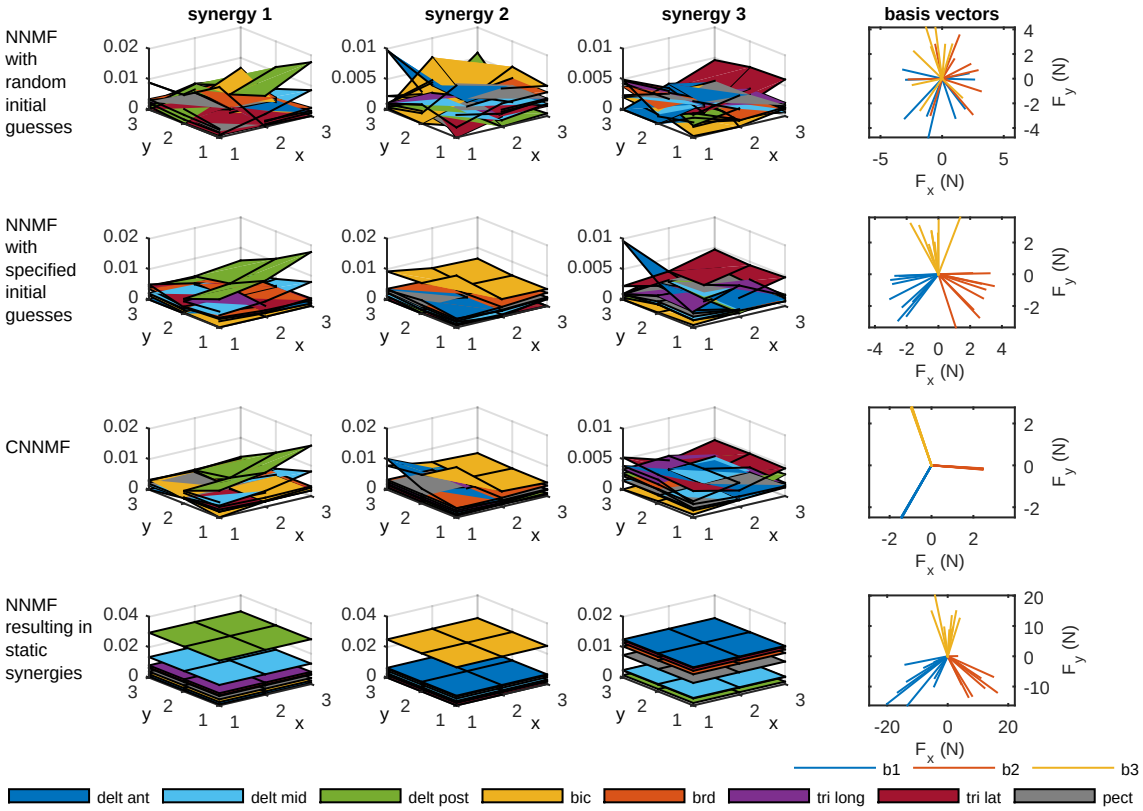

Figure 3.5: The comparison of various synergy extraction methods. The plots show how moving in x and y directions in the 2D task space affect the muscle activations in the synergies. Each coloured surface shows the activation level of a muscle in a synergy. The panels in the right column show the basis vectors associated with the synergies at 9 different positions in the task space. **Top row**: The application of NNMF with random initial guesses to the data matrices separately in various postures. No consistency exists between the synergies in the neighbouring points; the basis vectors are randomly distributed. **Second row**: The application of NNMF to separate data matrices with specified initial guesses; the synergies show smooth transition between neighbouring points, and the basis vectors are more clustered. **Third row**: The application of the CNNMF to the concatenated data matrix that is built by vertically stacking all the data matrices. The synergies are smooth, and the basis vectors are essentially posture-invariant. **Last row**: The application of the NNMF to the data matrix that considers all the available data as different samples. As a result, synergies are posture-invariant, but basis vectors do change with posture.

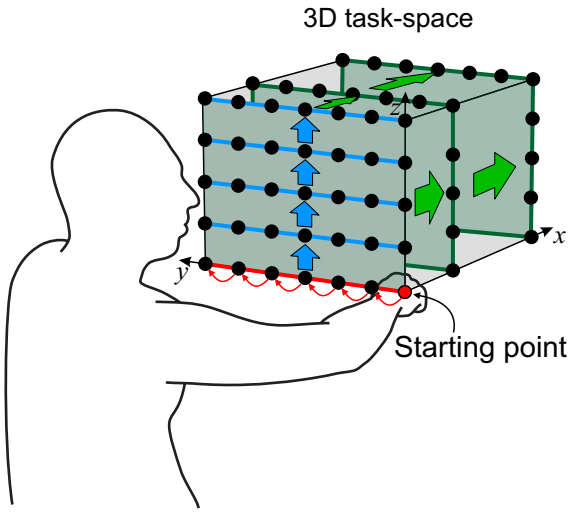

Figure 3.6: The schematic of the progression through a 3D task-space. The initial point is at the corner (the red dot). Each point along the first dimension (the red coloured line) uses the previous point results as the initial guess of the NNMF. Moving along the second dimension (the lines coloured blue), each point uses the result of the previous line as the initial guess. Finally, moving along the third dimension (the green "pages"), the previous page data is used as the initial guess of the current point.

Synergies with shared (posture-invariant) basis vectors

The method presented in the previous section results in posture-dependent synergies that produce posture-dependent basis vectors. It is possible to overcome the inconsistency issue mentioned earlier using a slightly different factorization approach. However, it comes at the expense of being restricted to posture-invariant bases.

In this method, the data matrices $\mathbf{A}$ from all postures are vertically stacked in a larger matrix (Shourijeh et al., 2016) as:

$$\mathbf{A}_{con} = \begin{bmatrix} \mathbf{A}^1_{m\times n} \\ \mathbf{A}^2_{m\times n} \\ \vdots \\ \mathbf{A}^P_{m\times n} \end{bmatrix}_{mP\times n} \tag{3.24}$$

where $\mathbf{A}_{con}$ is the *concatenated data matrix* and $\mathbf{A}^i, i = 1 \dots P$ are the data matrices in all P postures. Application of NNMF to this concatenated matrix (referred to as the concatenated-NNMF, or CNNMF method) gives a concatenated synergy matrix and a shared coefficient matrix:

$$\mathbf{A}_{con} = \begin{bmatrix} \mathbf{A}^1_{m\times n} \\ \mathbf{A}^2_{m\times n} \\ \vdots \\ \mathbf{A}^P_{m\times n} \end{bmatrix}_{mP\times n} \simeq \begin{bmatrix} \mathbf{S}^1_{m\times k} \\ \mathbf{S}^2_{m\times k} \\ \vdots \\ \mathbf{S}^P_{m\times k} \end{bmatrix}_{mP\times k} [\mathbf{C}_{k\times n}] \tag{3.25}$$

where each of the $\mathbf{S}^i$ matrices represent a synergy matrix at a specific posture. In the CNNMF formulation, the same coefficient matrix $\mathbf{C}$ is used to explain the data matrices $\mathbf{A}^i$. Since the acceleration vectors that the columns of $\mathbf{A}^i$'s produce are the same, this formulation implies that the synergy-produced basis vectors are the same for all postures. An example of CNNMF that results in posture-dependent synergies and posture-invariant bases is shown in the third row of Figure 3.5.

The posture-invariance bases are interesting from the implementation point of view. Since the bases are the same for all postures, the A2A mapping has an easier job decomposing the reference acceleration vector onto the basis set, as it does not need to interpolate the stored basis sets.

Furthermore, because the coefficient matrix is shared between all synergies in the factorization, and because the original data matrix contained smooth transitions from one point to the neighbouring one, the synergies' transitions are also necessarily smoothly across various postures (resolving the inconsistency issue).

The drawback of the CNNMF method is the possibility of sub-optimality of the extraction, since some flexibility is lost as a result of using a shared coefficient matrix for all postures. On the other hand, it has the advantage of being easier to implement.

Number of synergies

There is no systematic way to choose the number of synergies (except for the simpler cases described in section 3.3.2). The usual practice is to pick the smallest number of synergies that reconstruct the data with little error in an *inverse* manner; i.e. the goal is to explain the data with as few synergies as possible. The reconstruction error usually decreases as the number of synergies increase, and the number of synergies beyond which no significant improvement is observed is usually chosen.

However, the objective in the proposed motor control framework is to maximize the overall performance of the A2A process as a *predictive method*. Thus, instead of the reconstruction error of the original data (e.g. the error in (3.20)), a quantitative measure for the predictive capabilities of the method is needed. Therefore, the *variance accounted for* (VAF) of A2A mapping results is chosen as the measure. The VAF is defined as:

$$VAF = 1 - \frac{\sum (u_{a2a} - u)^2}{\sum u^2} \tag{3.26}$$

where u_{a2a} is the muscle activation calculated by the A2A mapping, and u is the *gold standard* value (usually measured EMG data, or optimally calculated muscle activation). The summation is usually taken over the entire number of muscle and samples. As it will be shown later in this thesis, the highest VAF value is usually attained with a relatively low numbers of synergies ($k \ll m$).

3.3.2 Synergies from optimal control

It is usually observed that the muscle activations obtained by minimizing an exertion index (e.g. minimizing muscle force or activation) have highly modular structures (Steele et al.,

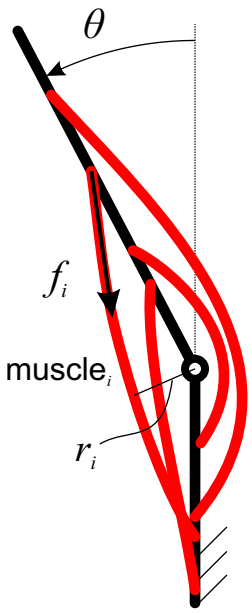

Figure 3.7: An example of a 1-DoF musculoskeletal system with mono-articular muscles. A muscle's force, f, and moment arm, r, is illustrated here.

2013). This section presents an alternative approach to identify the muscle synergies via analytical optimal control methods.

Assume a musculoskeletal system with a 1D task space. An example is shown in Figure 3.7, where the *task variable* is the joint angle, θ.

Since the model contains only mono-articular muscles, it is possible to analytically solve for the optimal muscle activations, a_i, that minimize the instantaneous cost function J:

$$J = \sum_{i=1}^{m} u_i^2 \qquad (m = \text{number of muscles}) \tag{3.27}$$

subject to the constraints:

$$\sum_i f_i r_i(\theta) = T \tag{3.28}$$

and

$$0 \leq u_i \tag{3.29}$$

The cost function J in (3.27) represents the muscular effort at each instant of time. Equation (3.28) is the moment balancing constraint that requires the muscles to generate a certain torque T in the task space. The muscle forces, f_i, act at posture-dependent moment arms $r_i(\theta)$, which are positive for the flexors, and negative for the extensors.

The inequality constraint (3.29) enforces the activations to be positive. No explicit upper bound (i.e. $u_i \leq 1$) is assumed for the activations since lower activations are strictly preferred by the cost function, resulting in optimal activations that do not violate the upper bound constraint. Therefore, the following arguments are only valid for *sub-maximal* motions.

The muscle force can be estimated from the activation level using a Hill muscle model as:

$$F = uF_{0_{max}} f_l(\theta) f_v(\dot{\theta}, u) \cos(\alpha) \tag{3.30}$$

In the Hill muscle model, muscle activation, u, scales the maximum muscle force $F_{0_{max}}$. Additionally f_l and f_v are force-length and force-velocity relations (Thelen, 2003) that also alter the muscle force. Lastly, muscle force in the tendon direction is affected by the pennation angle α.

It is possible to combine the non-linear terms in (3.28) and (3.30) and rewrite the constraint equation (3.28) as:

$$\sum_i u_i h_i(\theta, \dot{\theta}) = T \tag{3.31}$$

where $h_i(\theta, \dot{\theta})$ is the non-linear function that transforms muscle activity to the torque in the operational space (similar to a Jacobian that transforms joint torque to end-effector

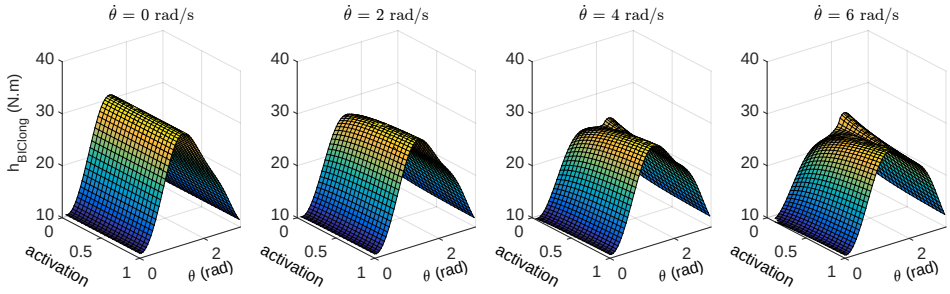

Figure 3.8: The simulated transformation $h_{BIClong}$ as a function of the elbow flexion angle θ and activation u, for various joint angle velocities. The plots show small dependence of h on activation.

force); it accounts for the force-length relation f_l, force-velocity relation f_v, maximum force $F_{0_{max}}$, pennation angle α, and moment arm $r(\theta)$ of muscle i. Therefore, h is positive for the flexors and negative for the extensors. It should be noted that in (3.31), the dependency of the force-velocity term on the activation is neglected (i.e. $f_v = f_v(\dot{\theta})$). Figure 3.8 shows the simulated value of h for the long head of biceps brachii as a function of elbow flexion angle θ and activation for $\dot{\theta} = 2$ rad/s. As can be seen, h is not a significant function of activation.

To solve the optimization problem, the cost function (3.27) can be augmented using a Lagrange multiplier, λ (Kirk, 2004).

$$\hat{J} = \sum_i u_i^2 + \lambda \left[\sum_i u_i h_i(\theta, \dot{\theta}) - T \right] \tag{3.32}$$

The inequality constraints (3.29) can be rewritten using the slack variables δ_i in the form:

$$u_i - \delta_i^2 = 0 \tag{3.33}$$

where δ_i are assumed to be unbounded. Substituting (3.33) into (3.32) yields:

$$\hat{J} = \sum_i \delta_i^4 + \lambda \left[\sum_i \delta_i^2 h_i(\theta, \dot{\theta}) - T \right] \tag{3.34}$$

$$\sum_i \delta_i^2 h_i(\theta, \dot{\theta}) = T \tag{3.35}$$

At a local minimum, the gradient of the cost function should be zero.

$$\frac{\partial \hat{J}}{\partial \delta_i} = 4\delta_i^3 + 2\lambda \delta_i h_i(\theta, \dot{\theta}) = 0 \tag{3.36}$$

One solution to this equation is:

$$\delta_i = 0 \tag{3.37}$$

which yields the optimal muscle activation, u_i^*:

$$u_i^* = 0 \tag{3.38}$$

If $\delta_i \neq 0$, (3.36) can be divided by δ_i to get:

$$2\delta_i^2 + \lambda h_i(\theta, \dot{\theta}) = 0 \tag{3.39}$$

which leads to:

$$\delta_i^2 = -\frac{\lambda}{2} h_i(\theta, \dot{\theta}) \tag{3.40}$$

By substituting this expression into the constraints (3.35), the Lagrange multiplier can be found:

$$\sum_i \left[-\frac{\lambda}{2} h_i(\theta, \dot{\theta}) \right] h_i(\theta, \dot{\theta}) = T \tag{3.41}$$

or:

$$\lambda = \frac{-2T}{\sum_i h_i^2(\theta, \dot{\theta})} \tag{3.42}$$

Therefore, the optimal solution (in sub-maximal contractions) can be found:

$$\delta_i^2 = u_i^* = \frac{h_i(\theta, \dot{\theta})}{\sum_j h_j^2(\theta, \dot{\theta})} T \tag{3.43}$$

To summarize the optimal solutions are:

$$u_i^* = 0 \tag{3.44}$$

or

$$u_i^* = \frac{h_i(\theta, \dot{\theta})}{\sum_j h_j^2(\theta, \dot{\theta})} T \tag{3.45}$$

The optimal solutions (3.44) and (3.45) are both valid answers in different situations. When the joint torque T is positive, the solution (3.45) is valid for the flexor muscles, which have $h(\theta, \dot{\theta}) > 0$. For the extensors, however, h is negative resulting in a negative (infeasible) answer if (3.45) is used. Therefore, the optimal extensor activations when $T > 0$ are stated by (3.44) (i.e. no extensor activity.) The opposite argument can be made when the joint torque is negative. In this case, the optimal extensor activations are found using (3.45), while flexors are inactive. A subtle detail that needs to be considered in (3.45) is that, depending on which group is active, the summation in the denominator has to be calculated over the *same-action* muscles (either flexors, or extensors). Therefore, the closed-form solution of (3.45) can be used to efficiently calculate the optimal muscle activations that generate a certain joint torque, T.

Alternatively, it can be observed that the ratio of the activations for the same-action muscles is independent of the required torque; they all activate with fixed (posture-dependent) relations—the same notion as muscle synergy.

$$\frac{u_i^*}{u_j^*} = \frac{h_i}{h_j} = f(\theta, \dot{\theta}) \tag{3.46}$$

It is possible to define two *synergies* for this operational space: one for a positive joint torque (flexor, S^f), and one for a negative one (extensor, S^e). One can identify two representative muscles (i.e. a flexor and an extensor) from the full set of muscles, and calculate the *synergy ratios* of (3.47) and (3.48).

$$s_i^f = \begin{cases} \dfrac{u_i^*}{u_f^*} = \dfrac{h_i}{h_f} & s_i^f > 0 \\ 0 & s_i^f \leq 0 \end{cases} \tag{3.47}$$

$$s_i^e = \begin{cases} \dfrac{u_i^*}{u_e^*} = \dfrac{h_i}{h_e} & s_i^e > 0 \\ 0 & s_i^e \leq 0 \end{cases} \tag{3.48}$$

In these relations, s_i^f and s_i^e are the flexor and extensor synergy ratios for muscle i, respectively. One can then calculate the optimal muscle activations based on the flexor and extensor representatives (u_f, u_e) using the synergies:

$$\mathbf{u} = \begin{bmatrix} S^f & S_i^e \end{bmatrix} \begin{bmatrix} u_f \\ u_e \end{bmatrix}_{rep} \tag{3.49}$$

where S^f and S^e are column vectors that contain the synergy ratios s_i^f and s_i^e, respectively. The representative activations themselves can be calculated either from the optimal values (3.45), or from any other control logic (e.g. PID). It is important to note that, regardless of the values of (u_f, u_e), if the synergy ratios of (3.47) and (3.48) are used, the resulting torque is optimally produced.

The calculation of synergy ratios are straightforward in simulations; they are the ratio of non-linear transformation of muscle i to that of the representative muscle. Although h is in general a function of activation, it is safe to neglect such dependency and calculate

$h|_{u=0.5}$. As will be shown in the simulation results in the next chapter, this approach results in near-optimal solutions.

3.3.3 Static versus posture-dependent synergies

The conventional method in the literature to extract synergies from the data matrices results in *static* synergies. In this context, static means that the synergies do not change with posture. The way these methods extract synergies involves gathering the muscle activity samples from a variety of situations. The samples in the data matrix may vary based on the experiment or simulation; they can be snapshots of the time-varying muscle activities, or the average of the recordings from multiple trials. Regardless, applying NNMF to such data results in synergies that are essentially static—they are the same for all samples. In contrast, both of the presented methods (the factorization and the analytic methods), result in posture-dependent synergies.

As shown in the next chapter (section 4.1), by adding the flexibility to the synergies to change with posture, it is possible to achieve higher control efficiency with a small number of synergies. Static synergies, on the other hand, fail to consider the changing capacity/function of the muscles as the posture changes. As a result, more synergies are required to capture the richness of muscle activity patterns.

For the sake of completeness, a method to extract static synergies is briefly described here. An example of static synergies is shown in the last row of Figure 3.5. To obtain these results, the data from various postures were stacked *horizontally* according to:

$$\mathbf{A}_{con} = [\mathbf{A}_1, \mathbf{A}_2, \cdots, \mathbf{A}_P]_{m \times Pn} \tag{3.50}$$

which essentially discards the dependence of the data on posture, and assumes them only as different samples without distinguishing them (a total of Pn samples). Therefore, the result of applying NNMF on this matrix is a set of static (posture-invariant) synergies, which produce posture-dependent bases.

3.4 Experimental evaluation of the methods

This section describes two experimental procedures designed to evaluate the performance of the A2A mapping. In these experiments, it is assumed that the human movements are governed by some high-level controller; the nature of this controller is not the focus of these experiments. Instead, the goal of the experiments is to test whether the A2A mapping can successfully be used to estimate muscle activities using the measured task space kinematics/dynamics (as the outputs of the high-level controller). If the estimates are close to the measured muscle activities, it is then possible to argue that the A2A mapping can be used for fast and biologically plausible feedback control of musculoskeletal systems.

In the next section, first the two experiments are described and the results are shown. The discussion about both experiments is presented afterwards.

3.4.1 Experiment #1: synergies in 2D horizontal plane

The first experiments uses the set-up shown in Figure 3.9. This set-up includes a two-DoF haptic robot (Quanser Inc.) that allows motion in the horizontal (table top) plane. The subject was asked to hold and move the robot end-effector. Therefore, the task space is the 2D (x, y) position of the hand/end-effector. The end-effector is equipped with a six-axis force sensor (Nano25, ATI Industrial Automation, Inc.) to measure the task space forces. The end-effector position was also measured by the robot. The subject's arm was suspended to remove the effects of gravity and arm/table friction (arm does not move off-plane). The robot's control loop and the force sensor had a 500 Hz sampling rate.

Surface electromyogram (EMG) data from eight muscles (Table 3.1) were recorded at 1926 Hz (Trigno Wireless EMG, Delsys Inc.). The EMG data was processed with the common procedure (raw EMG $\rightarrow$ zero-mean $\rightarrow$ digital band-pass filter with 5-800 Hz cut-off frequency $\rightarrow$ full-wave rectify $\rightarrow$ low-pass filter with 2 Hz cut-off frequency). The EMGs

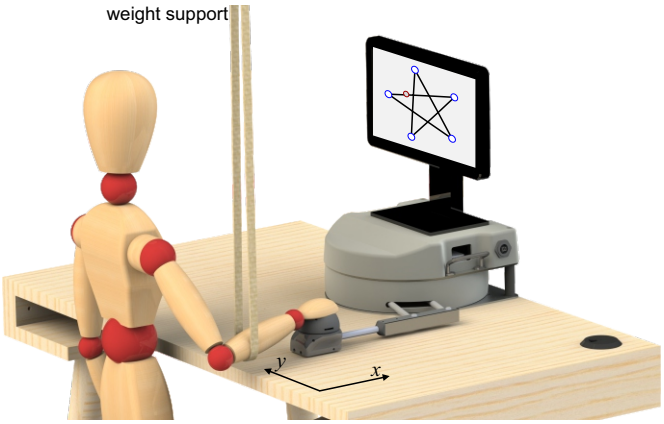

Figure 3.9: The set-up for experiment #1 includes a 2DoF haptic robot to measure force/position in the 2D task space. The arm is lifted above the table surface to support its weight and minimize friction.

#	Muscle	#	Muscle
1	Deltoid anterior	5	Brachioradialis
2	Deltoid middle	6	Triceps long
3	Deltoid posterior	7	Triceps Lateral
4	Biceps brachii	8	Pectoralis major

Table 3.1: The muscles recorded in the experiments

for each muscle were normalized with respect to the maximum voluntary contraction (see Appendix C for more details about the experiments).

The experiment was conducted in two phases. In phase one, the synergies were obtained and stored. In phase two, these synergies were used in the same A2A algorithm to reconstruct the muscle activities during motion trials. The only difference from the original algorithm is that the task space force vectors are used instead of the acceleration vectors (therefore, the mapping is a force-to-activation, F2A).

Force vectors are chosen because they are easier to measure in the experiments than

accelerations. However, working with force in the F2A mapping introduces error in the estimation of muscle activities. Due to the dynamics of the system (i.e. inertias), the measured hand force does not include all the information about the task space motion (system equations are needed to account for the dynamic terms). Therefore, to reduce the adverse effects of the arm and robot dynamics, the motion trails are conducted with high resistive force from the robot, and at low speeds and accelerations. In this condition, the hand/robot interaction force outweighs the dynamics effects, and the error is expected to be small.

Phase one: obtaining the synergies

The robot end-effector was locked in 9 different positions in the task space, and in each position, the subject applied isometric force to the end-effector. A display showed the measured force vector, which the subject had to match with multiple targets. The target forces were 5 N (setup's limitation) along 15 equally-spaced directions in the horizontal plane. The subject had to hold the force for at least 2 s within 0.5 N accuracy range to successfully match a target.

The EMG data in each posture was averaged for each muscle in the 2-s window before the successful target matching. The collection of these data for all 15 targets formed a data matrix $\mathbf{A}_{8\times15}$ for that specific posture. The concatenated data matrices from all 9 postures were given to the CNNMF algorithm to obtain the posture-dependent synergy and the shared coefficient matrices ($\mathbf{A}_{(9\times8)\times15} = \mathbf{S}_{(9\times8)\times k}\mathbf{C}_{k\times15}$, with k synergies)

The basis set $\mathbf{B}$ corresponding to each synergy matrix was also obtained by solving the following equation using a least square method:

$$\mathbf{F}_{2\times15} = \mathbf{B}_{2\times k}\mathbf{C}_{k\times15} \tag{3.51}$$

The matrix $\mathbf{F}_{2\times15}$ contained the measured 2D force vectors in the 15 directions in the specific posture.

Phase two: motion trials and muscle activation estimation

Next, the subject performed multiple point-to-point reaching movements in the 2D task space with self-selected speed, and the task space forces and positions were collected. At each point during the motion, the posture-specific synergy and basis matrices were estimated by interpolating the previously obtained matrices. Then, the measured force vector was decomposed onto the basis set to calculate the corresponding coefficients, which were multiplied by the synergy matrix to reconstruct the muscle activities. The only data available to this mapping were: the current task space force (F_x, F_y) and position (x, y), as well as the previously obtained synergy and basis matrices ($\mathbf{S}$ and $\mathbf{B}$).

To quantify the estimation performance, VAF (3.26) is calculated, where the summation is across all the muscles and for the entire duration of the movements. In (3.26), u_{A2A} is the estimated muscle activities using the presented synergy approach, which is compared against the gold standard, u (the measured EMGs).

Results

Three subjects participated in the experiment. The experimental results (the 2D task space) for subject #1 are shown in Figures 3.10 and 3.11 (Appendix A contains the rest of the results). Applying the CNNMF algorithm to the collected EMG datasets results in the posture-dependent synergy matrices, which are visualized in Figure 3.10a. The results with three synergies ($k = 3$) are shown here. Each surface in the visualization of the synergies in Figure 3.10a illustrates the variation of a muscle share in a synergy across various positions in the task space. Associated with each synergy is a basis vector shown in Figure 3.10b. The implementation of the CNNMF results in basis sets that are consistent across all postures. The point-to-point motion trials in the 2D task space and the associated task space forces are shown in Figure 3.10c. A *segment* is the movement from one target to the next (5 segments in total), and the motion in each segment was repeated 10 times. Finally, the measured EMGs during the movements are shown in Figure 3.11, super-imposed by

the estimated activations from the presented method.

The motor control framework presented here is a general method; however, the results (specifically the synergies) are subject-specific, and an inter-subject comparison is hard. Therefore, only one subject's results were shown here. The results for subject 2 and 3 are presented in Appendix A. The three subjects' results were similar with VAF calculated to be 0.726 ± 0.005, 0.635 ± 0.006, and 0.661 ± 0.005 (for $k = 3$).

The effect of the number of synergies on the framework performance (VAF) as well as the CNNMF error (e in (3.20)) is shown in Figure 3.12. Multiple runs of the method (20 sets) is performed (because CNNMF results are sensitive to the randomly-chosen initial guesses), and Figure 3.12 shows the mean and standard deviation of the obtained results. It can be seen that the minimum number of synergies for a 2D task space ($k = 3$) results in the best VAF performance, and the inclusion of more synergies does not improve the results. This is the reason why $k = 3$ was used in the presented results in Figures 3.10 and 3.11.

3.4.2 Experiment #2: synergies in a redundant system

In the second experiment, the goal has been to investigate how the assumption of the task/redundant space orthogonality works in practice.

To tackle this problem, the experimental set-up of Figure 3.13 was designed to impose certain constraints on the body. The subject was asked to hold the handle, and the forearm was strapped to the armrest. As a result, the set-up allowed only two degrees of freedom: a linear motion of the hand in the x direction (which is considered as the *task space*), plus a rotation of the arm about the same axis (the *redundant space*, denoted by angle ϕ). These two DoFs are shown in Figure 3.13.

Surface electromyogram (EMG) data from eight muscles (Table 3.1) was recorded at 1926 Hz (Trigno Wireless EMG, Delsys Inc.). The arm motion was registered at 150 Hz (Optotrak Certus, Northern Digital Inc.), with optical markers placed on the shoulder

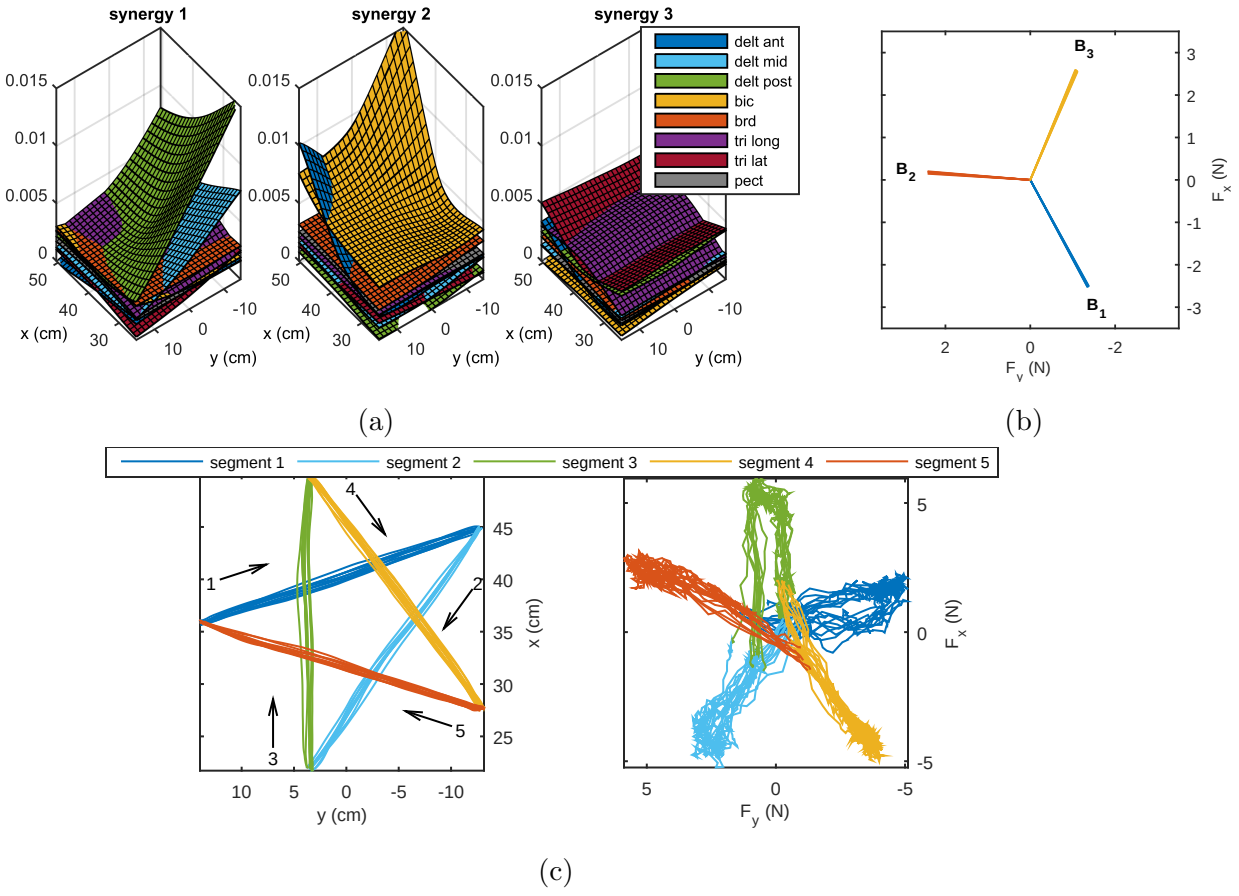

Figure 3.10: The experiment #1 results, belonging to subject #1. (a) The synergies obtained by applying CNNMF to the experimentally measured EMG data. (b) The basis vectors associated with the synergies. (c) The motion (on the left) and force (on the right) in the task space during the motion trials. The motion is divided into 5 segments (color coded).

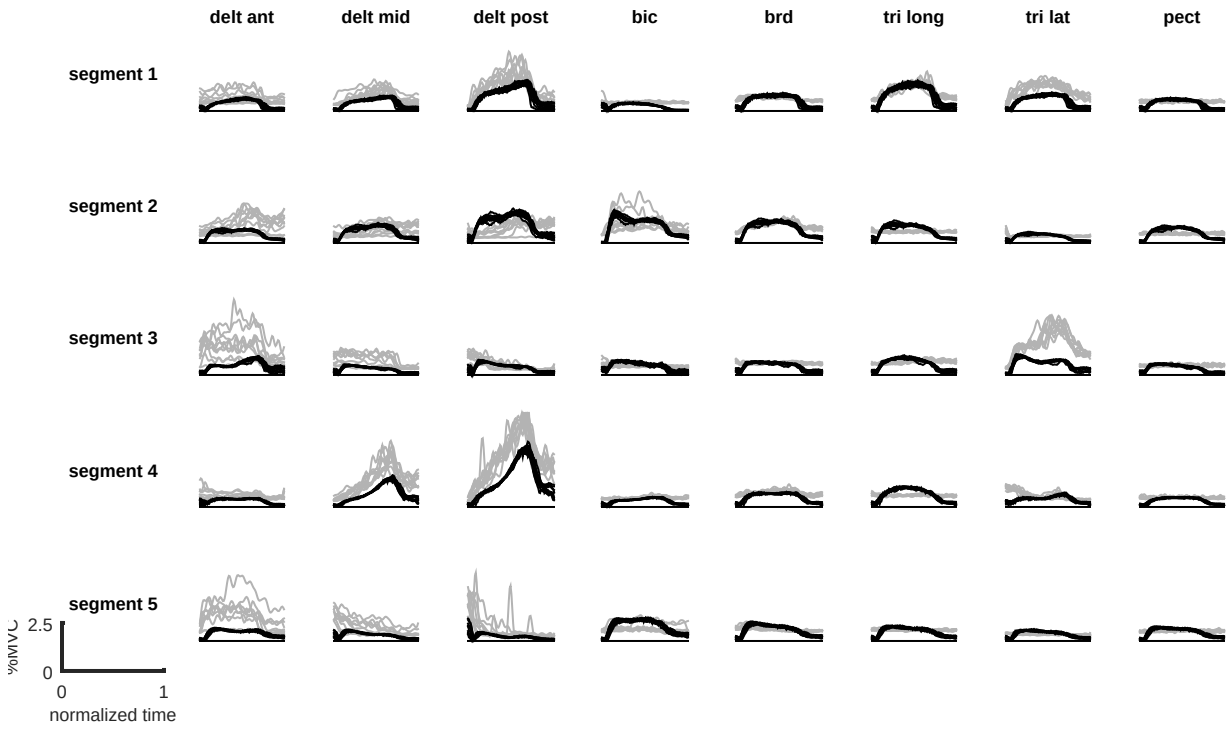

Figure 3.11: The measured EMG and the reconstructed activities for the eight muscles and for each motion segment in experiment #1. The grey and black lines, respectively, show the measured EMG data, and the reconstructed muscle activations. Each line represents a single trial.

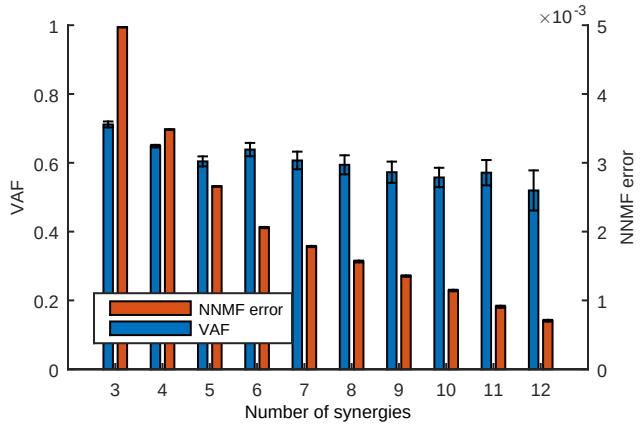

Figure 3.12: The effect of the number of synergies on the performance of the motor control framework. Because CNNMF is sensitive to the initial guesses, multiple runs of CNNMF are performed. The plots show the mean and standard deviation of the results. When a small number of synergies are used, the standard deviation is small.

(acromion process), elbow (lateral epicondyle), wrist (ulnar styloid process) and hand (distal end of the third metacarpal bone). Force plate data was also recorded at 100 Hz (AccuGait, Advanced Mechanical Technology, Inc.). By assuming negligible body motion, the same forces at the hand can be sensed by the force plate beneath the stool.

The EMG data was processed with the common procedure (raw EMG $\rightarrow$ zero-mean $\rightarrow$ band-pass filter with 5-800 Hz cut-off frequency $\rightarrow$ full-wave rectify $\rightarrow$ low-pass filter with 2 Hz cut-off frequency). The EMGs for each muscle were normalized with respect to the maximum voluntary contraction (see Appendix C).

Similar to experiment #1, this experiment is also conducted in multiple phases.

Phase one: obtaining the synergies

The subject was asked to exert isometric positive (push) and negative (pull) forces along the task space, as well as positive (rotate upwards) and negative (rotate downward) torques in the redundant space. The set-up was locked at nine different positions (three positions

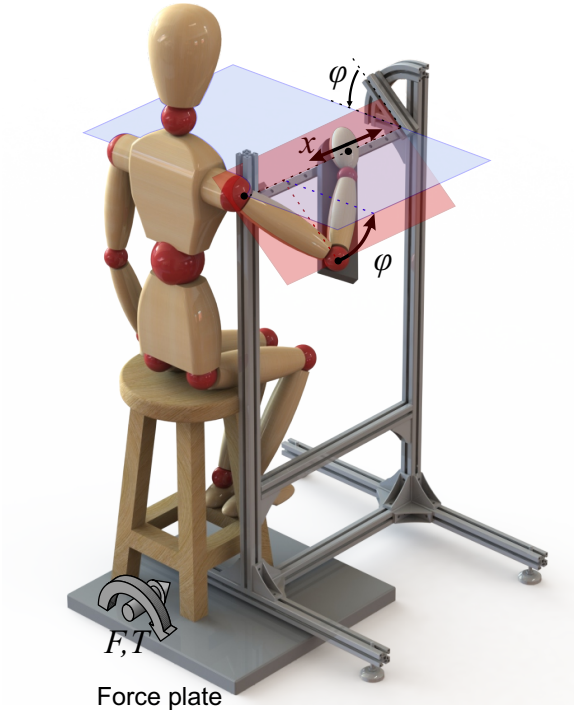

Figure 3.13: The experiment #2 set-up to study the orthogonality of the synergies in task and redundant spaces. The apparatus allows a 1D motion along the slider (the task space, x), and a rotation about the slider's axis (the redundant space, ϕ). Therefore, the entire systems has 2 degrees of freedom.

in the task space {close, middle, far}, each at three angles in the redundant space {0°, −45°, −90°}). Therefore, a total of 36 sessions were recorded.

The processed EMG from each of the eight muscles was averaged for the last 2 s of the isometric force/torque production episodes. These averaged EMG data were then normalized by the corresponding measured force (F in the task space) or torque (T in the redundant space) to obtain the "synergies" (S) that produce unit force/torque in the task/redundant spaces; i.e.:

$$S_{task} = \frac{1}{F} \begin{bmatrix} \overline{EMG}_1 \\ \overline{EMG}_2 \\ \vdots \\ \overline{EMG}_8 \end{bmatrix} \qquad \text{(when pulling/pushing in the task space)} \tag{3.52}$$

$$S_{red} = \frac{1}{T} \begin{bmatrix} \overline{EMG}_1 \\ \overline{EMG}_2 \\ \vdots \\ \overline{EMG}_8 \end{bmatrix} \qquad \text{(when rotating up/down in the redundant space)} \tag{3.53}$$

$$\tag{3.54}$$

These *posture-dependent* synergies and the corresponding basis set can be represented as:

$$\hat{\mathbf{S}}_{8\times4}(x,\phi) = [S^{+}_{task}\ S^{-}_{task}\ S^{+}_{red}\ S^{-}_{red}] \tag{3.55}$$

$$\hat{\mathbf{B}}_{2\times4} = \begin{bmatrix} +1 & -1 & 0 & 0 \\ 0 & 0 & +1 & -1 \end{bmatrix} \tag{3.56}$$

where S_{task} and S_{red} are the task and redundant space synergies, respectively, and the superscripts $^{+}$ and $^{-}$ denote the positive and negative directions in the two spaces. The basis vectors are the unit force/torque in the 2D space.

Phase two: motion trials

Next, the subject was instructed to reach forward and backward along the slider with a self-selected speed (the *task* is a point-to-point reach), while a small resistance was imposed on the slider to increase the muscular activity. The redundant DoF was once fixed (locked

Table 3.2: The motion trials in the experiments

Trial name	Redundant DoF	Trial name	Redundant DoF
Fixed-0	Fixed at 0°	Controlled-0	Free, held at 0°
Fixed-45	Fixed at -45°	Controlled-45	Free, held at -45°
Fixed-90	Fixed at -90°	Controlled-90	Free, held at -90°
		Uncontrolled	Free, unattended

at three different angles $\{0°, -45°, -90°\}$), and once left free to rotate. In the free motion trials, the subject was asked to actively hold the arm at specific angles $\{0°, -45°, -90°\}$ while reaching forward and back. Lastly, the subject was asked to disregard the redundant angle, and *naturally* move back and forth in the task space. The three sets of trials are designated by *fixed*, *controlled*, and *uncontrolled* trials, respectively, and are summarized in Table 3.2.

Phase three: EMG reconstruction

In this part, it was assumed that a task space controller (unknown nature at this moment) had decided on the movement trajectories that satisfied the tasks mentioned above. The task/redundant space forces are assumed to be the outputs of this high-level controller. The goal has been to use these observed task/redundant space forces to estimate the muscle activations. Therefore, the same procedure introduced previously in section 3.2.2 has been used to reconstruct the muscle activities. However, instead of the acceleration vectors, the measured force/torque vectors were used.

Mathematically, at a given sample time during the motion, the coefficients $\hat{\mathbf{C}}_{4\times1} = [c^+_{task}, c^-_{task}, c^+_{red}, c^-_{red}]^T$ were found such that:

$$\begin{bmatrix} F(t) \\ T(t) \end{bmatrix}_{measured} = \hat{\mathbf{B}}_{2\times4}\hat{\mathbf{C}}_{4\times1} \tag{3.57}$$

and then multiplied by the synergy matrix:

$$\hat{\mathbf{u}}(t) = \hat{\mathbf{S}}\left(x(t), \phi(t)\right)_{8\times 4}\, \hat{\mathbf{C}}_{4\times 1} \tag{3.58}$$

to estimate the muscle activations.

Note 1 Since the basis vectors in (3.56) are orthonormal (they are unit vectors orthogonal to each other), the decomposition in (3.57) is essentially a separation of positive and negative portions of the measured force/torque.

Note 2 The synergy matrix $\hat{\mathbf{S}}\left(x(t), \phi(t)\right)$ in (3.58), is the posture-specific synergy matrix, which is calculated by interpolating the previously obtained synergy matrices $\hat{\mathbf{S}}(x, \phi)$ in part one, at the measured posture $(x(t), \phi(t))$.

Note 3 It was assumed that the redundant DoF was not controlled in the *fixed* and *uncontrolled* trials. Therefore, zero redundant space torque ($T = 0$) was used in (3.57) to reconstruct the muscle activations. In the *controlled* trials, the redundant space torque could not be measured; thus it was estimated as:

$$T = T_{max} \cos(\phi) \frac{d}{d_{max}} \tag{3.59}$$

In this relation, T_{max} is the torque measured when the arm is resting on the fixed arm rest at $\phi = 0^\circ$ and the elbow is fully flexed. In this posture, the distance of the elbow from the axis of rotation is d_{max}, which is used to scale the measured distance d during the movements.

Results

Two subjects participated in the second experimental trials. In the following, the results belonging to subject #1 is shown (Complete results are shown in the Appendix B).

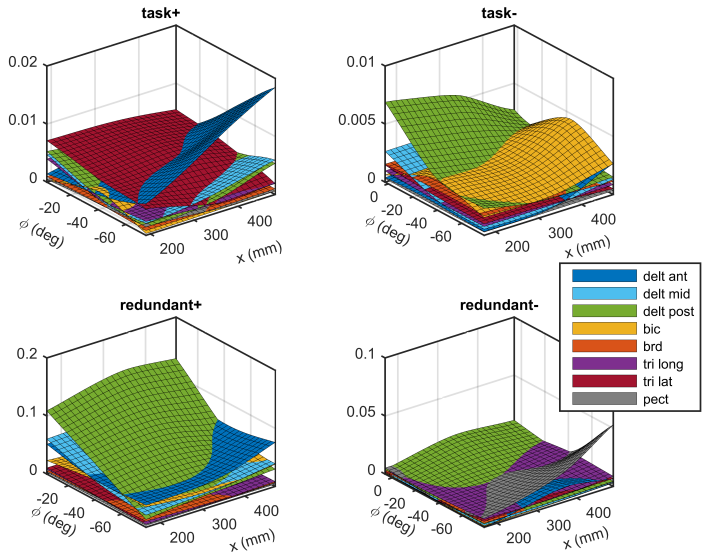

Figure 3.14: The synergies in experiment #2; the synergies that correspond to the task space are shown in the top row, and the redundant space ones in the bottom row. The plots show fitted spline functions to the measured data.

The experimentally obtained synergies are shown in Figure 3.14. These plots show how the share of the muscles in the synergies changes across various postures. At a given posture, (x, ϕ), the value of each surface corresponds to the elements of the synergy matrix S. The plots "task+" and "task−" show the task space synergies (pushing and pulling along the linear guide respectively), while the "redundant+" and "redundant−" plots show the redundant space synergies (roughly translate into elevating the arm and lowering it, respectively).

The recorded motion in the task and redundant spaces are shown in the top two rows of Figure 3.15. The plots show the average and standard deviation of the variables in five repetitions of the motion (reach out, rest, and return). The third row shows the measured task space force, as well as the estimated redundant space torque. Finally, the comparison of the measured and estimated muscle activities during movements are shown

in the subsequent rows of Figure 3.15. To obtain these results, the measured x and ϕ values at a given time are used to interpolate the synergies shown in Figure 3.14. Next, the obtained synergy matrix, along with the measured force at this sample time are used in (3.57) and (3.58). This process is done for the entire duration of the movement.

The presented results in Figure 3.15 are essentially subject-specific, and inter-subject comparison is not possible. To quantify the estimation performance and compare the subjects, the same VAF measure (3.26) is used. The calculated VAF for subjects #1 and #2 are 0.619 and 0.587, respectively.

3.4.3 Discussion

The experimental trials presented in this section meant to evaluate the performance of the F2A (equivalently A2A) methodology only. Therefore, not much attention was given to how the motions are generated. Instead, the goal was to test whether the muscle activations could be estimated using only the high-level controller's output, which was assumed to be the task space forces (and redundant space torque). Therefore, only the measured task space forces and posture information were used to reconstruct the muscle activations.

The calculated VAF values (about 60%) were lower than the reported values in the muscle synergy literature (above 90%, e.g. in Moghadam et al., 2013). There are many reasons for this difference. The most important one is due to the approach taken. In most of the muscle synergy studies, the VAF is calculated for how well the extracted muscle synergies (e.g. using NNMF) can explain the same set of experimental data. In the presented method, however, a *predictive* approach is taken: the muscle activations were predicted using a different set of measurements (i.e. the task space forces/positions). Because of the different approaches, comparing the calculated VAF with the values reported in the literature bears little significance. The only comparable work in the literature is (Lockhart and Ting, 2007), in which muscle activities are estimated using a feedback balance controller. Lockhart and Ting have reported VAF>80% in various conditions;

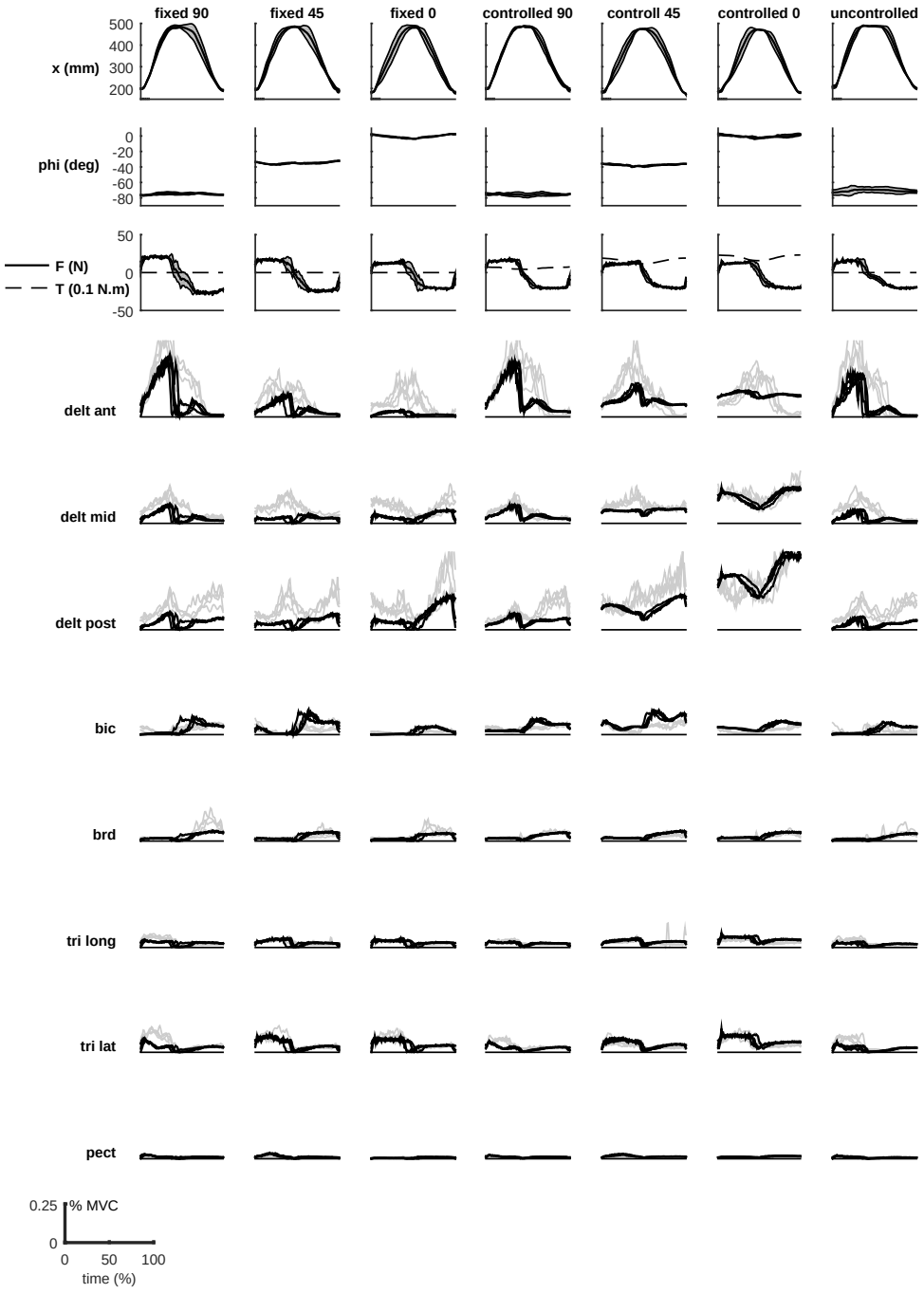

Figure 3.15: experimental results during the motion trials in experiment #2. The measured motion in the task space and redundant space, measured forces, and the recorded EMGs are shown. The EMGs (grey lines) are overlaid with the estimated activities (black) during the multiple motion trials

however, to obtain these results, the same set of data that was used to train the model was used for comparison, which potentially results in higher VAF.

The properties of the measured EMG signals are also worth discussing. The measured surface EMG signals are less reliable at low activation levels (mostly because of the high noise-to-signal ratio), which may be a potential source of discrepancy observed in the results. Furthermore, the filtering of the EMG signals introduces non-linearities to the system, which conflicts with the linearity requirement of the presented framework.

Another potential source of inaccuracy, as mentioned earlier, is the use of forces instead of accelerations in muscle activation estimation (i.e. F2A instead of A2A). Although motions were slow and robot resistance was high, the arm and robot inertia still affected the measurements and introduced error.

Lastly, the amplitudes of muscle activations were usually under-estimated by the method, which is speculated to be mostly due to agonist/antagonist co-contractions and other compensatory movements. Informal observations during the experiments revealed that the estimation error decreased if the subjects were asked to relax (to eliminate co-contraction) and fully rest their arm on the arm rest (to remove the extra muscle activities that were required to hold the arm against gravity).

Despite all these factors, it was shown that the proposed method could (qualitatively) capture the pattern and relative activation of the muscle activations.

It was mentioned before that the F2A methodology relies on superposition. Although the linearity assumption was not rigorously tested in these experiments, the results suggest that the linear scaling of the task space forces with the amplitude of the synergies is feasible.

Although the experimental results showed that the A2A method could be used to estimate the muscle activities from the task space measurements, it is not conclusive whether the presented motor control model is, in fact, the process happening in the nervous system to control the movement. For more rigorous testing of the entire motor control model, one should devise an experiment to isolate high-level controller from the rest of the control loop, to verify its behaviour.

3.5 Chapter conclusions

This chapter presented the basics of the proposed motor control framework. This framework is based on a hierarchical structure. There is a high-level (task space) controller which handles the path planning and error compensation. The output of this controller is a command in the task space (an acceleration vector) which needs to be translated to muscle activations. The presented acceleration-to-activation (A2A) mapping in the lower-level of the control hierarchy performs this translation. The A2A mapping decomposes the reference acceleration vector onto a basis set, which is produced by a number of muscle synergies. The decomposition coefficients are then used to combine the muscle synergies to calculate the required muscle activations.

The experimental data to evaluate the performance of the A2A mapping was also presented. The results showed that the synergy-based approach could capture approximately 60% of muscle activations variability, both in fully-determined and redundant kinematic conditions.

In the next chapters, the application of the motor control framework to musculoskeletal simulations as well as feedback control of functional electrical stimulation systems will be presented.

Chapter 4

The Motor Control Framework for Musculoskeletal Simulations

The previous chapter presented the basics of the proposed motor control framework. This chapter gives examples where this motor control model is used to control the motion of musculoskeletal systems of various complexities. The examples include simulation results of musculoskeletal systems ranging from a simple 1-DoF to a redundant 4-DoF system, each of which emphasizes a different aspect of the motor control framework.

In the following sections, first the details of the musculoskeletal systems, the motor control models, and the simulation results are presented. A thorough discussion about the framework, the results and their implications is presented at the end of the chapter.

4.1 Example 1: one degree of freedom systems

4.1.1 The musculoskeletal systems

The first examples to showcase the presented motor control framework are a 2D/1-DoF musculoskeletal forearm model (taken from Sharif Razavian et al., 2015; Sharif Shourijeh

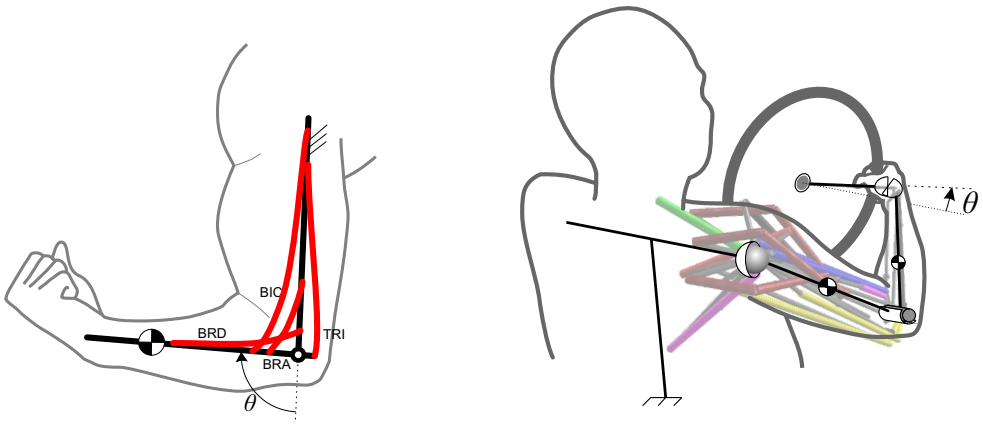

(a) (b)

Figure 4.1: The 1-DoF musculoskeletal models. (a) The 2D forearm model. (b) The 3D driver model. Although, both models are 1-DoF, the task spaces are different.

and McPhee, 2013, see Figure 4.1a) and a 3D/1-DoF human driver model (taken from Mehrabi et al., 2015a,b, see Figure 4.1b).

The 2D forearm model consists of a single-DoF revolute joint, which allows for forearm flexion/extension motion. Seven muscles actuate this model: brachioradialis, brachialis, biceps brachii (long and short heads) and triceps brachii (long, lateral, and medial heads). The physical parameters for these muscles are taken from (Sharif Shourijeh and McPhee, 2013; Garner and Pandy, 2001) and are given in Appendix E.

The 3D driver model consists of four body segments: trunk, upper arm, forearm, and hand. The trunk is assumed to be fixed, and the upper arm is attached to the trunk using a spherical joint. The elbow is modelled as a revolute joint, and the hand is connected to the forearm via a universal joint. Since the hand is assumed to grip the steering wheel firmly, the whole system has only one DoF. Therefore, knowing the steering wheel angle is sufficient to find the arm joint angles. This argument is not valid in general, as there is one extra DoF (forearm supination/pronation) that is neglected here for the sake of simplicity. This model is actuated by 15 muscles listed in Mehrabi et al. (2015b).

The muscles in both examples are modelled using the Hill-type formulation (Thelen, 2003). For simplicity (in these models as well as in the models in the next sections), only the contractile element of the muscle model is implemented, and no explicit joint stiffness is considered. The input to the models is the set of muscle activations, u, which result in muscle forces that generate motion. Forward dynamics is the predictive simulation method used in these examples.

4.1.2 The motor control model

The task space (the variable that is actively controlled in the motor control model) in the forearm model is a 1D space containing the elbow angle ($\mathcal{T}_1 = \{\theta_{elbow}\}$), while the task space in the driver model is a 1D space containing the steering wheel angle ($\mathcal{T}_1 = \{\theta_{steering}\}$). For simplicity, the subscripts are dropped and both angles are denoted by θ in Figure 4.1. Although substantial differences exist in the aforementioned tasks and recruited muscles, since the task spaces in both systems are one-dimensional, the same motor control structure can be used to control their movements.

Since the task spaces are one-dimensional, two basis vectors are required to *positively decompose* the needed reference command (one basis vector to handle positive commands, and one for negative ones). Therefore, the task space vector decomposition in these examples is simply a separation of positive and negative portions of the high-level controller's command. As a result, the definition of posture-dependent muscle synergies yields a unique solution for the force-sharing problem, thereby eliminating the need for any on-line optimization, resulting in a significantly faster feedback control scheme.

The schematic of the motor control model for the 1-DoF examples is presented in Figure 4.2. Because of the simpler structure of the task space in these cases, a simplified version of the motor control framework is used. The output of the high-level controller, instead of being an acceleration command, is a signed activation (a scalar value) that is separated into two representative muscle activation signals.

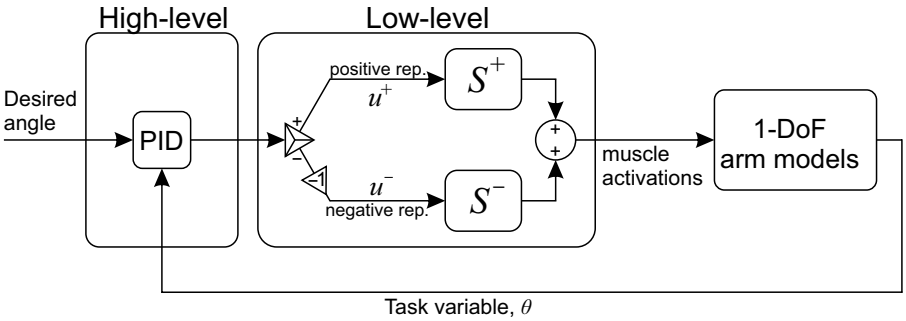

Figure 4.2: The schematic of the motor control model for the control of 1-DoF systems. The output of the high-level controller is a signed activation. The positive and negative portions of the signal are used to create muscle activations from the two synergy ratios.

The representative muscle activations can be found using various control methods such as optimal control (e.g. model predictive controller, MPC, or linear quadratic regulator, LQR) or error driven (e.g. proportional-integral-derivative, PID) controller.

To show the effectiveness of the synergies for real-time control, a simple PID controller is used as the high-level controller as shown in Figure 4.2. The positive and negative portions of the activation command are separated. The positive values are interpreted as the representative muscle activation for the positive direction in the task space. Similarly, the negative portion is interpreted as the representative activation in the negative direction. The representative activations can subsequently be multiplied by the corresponding synergy ratios (4.4) to calculate all muscle activations.

In these examples, the synergy ratios calculated from the optimal control method (section 3.3.2) are employed. Applying the optimal control method to the 2D forearm model is straightforward and is the same as the method described in section 3.3.2. The resulting synergy ratios are shown in Figure 4.3.

For the more complex 3D driver model, however, the mathematical arguments similar to (3.27)-(3.45) are harder to make (because of the larger number of joints, and the existence of bi-articular muscles). However, since the model has only one DoF, it is possible to

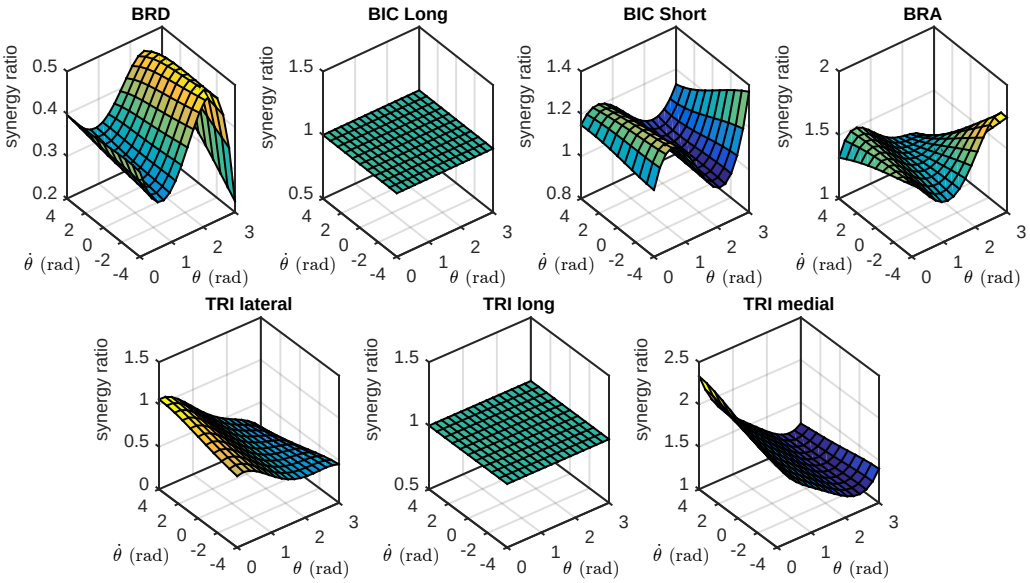

Figure 4.3: The synergy ratios in the 2D forearm model. Top row: the flexor synergy ratios (representative muscle is the long head of biceps). Bottom row: the extensor synergy ratios (representative muscle is the long head of triceps).

modify the arguments to accommodate this 3D arm as well.

Given the complex kinematics in this model, a direct solution for h (as used in (3.31)) is challenging. An efficient method is to calculate it from the response of the musculoskeletal system similar to the experimental procedure in Berger and D'Avella (2014). In a certain posture, activation of each muscle will produce a torque in the task space (steering wheel rotation). Therefore, one can define the non-linear transformation $h(\theta)$ as:

$$h_i(\theta) \triangleq \frac{T_i}{u_i} \tag{4.1}$$

where u_i is the activation of muscle i and T_i is the resulting torque in the task space. Having h calculated from (4.1), it is now possible to use the constraint of (3.31), thereby making similar arguments to calculate the optimal activations and the synergy ratios:

$$S_i^{cw} = \begin{cases} \dfrac{u_i^*}{u_{cw}^*} = \dfrac{h_i}{h_{cw}} & S_i^{cw} > 0 \\ 0 & S_i^{cw} < 0 \end{cases} \tag{4.2}$$

$$S_i^{ccw} = \begin{cases} \dfrac{u_i^*}{u_{ccw}^*} = \dfrac{h_i}{h_{ccw}} & S_i^{ccw} > 0 \\ 0 & S_i^{ccw} < 0 \end{cases} \tag{4.3}$$

These synergy ratios are calculated based on two representative muscle activations: a counter-clockwise rotator and a clockwise rotator, which are denoted by the subscripts *cw* and *ccw*, respectively.

In general, h is a function of both the steering angle and angular velocity. However, as previously shown in the 2D forearm results (Figure 4.3), h and synergy ratios, s, are not significantly affected by $\dot{\theta}$. Therefore, it is assumed that h is only a function of θ; i.e. $h = h(\theta)$. This assumption significantly reduces the complexity of the synergies and the memory required to store them. However, it comes at the expense of sub-optimality if the synergy ratios of (4.2) and (4.3) are used (it will be shown later that they are close to optimal). Furthermore, such an assumption aligns well with the concept of posture-dependent synergies, whereas, velocity-dependency has not been reported before. The synergy ratios for the 3D driver model are shown in Figure 4.4, where the *cw* and *ccw* representatives are chosen to be anterior deltoid and long head of triceps, respectively.

With the synergy ratios calculated a priori, it is possible to control the musculoskeletal system in an optimal manner by calculating only the representative muscle activations. All other muscle activations can optimally be constructed using the synergy ratios:

$$\mathbf{u} = [S^+, S^-] \begin{bmatrix} u^+ \\ u^- \end{bmatrix} \tag{4.4}$$

where S^+ and S^- are synergy vectors with the bases in positive and negative directions in the task space, respectively. $[u^+ u^-]^T$ is the vector of the two representative muscle activations.

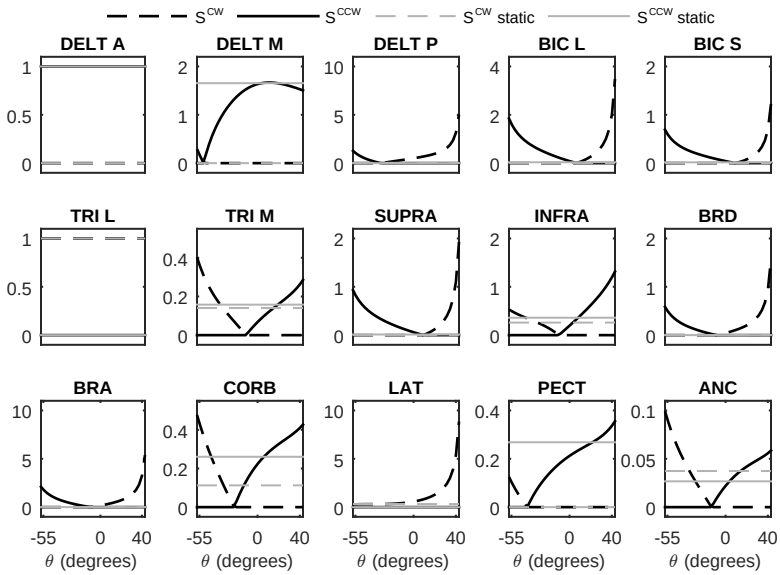

Figure 4.4: The synergy ratios for the 3D driver model. The representative *cw* and *ccw* muscles are anterior deltoid and long head of triceps, respectively. The *static* synergies are also shown in the plots with gray lines.

In the forearm model, the task space is the elbow flexion angle, with the positive direction being flexion and negative being extension. The representative muscles for the two directions are long heads of biceps and triceps brachii, respectively.

In the driver model, the task space is the steering wheel angle. The positive direction is arbitrarily chosen to be the clockwise rotation of the steering wheel, and the negative direction is the counter-clockwise rotation. The interesting point in this model is that only anterior deltoid remains a counter-clockwise rotator in the entire simulated range of motion of the steering wheel. Likewise, only triceps (long head) and latissimus dorsi remain clockwise rotators. This observation emphasizes the importance of defining posture-dependent synergies (for an individual), as the muscle may change function as the posture changes.

4.1.3 Simulation results

The simulation results for both 1-DoF models are presented here. In these simulations, the objective was to efficiently follow a desired trajectory in their task spaces.

Two feedback control methods were used: an optimal controller (forward static optimization, FSO, Sharif Shourijeh et al., 2015, 2017), and the proposed motor control models. FSO was selected as the optimal controller because of its forward dynamics properties and optimal behaviour Anderson2001a. It must be noted that FSO is not an *optimal controller*, as the state trajectories should be specified (FSO is optimal only for the given path). For the FSO controller, a weighted sum of the muscular effort and tracking error is considered as the objective function:

$$J = w_1 \sum_{i=1}^{m} u_i^2 + w_2(\theta - \theta_{des})^2 + w_3(\dot{\theta} - \dot{\theta}_{des})^2 \tag{4.5}$$

Two sets of simulations were run. First, the musculoskeletal systems were driven by the optimal controller, resulting in our *gold standard* muscle activation patterns. In these simulations, the activation levels of all the muscles were individually modulated by the FSO controller for each time step. In the second set of simulations, the proposed motor control model calculated the muscle activity levels using muscle synergies (4.4). These muscle activities were used to drive the musculoskeletal systems.

Figure 4.5 shows the performance of the two controller methods for the forearm model. In this figure, the FSO and the synergy-based controllers are denoted by "optimal" and "synergy+PID", respectively. As can be seen in this figure, the performance of the two controllers is very close. The tracking error is comparable using the two controllers, and the muscle activation patterns are also very similar.

The similarity of the activations resulting from the synergistic controller and the optimal controller suggests that the synergies defined in the previous sections result in near-optimal behaviour. The numerical values of the physiological cost ($\sum_i \int_0^{T_f} u_i^2 dt$) in Table 4.1 further

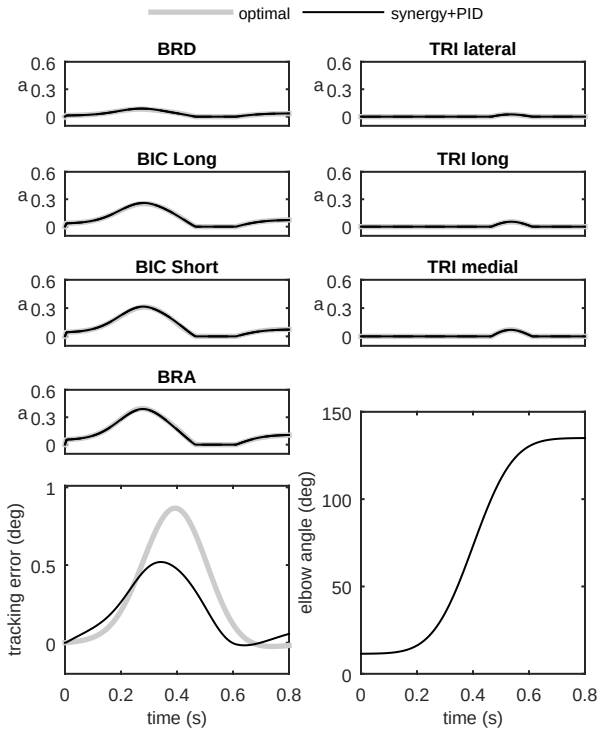

Figure 4.5: Comparison of the two control methods in the control of the 2D forearm model

show the closeness of the two methods. Previous reports (Erdemir et al., 2007) have shown that the optimal muscle activities (calculated by the FSO controller) estimate realistic muscle activities, which implies that the synergistic controller results in realistic activity patterns.

Figure 4.6 presents the 3D driver model simulation results, which contains an extra set of simulations to compare the static synergies with the posture-dependent synergies.

To obtain the static synergies, the optimal muscle activities were found such that the musculoskeletal system followed a random motion in the task space. These time-varying optimal muscle activities were then be gathered in the matrix $\mathbf{A}$ (the samples are muscle activities in different time steps), and fed to the NNMF algorithm to find the static synergies and time-dependent coefficients.

Table 4.1: Comparison of the control methods in the simulation of one-DoF systems

	Physiological effort[†]		Computation time (s)[§]	
Method	forearm model	driver model	forearm model	driver model[‡]
Optimal (baseline)	1	1	26.51	135.99
Synergy+PID	1.0082	1.0179	2.04×10^{-2}	2.25
Static synergy+PID	—	1.125	—	2.25

[†] The reported values are normalized with respect to the baseline

[§] CPU: Core i7 4790, RAM: 16Gb, running Matlab/Simulink 64 bit

[‡] Total simulation time, which includes the time required for controller calculations, plus the integration time of the musculoskeletal model

Similar to the forearm model results, the optimal muscle activities are well-matched by the optimally obtained synergies. However, the static synergies could not accurately recreate the optimal muscle activities. This happens because the NNMF algorithm was applied to the data matrix containing muscle activations in the entire range of steering wheel angles. Thus, the NNMF essentially averages the relative muscle activities for the entire range, neglecting the changing importance and function of the muscles. As a result, some muscles are over-activated (e.g. medial head of triceps), incorrectly activated (e.g. posterior deltoid) or even completely neglected (e.g. brachioradialis and brachialis). The posture-dependent definition of synergies allows for high reconstruction accuracy with the minimum number of synergies (in these cases only two synergies). The comparison of the numerical values of the physiological cost (Table 4.1) further shows that the two static synergies cannot reconstruct the optimal muscle activities as well as the posture-dependent ones (the physiological cost increases by 12% using static synergies).

The synergistic motor control model performed similar to the optimal controller, but was 2-3 orders of magnitude faster (Table 4.1). These results show that the synergistic controller can run very fast, which is an essential requirement in many applications including real-time control of functional electrical stimulation and rehabilitation devices (see

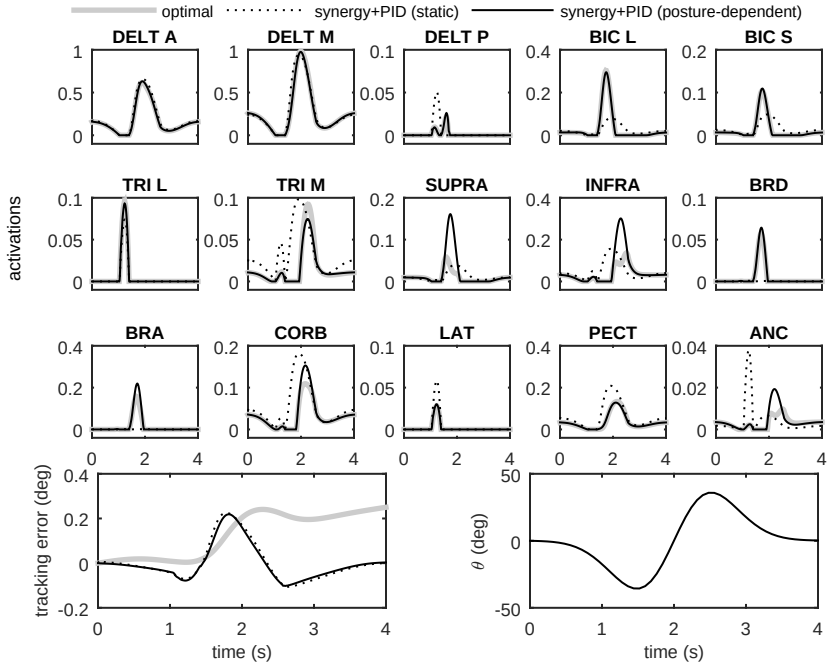

Figure 4.6: Comparison of the three control methods in the control of the 3D driver model

chapter 5).

4.2 Example 2: a two degree of freedom system

4.2.1 The musculoskeletal system

In the second example, the motor control framework is used to control the motion of a 2D and 2-DoF arm model (shown in Figure 4.7). This arm model is obtained by mapping a high-fidelity 3D arm model into a 2D space (Ghannadi et al., 2015); it consists of two links, representing the upper arm and forearm/hand, which are connected to each other and to the torso via 1-DoF revolute joints. Therefore, this model has 2 DoFs which allow it to reach to any 2D point in its reachable space.

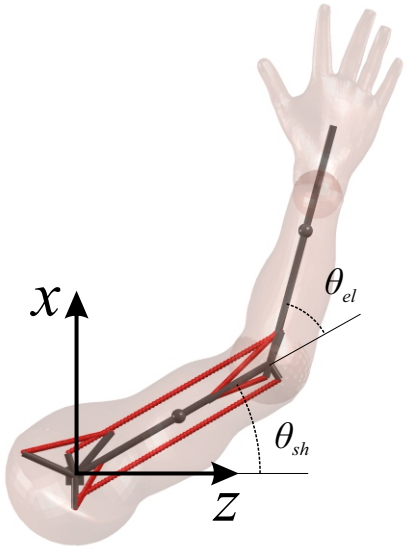

Figure 4.7: The planar 2-DoF arm model. The task space in this model is the 2D position of the hand.

This model is actuated by six muscle groups (shoulder and elbow flexors and extensors, plus a bi-articular flexor and a bi-articular extensor), which are modelled using a Hill-type formulation (Thelen, 2003).

4.2.2 The motor control model

The task in this model is to reach to arbitrary points in the 2D space. Therefore, the task space is the 2D space defined by the (z, x) position of the hand ($\mathcal{T}_2 = \{(z, x)\}$). To implement the motor control framework for this model (schematic shown in Figure 4.8), the synergies that are obtained from the NNMF algorithm (non-concatenated method, as described in section 3.3.1) are used. Figure 4.9a shows how the muscle activations in the synergies change as the hand moves in the 2D task space, and Figure 4.9b shows the basis vectors in the task space.

The A2A mapping calculates the muscle activations from the 2D reference acceleration

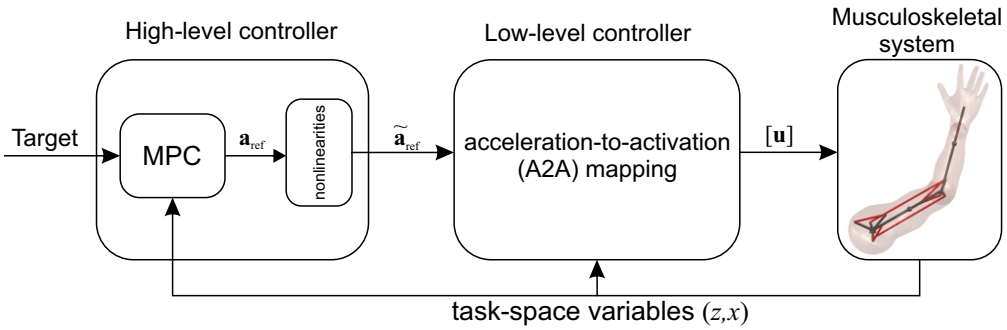

Figure 4.8: The schematic of motor control model for the control of the 2D planar arm model

vector that is defined by the high-level controller. In this example, a Model Predictive Controller (MPC) is chosen as a semi-optimal high-level controller, in order to show the diverse potential of this framework (instead of a non-optimal error-driven PID controller). MPC requires a representation of the system (called the *control-oriented model*) to decide on the optimal control commands. Since the high-level controller only considers the motion in the task space, the control-oriented model of the MPC controller in this framework uses a trivial kinematic model described by the state-space equations:

$$\dot{\mathbf{X}} = \begin{bmatrix} \dot{x} \\ \dot{z} \\ \dot{v}_x \\ \dot{v}_z \end{bmatrix} = \begin{bmatrix} 0 & 0 & 1 & 0 \\ 0 & 0 & 0 & 1 \\ 0 & 0 & 0 & 0 \\ 0 & 0 & 0 & 0 \end{bmatrix} \begin{bmatrix} x \\ z \\ v_x \\ v_z \end{bmatrix} + \begin{bmatrix} 0 & 0 \\ 0 & 0 \\ 1 & 0 \\ 0 & 1 \end{bmatrix} \begin{bmatrix} a_x \\ a_z \end{bmatrix} \tag{4.6}$$

$$\mathbf{Y} = \begin{bmatrix} 1 & 0 & 0 & 0 \\ 0 & 1 & 0 & 0 \end{bmatrix} \begin{bmatrix} x \\ z \\ v_x \\ v_z \end{bmatrix} \tag{4.7}$$

where x and z are the positions, v_x and v_z are the velocities, and a_x and a_z are the controller command (accelerations) in the 2D space. $\mathbf{Y}$ is the vector of system measurements.

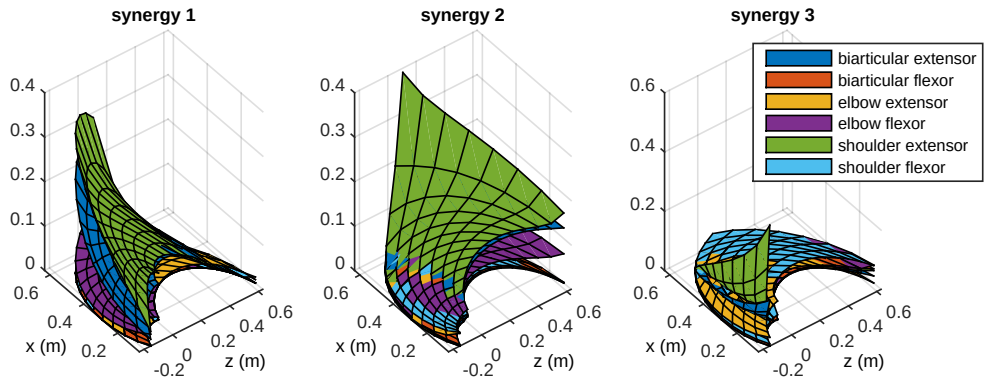

(a)

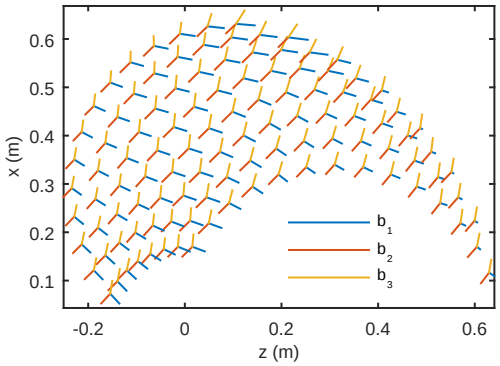

(b)

Figure 4.9: (a) The changing muscle activities in the three synergies as functions of the hand position in the 2D task space. (b) The basis vectors in the 2D task space.

The high-level MPC controller is then designed using this linear model, with a 200-step prediction horizon length, and 20-step control horizon length (controller sampling time is 1 ms).

To further improve the control performance, the output of the high-level controller (the task space acceleration) is adjusted to account for system dynamics according to the method presented in section 3.2.3.

Four control methods are compared here: 1) an optimal controller that controls all mus-

cle activations individually; 2) an optimal controller that adjusts the synergy coefficients instead of individual muscles; 3) the proposed motor control model with an MPC as the high-level controller; and 4) the proposed motor control model with a PID controller as the high-level controller. These four controllers are denoted by *optimal*, *synergy+optimal*. *synergy+MPC*, and *synergy+PID*, respectively. The two optimal controllers are nonlinear model predictive controllers (Mehrabi et al., 2017) with 7-step prediction horizon and the cost function:

$$J = w_1 \sum_{i=1}^{m} \int u_i^2 dt + w_2 \int (e_p)^2 dt + w_3 \int (e_v)^2 dt + w_4 \int (e_a)^2 dt \tag{4.8}$$

where e_p, e_v, and e_a are the position, velocity and acceleration error in the task space, respectively. The weightings w_i are found through trial and error and are given in Appendix E.

4.2.3 Simulation results

The simulation results are shown here. In all simulations, the reference motion has been the same; it is a sinusoidal movement in the z (lateral direction, see Figure 4.10). The muscle activities and the resulting motion from the four controllers are shown in Figure 4.11.

The comparison of the physiological effort between these four controllers is presented in Table 4.2. As it can be observed from this table and Figure 4.11, the motor control framework with MPC and PID are both able to control the motions, however with slightly less tracking accuracy than the two optimization-based methods. By comparing the physiological effort, it is clear that the PID-based controller demands the highest effort. The MPC-based controller uses identical motor control architecture, but is significantly more efficient than the PID controller, and very close to the controller that optimally calculates the synergy coefficients. This example further supports the previous example results that the A2A mapping is capable of providing computationally-efficient control of complex movements.

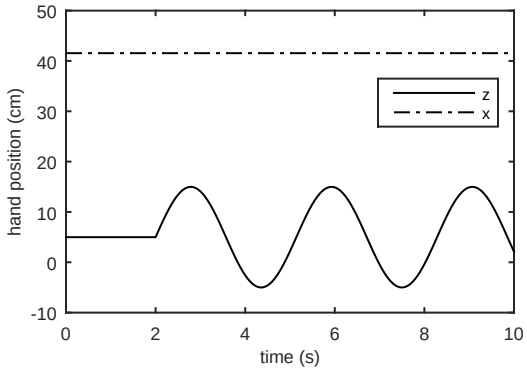

Figure 4.10: The reference motion for the simulation of the 2D planar arm model. The maximum velocity is 20 cm/s.

Table 4.2: The comparison of the four controller performances in the 2D planar simulations.

	Optimal	Synergy+optimal	Synergy+MPC	Synerg+PID
Effort $(\int \mathbf{u}^T\mathbf{u}dt)^\dagger$	1	1.080	1.568	2.528
CPU time (s)$^{\ddagger\ \S}$	93.17	85.11	30.70	12.77

† All the values are normalized with respect to optimal

‡ CPU: Core i7 4790, RAM: 16Gb, running Matlab/Simulink 64 bit

§ Total simulation time, which includes the time required for controller calculations, plus the integration time of the musculoskeletal model

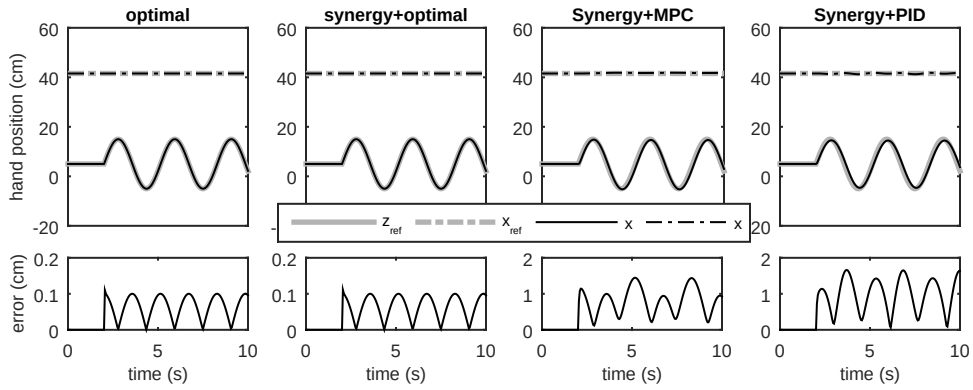

(a)

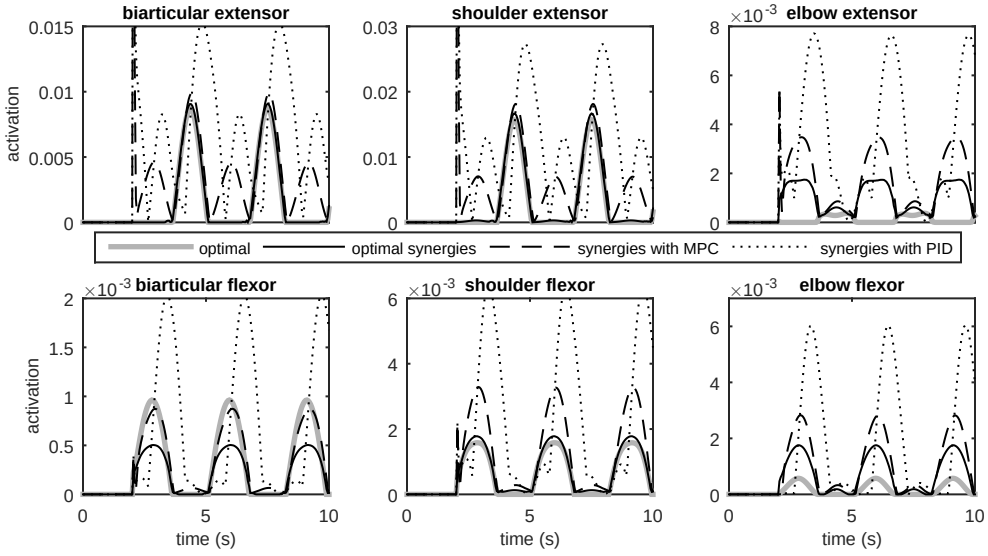

(b)

Figure 4.11: The simulation results of the planar arm model, using the four control methods. (a) The tracking performance. (b) the resulting muscle activations.

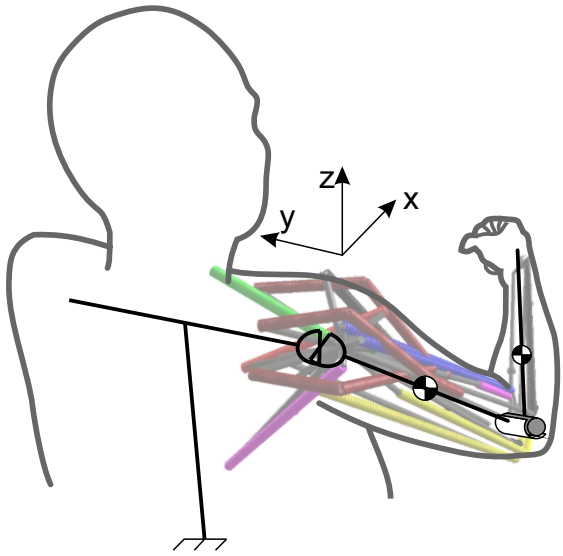

Figure 4.12: The schematic of the 3-DoF arm model

Lastly, the simulation results revealed that the compensatory accelerations calculated from the dynamical equations of motion (section 3.2.3) have small effect on the tracking performance of the motor control models. The maximum amplitude of the compensatory acceleration turned out to be roughly 3.7% of the high-level controller's output. Thus, in the next examples, the system dynamics are neglected in the motor control model.

4.3 Example 3: a three degree of freedom system

4.3.1 The musculoskeletal model

In this example the musculoskeletal model is the same as the driver model described before (Figure 4.12). The differences are: 1) the steering wheel is removed, 2) the shoulder joint is replaced with a 2-DoF universal joint, and 3) the wrist joint is locked. As a result, this 3D arm model has three DoFs, which allows for reaching to any 3D point in the task space.

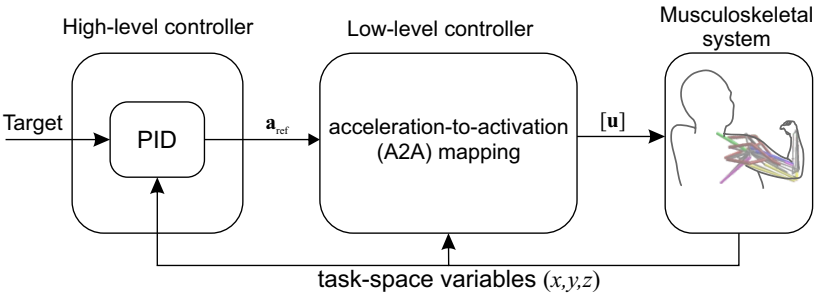

Figure 4.13: The hierarchical structure of the synergy-based motor control framework for the 3D 3-DoF arm model

4.3.2 The motor control model

The goal of the motor control model in this example is to drive the hand to any arbitrary target in the 3D task-space ($\mathcal{T}_3 = \{(x, y, z)\}$). Since this model does not have any redundant degrees of freedom, all of its degrees of freedom are controlled (in other words, the uncontrolled manifold is empty, $\mathcal{R} = \varnothing$).

The schematic of the motor control model for this example is shown in Figure 4.13. Similar to the previous examples, this model has a hierarchical structure. The high-level controller is a PID controller which only deals with the 3D hand position error, and disregards all the complexities of the musculoskeletal system. This controller compares the current location of the hand with the target, and defines the 3D acceleration required to reach to the target.

The A2A mapping receives the reference acceleration, and calculates the required muscle activations using the muscle synergies and the corresponding basis set. To obtain the synergies for this A2A mapping, the NNMF method that results in *posture-dependent* basis vectors (section 3.3.1) is used. This method of extracting the synergies gives higher flexibility to define the synergies, resulting in more efficient control performance. Figure 4.14 illustrates the calculated synergies.

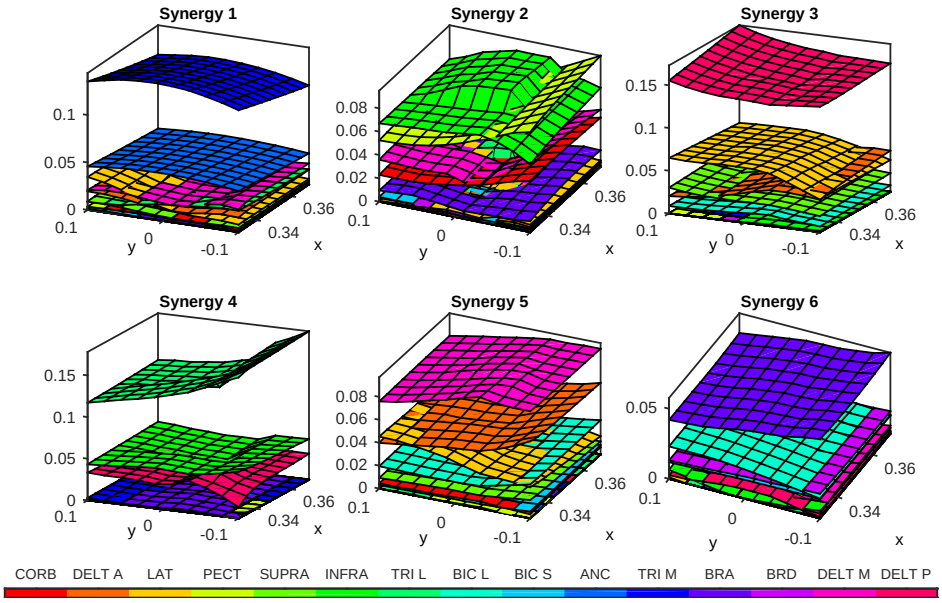

Figure 4.14: The posture-dependent synergies that are used in the control of the 3D 3-DoF model. In this example, six synergies are used. The plots show the variation of the muscles' shares in the synergies as functions of the hand's (x, y) position. In these plots, hand elevation is at shoulder level ($z = 0$).

4.3.3 Simulation results

Number of synergies

The effect of the number of synergies on the VAF and NNMF reconstruction error is shown in Figure 4.15. In the calculation of VAF, the gold standard has been the set of optimal muscle activations that produce various acceleration vectors (they are 15 uniformly-distributed vectors in 3D space). The activations from the A2A mapping for the same acceleration vectors were also calculated to be used in the VAF formula (3.26). Furthermore, the set of optimal activations was fed to NNMF to calculate the reconstruction error, e.

Because the NNMF is sensitive to the initial guess, each run of the NNMF may result in a different synergy matrix, and consequently a different estimation error. Therefore, 20

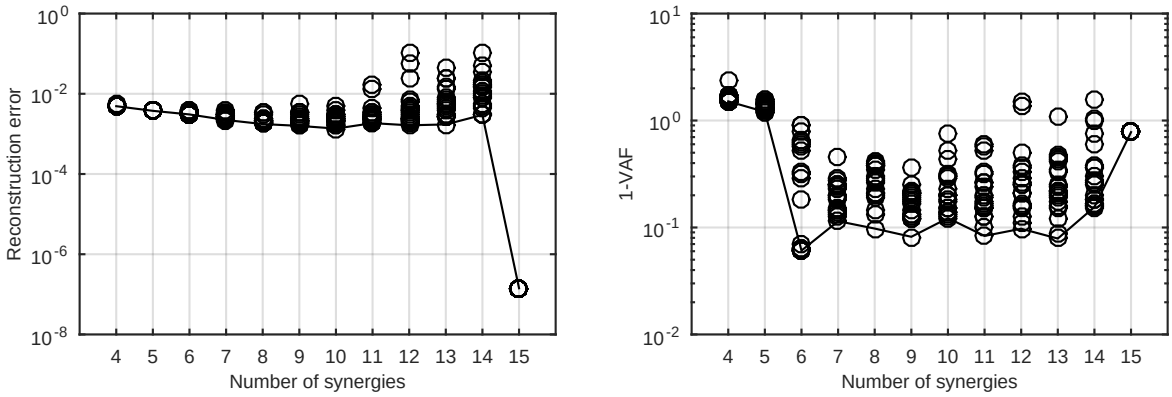

(a) (b)

Figure 4.15: The effect of number of synergies on (a) the NNMF reconstruction error, and (b) the variance accounted for, in the simulation of the 3D 3-DoF arm model. Each circle represents one run of the NNMF algorithm. The solid lines indicate the best results.

runs of NNMF are performed (shown by the circles in Figure 4.15), and the best result was selected (shown by the solid lines). It can be seen in Figure 4.15a that by increasing the number of synergies, the reconstruction error decreases until $k = 10$, after which it starts to increase again. When 15 synergies are used, the reconstruction error is negligible, as each synergy will include only one muscle.

The VAF measure is shown in Figure 4.15b (it should be noted that for better visualization, $1-\text{VAF}$ is shown here). As can be seen, small numbers of synergies (four and five) result in poor performance as expected. Counter-intuitively, we can observe that increasing the number of synergies beyond six does not improve VAF (reasons are discussed in section 4.5). Therefore, for the next set of simulations, six synergies has been used.

Motor control performance

The closed-loop control performance of the proposed motor control framework is shown in Figure 4.16. The desired motion is a 20 cm periodic motion in y (medial-lateral) direction

Table 4.3: The physiological effort and computation time of the two control methods in the simulation of 3D 3-DoF arm model

Control method	Physiological effort[†]	CPU time (s)[‡] [§]
Optimal	1	102.51
Synergy+PID	1.0237	8.21

[†] The values are normalized with respect to optimal

[‡] CPU: Core i7 4790, RAM: 16Gb, running Matlab/Simulink 64 bit

[§] Total simulation time, which includes the time required for controller calculations, plus the integration time of the musculoskeletal model

shown in Figure 4.16a. Two control methods are used to track the motion: the proposed framework, and a nonlinear model predictive controller with 3-step prediction horizon and the objective function in (4.8). In the results shown, these two controllers are denoted by "synergy+PID" and "optimal", respectively. The tracking error obtained from the two controllers are shown in Figure 4.16a, with the muscle activations presented in Figure 4.16b. The performance of the two controllers are similar in tracking error (maximum error 1 mm), and the muscle activations are also similar (VAF = 0.974). The total physiological effort (defined as: $\int_0^{t_f} \mathbf{u}^T\mathbf{u}\ dt$) and the CPU time of the two controllers are given in Table 4.3.

4.4 Example 4: a four degree of freedom system with kinematic redundancy

4.4.1 The musculoskeletal model

The last example in this chapter is the application of the motor control framework to control the motion of a kinematically redundant musculoskeletal system. This example also uses the same 3D arm model as before (Figure 4.17a), but with a spherical joint as

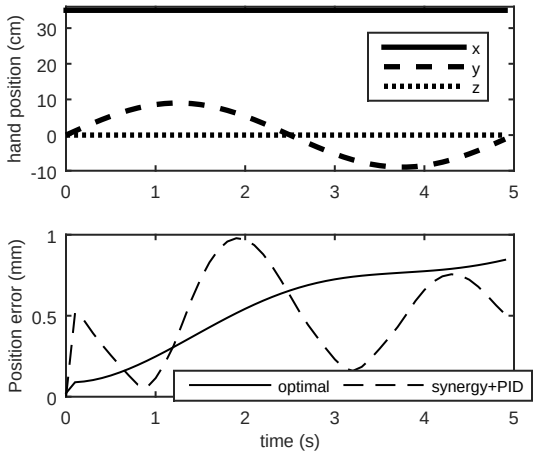

(a)

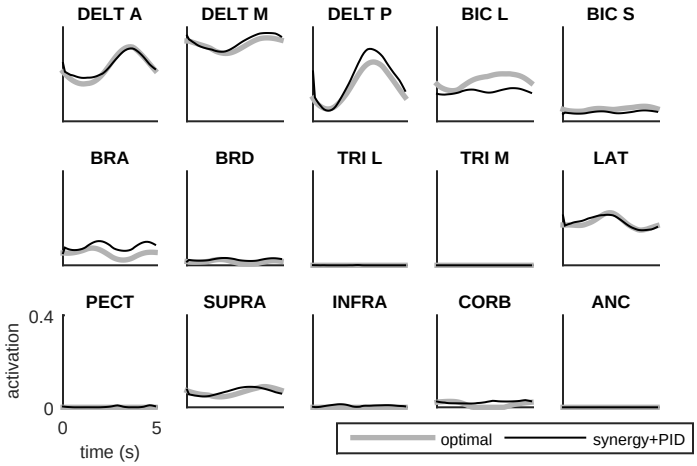

(b)

Figure 4.16: The simulation results for the 3D/3-DoF musculoskeletal system. Two control methods are compared here: and optimal controller, an the proposed motor control model. (a) The reference motion, and the tracking performance of the two controllers. (b) The resulting muscle activations.

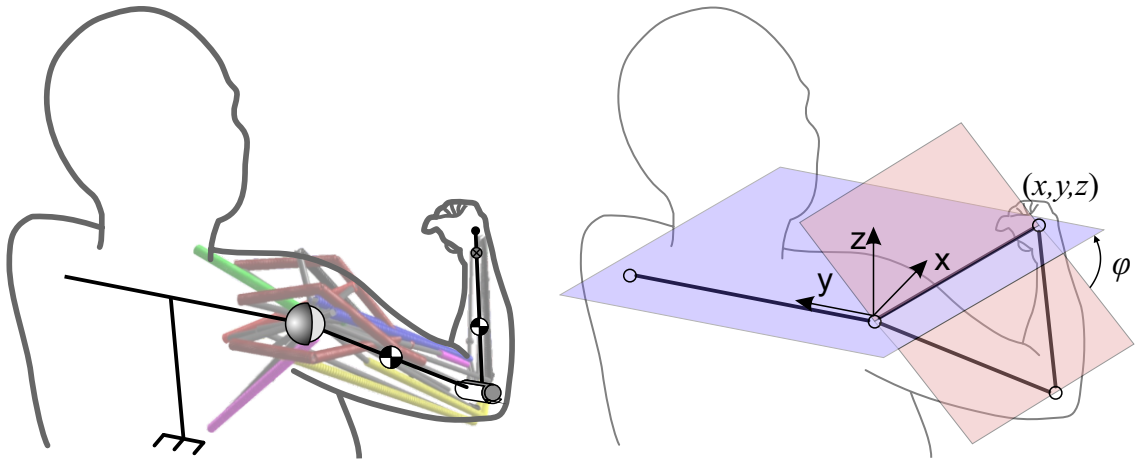

(a) (b)

Figure 4.17: (a) The 4-DoF redundant musculoskeletal system. (b) the task/redundant space representation.

the shoulder (3 DoFs), and a revolute joint as the elbow (1 DoF). As a result, this model has four degrees of freedom.

4.4.2 Motor control model for selective control of redundant degrees of freedom

The controller goal is to reach to 3D points in space with the hand; therefore, the task space is the 3D Cartesian space ($\mathcal{T}_3 = \{(x, y, z)\}$). Since the model has four DoFs, there remains one extra DoF that is irrelevant to the task (ϕ in Figure 4.17b); thus, the *redundant space* is a 1D space containing this extra degree of freedom ($\mathcal{R}_1 = \{\phi\}$).

It should be noted that all the degrees of freedom (x, y, z, ϕ) in this model are functions of the joint angles, and the task and redundant spaces are orthogonal—the task-dependent and redundant kinematic variables are independent of each other.

The proposed synergy-based motor control framework has the advantage of allowing

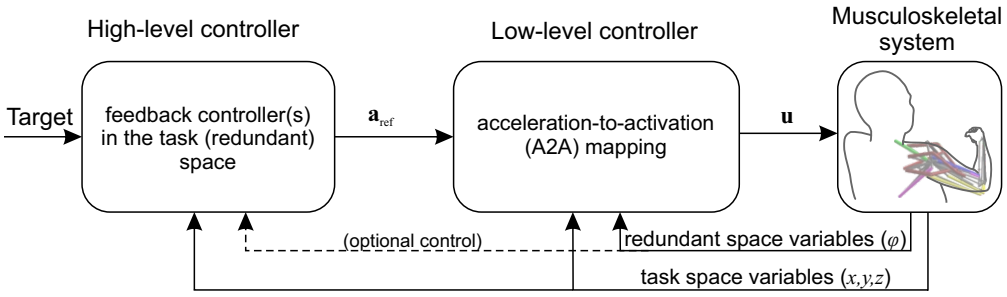

Figure 4.18: The schematic of the motor control framework for the control of the redundant system.

for the selective control of all or some of the degrees of freedom. When the task is to reach to a 3D target, the redundant DoF may be left uncontrolled. For such selective control of the degrees of freedom, the structure of the motor control framework remains the same (Figure 4.18), with slight changes.

As mentioned in section 3.2.2, to control only the task-related variables, the task space basis vectors should be orthogonal to the redundant space. This condition can be achieved by imposing constraints on the synergy identification process. Similar to the previous examples, synergies are found using the solutions to a large number of optimization problems. For a number of postures and desired task space acceleration vectors ($\mathbf{a}_{des}$), the optimization algorithm calculates the vector of muscle activation that minimizes the objective function:

$$\mathbf{u}_{m\times 1} = \underset{0\leq u_i\leq 1}{\arg\min} \left\{ J = w_1 \frac{1}{|\mathbf{a}_{des}|^2} |\mathbf{a}_{des} - \mathbf{a}|^2 + w_2 \mathbf{u}^T \mathbf{u} \right\} \tag{4.9}$$

subject to the extra constraint:

$$\bar{a}_{des} = \ddot{\phi} = 0 \tag{4.10}$$

The constraint (4.10) forces the resulting redundant space acceleration to be zero. The reason for this constraint is to ensure that the activation of synergies does not impose significant unwanted acceleration in the redundant space (to leave it uncontrolled).

The data obtained from the optimization solutions are then used in a *constrained* CNNMF (C2NNMF) to get the posture-dependent synergy matrices with shared basis sets that produce small accelerations in the redundant space.

A linear constraint of the following form is considered for this application:

$$\mathbf{L}_{q\times m}\mathbf{S}_{m\times k} = 0 \tag{4.11}$$

The matrix $\mathbf{L}$ in (4.11) is a mapping from the m-dimensional muscle space to a q dimensional *effect* space. This effect may be a physically meaningful measure (e.g. an acceleration vector), or abstract (e.g. fitting the synergies in a certain shape, or forcibly turning off certain muscles in some synergies). In this example, the effect is the acceleration in the 1D redundant space ($q = 1$), and the row-matrix $\mathbf{L}_{1\times m}$ contains the redundant space acceleration produced by full activation of each of the m muscles.

The iterative algorithms presented originally to solve the NNMF problem can be modified to accommodate such linear constraints. Here, the original ALS (alternating least square) and the modification to include the linear constraint is presented.

In each iteration of the original ALS algorithm, the solutions for $\mathbf{S}$ and $\mathbf{C}$ are updated as:

$$\text{First solve for } \mathbf{C}_{update} \text{ in the equation : } \mathbf{S}^T\mathbf{S}\mathbf{C} = \mathbf{S}^T\mathbf{A} \tag{4.12}$$

$$\text{Then use it to solve for } \mathbf{S}_{update} \text{ using : } \mathbf{C}\mathbf{C}^T\mathbf{S}^T = \mathbf{C}\mathbf{A}^T \tag{4.13}$$

In order to satisfy the constraint (4.11), $\mathbf{S}$ must be in the null space (or kernel) of $\mathbf{L}$ ($N_{\mathbf{L}} = ker(\mathbf{L}) = \{x \in \mathbb{R}^m | \mathbf{L}x = 0\}$). Therefore, the solution of $\mathbf{S}$ in each iteration is

projected onto this subspace, which is equivalent to:

$$\mathbf{S}_{proj} = \mathbf{PS} \tag{4.14}$$

where

$$\mathbf{P} = N_{\mathbf{L}}(N_{\mathbf{L}}^T N_{\mathbf{L}})^{-1} N_{\mathbf{L}}^T \tag{4.15}$$

This projection can be applied in every iteration of the NNMF algorithm after the solution of $\mathbf{S}_{update}$ is found in (4.13). The Matlab implementation of this algorithm is given in Appendix D.

Using C2NNMF on the optimized muscle activation data results in synergies whose basis set spans the task space, and produce small accelerations in the redundant space. Therefore, the motor control structure shown in Figure 4.18 can be used to control only the task-related variables (while leaving the movements in the redundant space uncontrolled).

To achieve full control of the motion (for example to avoid an obstacle), a new augmented task space should be considered ($\hat{\mathcal{T}}_4 = \{(x, y, z, \phi)\}$). To control the motion in this new task space, synergies with basis vectors orthogonal to the original ones (that spanned $\mathcal{T}_3$) should be defined. Since the original redundant space was 1D in this example, only two synergies would be required to control the motion in this space. These extra synergies can also be found by solving a number of optimization problems. In a given posture, the optimization algorithm calculates the muscle activations that minimize the cost function (4.9) with the task space condition $\mathbf{a}_{des} = 0$, but subject to the constraints:

$$\bar{a}_{des} = \ddot{\phi} = +1 \text{ or } -1 \tag{4.16}$$

These constraints requires the muscles to produce zero acceleration in the original task space ($\mathcal{T}_3$), and $+1$ or -1 (rad.s^{-2}) acceleration in the original redundant space($\mathcal{R}_1$). The set of posture-dependent muscle activations that produce positive redundant space acceleration are considered as one of the redundant space synergies, and the ones that

produce negative acceleration are the other synergy. It is therefore, evident that the basis vectors for these two synergies are $\bar{B}_1 = +1$ and $\bar{B}_2 = -1$.

Once the augmented synergy set ($\hat{\mathbf{S}}$) is identified (shown in Figure 4.19), the method presented in section 3.2.2 can be used to control some or all of the arm's degrees of freedom.

4.4.3 Simulation results

The simulation results for the 3D and 4-DoF musculoskeletal arm model are presented here. Figure 4.20 presents the simulation results when the target motion is a 20 cm hand elevation in the z direction. Two control methods are presented: The motor control framework, and a non-linear model predictive controller with 3-step prediction horizon and the cost function:

$$J = w_1 \sum_{i=1}^{m} \int u_i^2 dt + w_2 \int (e_p)^2 dt + w_3 \int (e_v)^2 dt + w_4 \int (e_\phi)^2 dt \tag{4.17}$$

in which the last term ($\int (e_\phi)^2 dt$) handles tracking in the redundant space.

The arm motion resulting from the two controllers is shown in Figure 4.20a, along with the muscle activations presented in Figure 4.20b (The two control methods are denoted in the results by "synergy+PID" and "optimal"). It must be noted that the synergy-based controller leaves the redundant DoF (ϕ) uncontrolled, (it falls due to the gravity), whereas the optimal controller has to control it. To obtain comparable results with the optimal controller, it was required to follow the same ϕ trajectory.

The results in Figure 4.20 were obtained using five synergies. The effect of the number of synergies on the framework performance (VAF) as well as the NNMF error (e in (3.20)) is shown in Figure 4.21. To calculate VAF in these simulations, the same equation as (3.26) is used. The muscle activations for VAF calculations correspond to the motion shown in Figure 4.20a. Five synergies result in the highest VAF in these simulations, which is the number that is used in the close-loop control performance showed in .

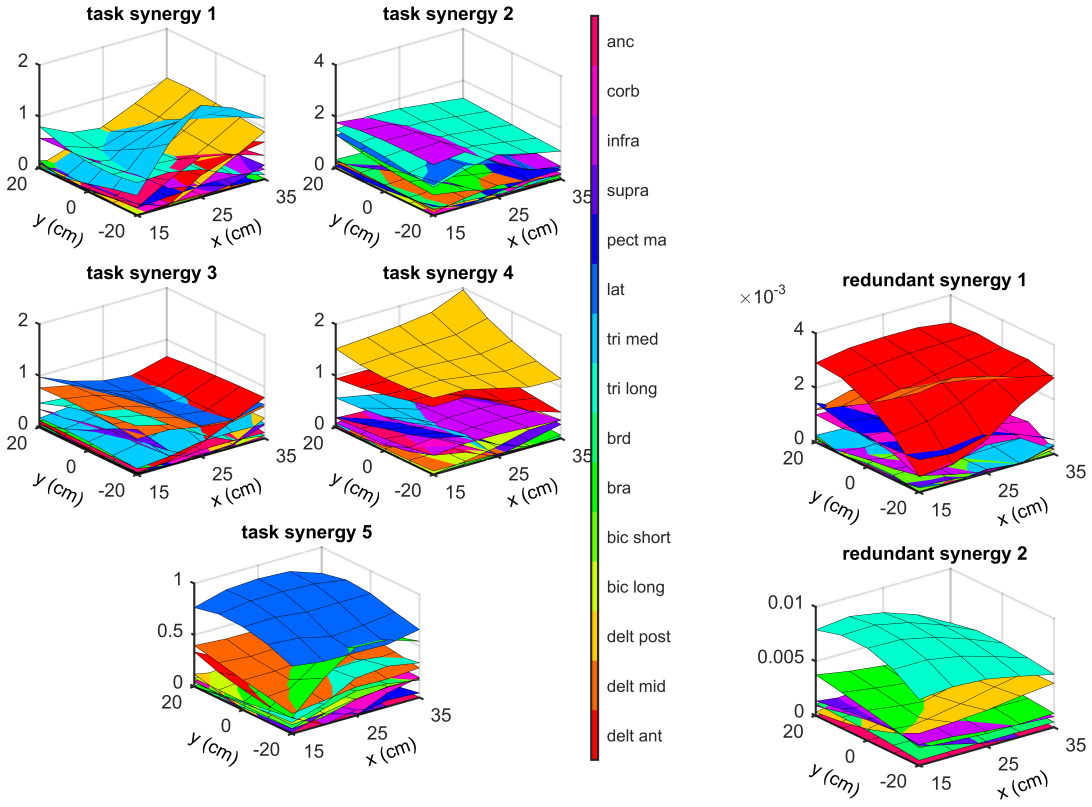

(a) (b)

Figure 4.19: The visualization of the synergies used for the control of the 3D 4-DoF arm model. (a) The task space synergies, and (b) the redundant space synergies. The surfaces show the changing muscle activities within each synergy, as the hand position changes in a 2D horizontal space. These synergies are shown when the hand elevation is 20 cm below the shoulder ($z = -20cm$), and $\phi = 0°$.

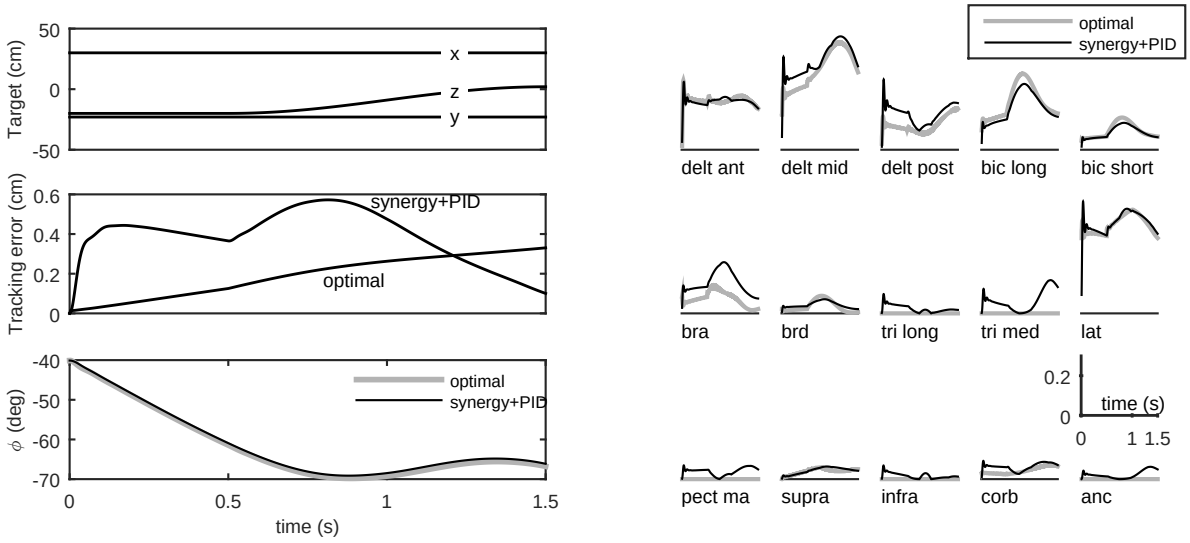

(a) (b)

Figure 4.20: The application of the motor control framework for the feedback motion control of the 3D 4D0F musculoskeletal arm model. (a) The trajectory for the hand position (moving 20 cm upwards), the tracking error, and the motion in the redundant space. Two control methods are compared: an optimal controller, and the synergy-based motor control model. (b) The muscle activations resulting from the two control methods.

With five synergies, the physiological effort ($= \int \mathbf{u}^T \mathbf{u} dt$) from the synergy-based controller turned out to be only 11.6% more than that of the optimal controller. The VAF between the optimal and synergy-produced activations also shows closeness of the results (VAF = 0.923). The computation time, on the other hand, is reduced by 88.3% (the total synergy+PID simulation took 5.55 s on a computer with a Core-i7 4790 CPU and 16 GB of RAM, while the optimal controller took 49.1 s).

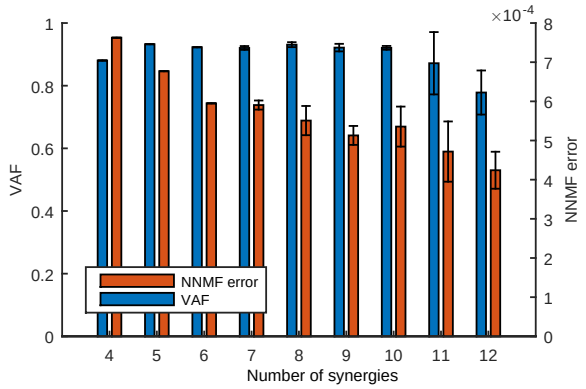

Figure 4.21: The effect of the number of synergies on the performance of the motor control framework. Because the NNMF is sensitive to the initial guesses, multiple runs of NNMF are performed. The plots show the mean and standard deviation of the results. When a small number of synergies are used, the variability is low.

4.5 Discussion

This chapter highlighted the potential of the proposed motor control framework in controlling the movement in a variety of musculoskeletal systems. The motor control models in all the examples were based on a hierarchical structure: a high-level control logic handled path planning and error compensation in the task space, while a low-level controller estimated the required muscle activities. It was shown that this framework was successful in controlling the motion in the task space and redundant space, with near-optimal muscle activations.

One should note that the proposed framework focused on the *active feedback* aspects of the movement control. In reality, however, there are numerous *passive and feedforward* pathways involved in the control of movements. For instance, passive muscle forces may play an important role in shaping the motion of the *uncontrolled* degrees of freedom. Furthermore, short-latency feedback loops (e.g. stretch reflexes) also affect the body/environment interactions that were left unattended in this framework.

4.5.1 High-level controller

The task-space controller chosen in most of the presented examples was a simple error-driven PID controller. Although the PID showed acceptable results in the simulations, it may not capture the essential properties of the human motor control system, such as prediction/expectation, adaptability, and robustness. To show the potential of the framework, an MPC controller was also used as a semi-optimal controller. It is possible to include more complex feedback control types, such as a robust/adaptive controller in the control loop. Furthermore, machine learning techniques may also be used as an approximation of the complex processes in the nervous system.

It is worth noting that the human motor control system is very complex, and the subtle changes in the goals of the task may change the underlying control mechanisms. For instance, during a normal reaching task, the goal is to move from one point to another; however if a joint is causing pain, another important goal is to restrict its motion. In this framework, this would be a new and more complex task space, which would engage a different set of high- and low-level controllers.

4.5.2 The A2A mapping

The major contribution of this research is the introduction of a method to translate task space control commands to muscle activations. The proposed motor control framework is based on a hierarchical structure, and the bridge between the task-space and muscle-space control signals is a posture-dependent mapping that employs muscle synergies.

It has been argued that muscle synergies may arise from a background optimization process (perhaps during evolution) (de Rugy et al., 2013, 2012). The presented method relies on these arguments and defines the synergies by employing optimization tools. However, unlike the on-line optimization methods, e.g. (Todorov and Jordan, 2002b; Todorov et al., 2005), the synergies are optimally calculated and stored off-line, and recalled during an on-line control process in the A2A mapping.

The A2A mapping introduced in this thesis employs muscle synergies to simplify the calculations and reduce the processing time. In this process, it was assumed that an internal representation of the arm (through the known basis vectors associated with each synergy) is available to the nervous system.

Muscle synergies, if they exist, are probably formed either through evolution (prior to the movement, an off-line method) or practice (concurrent with the movement, an on-line method). In this thesis, the off-line learning method was implemented; however, this assumption does not affect the generalizability of the presented motor control framework.

Another critical assumption that was made in this framework was the orthogonality of the basis sets in the task and redundant spaces. The experimental results presented in the previous chapter showed that, at least at the behavioural level (i.e. motion and EMG), this assumption yields close estimations (60-70% VAF). In other words, the control of movements in the task and redundant spaces can be separated by employing orthogonal basis vectors, and the results are not far from reality.

The orthogonality condition simplifies the computations, as the task-related synergies will not induce an acceleration in the redundant space and vice versa. This assumption also introduces the ability to switch on/off the redundant space control, without the need to change the control structure. The simulation results further showed that by assuming orthogonal bases for the task and redundant spaces, the feedback control performance is acceptable, and flexible control of movements in the task and redundant spaces is possible.

The downside of the orthogonality assumption, however, is the sub-optimality of the final results. It is possible that a general (non-orthogonal) n-D basis set would result in more efficient muscle activations. One hypothesis regarding this issue would be similar to the idea presented by Raphael et al. (2010) and Loeb (2012). It might be possible that in a novel situation, the nervous system starts employing the previously known solutions (a basis set for the task space, plus another one orthogonal to the first for the redundant space), and eventually explores the neighbouring solutions until it reaches a *good-enough* solution (a non-orthogonal basis set, with possibly fewer synergies).

Lastly, instead of the previous statistical methods (e.g. NNMF), a new model-based approach was proposed for defining the synergies based on the principles of optimality. In support of this optimization-based method, it has been reported that the muscle activities estimated by optimal control approaches correlate well with experimental EMG (Erdemir et al., 2007), and that the synergies extracted from such optimal muscle activities match the ones extracted from the EMG data (Steele et al., 2013). The comparison between the presented results and the synergies obtained from the common factorization methods (NNMF) also show the plausibility of the optimal arguments. Therefore, the presented method can be used as a theoretical model-based framework to study muscle synergy—a tool that was not available before.

The proposed A2A mapping, despite being successful in the fast control of musculoskeletal systems, has limitations including the inability to account for agonist/antagonist muscle co-contraction, and the combination of multiple tasks.

4.5.3 Task-dependent synergies

Muscle synergy has been considered as a possible mechanism employed by the nervous system to control movements. Previous investigations on muscle synergy usually relied on an *inverse* extraction method—the synergies were extracted from the measured muscle activities using a factorization algorithm (e.g. NNMF). These methods usually neglect the functional aspects of synergies and their correspondence with the task.

An important assumption in this motor control framework is the dependency of the control strategy (therefore the synergies) on the intended task. There are two schools of thought regarding the relationship between synergies and tasks: some researchers try to find the *shared* synergies that can explain muscle activities in a variety of motions (e.g. Sartori et al. (2013); Bizzi et al. (2008)), while others look at specific tasks (e.g. point-to-point reach, D'Avella et al. (2008), or wrist articulation, de Rugy et al. (2013)). Task-dependent synergies have been previously mentioned (e.g. in Zelik et al. (2014)), but no scientific method to distinguish the tasks and relate the synergies to the operational

space has been shown. The importance of the task-related kinematics and control strategy has been reported before (by the UCM (Scholz and Schöner, 1999), and the minimal intervention (Todorov and Jordan, 2002a) theories, respectively). Relying on these theories and the results presented in this thesis, one may speculate that task-specific synergies are necessary for the efficient control of a task by the CNS.

4.5.4 Posture-dependent synergies

Posture dependence is an important assumption in this motor control framework. The generalizability of static (posture-invariant) synergies across various postures has been discussed before (e.g. by Torres-Oviedo, 2006). However, the added flexibility of the posture-dependent synergies (as opposed to the fixed ones) gives a smaller set of synergies the richness that is necessary to control complex movements.

No explicit definition of posture-dependent synergies is available in the literature (perhaps because of the vast number of the required experimental trials). The proposed method is superior as fewer posture-dependent synergies can account for more muscle activity variations than fixed ones. The posture dependency, as mentioned earlier in this thesis as well as by de Rugy et al. (2012), might be an essential requirement of synergies, as muscles may change function depending on the posture (e.g. wrist muscles (Kakei et al., 1999)). The presented simulation results comparing the posture-dependent synergies and the fixed ones from NNMF (section 4.1) support the hypothesis that posture-dependent synergies can reduce the dimensions of the control space more effectively; fewer synergies are required to efficiently control the motion if synergies are posture-dependent.

4.5.5 Number of synergies

The number of synergies is still an uncertain matter in the literature. The data reproduction capability measure that is widely used in the literature has one problem: it is

an *inverse* method, in which the error continually decreases by increasing the number of synergies. Thus, one has to decide how much improvement is enough.

In the presented motor control framework, however, the reconstruction of the original data matrices bears little significance. Instead, the performance of the A2A mapping (as a *forward*, or *predictive* method) in estimating the muscle activations is a more meaningful measure. It was shown in multiple examples that the best A2A performance and lowest data reconstruction error do not correlate well. In the examples showed, there were certain numbers of synergies (usually small) where A2A performed the best.

One explanation for these observations could be that the performance of the A2A mapping depends on the number of synergies and how well the task space is spanned by the basis vectors. The NNMF does not take into account the task space, and results in a non-optimal distribution of basis vectors when a high number of synergies are used. Therefore, counter-intuitively, more synergies do not improve the overall performance, despite the decrease in the NNMF error.

4.5.6 Speculations on muscle synergies and motor learning

From an evolutionary point of view, the muscle synergies must be structured in such a way that result in the best performance in doing a task. The arguments in this thesis were based on physiological effort minimization, because a well-practised motion (such as reaching) is physiologically efficient. However, another important performance index that needs to be addressed is the robustness and generalizability in novel conditions (as observed by Gentner et al., 2013). The task-specific definition of the synergies raises the important question whether new synergies are formed for a new task, or the general-purpose synergies would still be used. In a similar note, are they hard-coded, or do they flexibly change by task?

One possible argument is that the synergies (especially the ones related to locomotion) are fine-tuned over the course of human evolution, and perhaps hard-coded into the spinal

cord circuitries (the so-called central pattern generators (Ijspeert, 2008) can be viewed as an example). The synergies for important, repeated, and specific task (e.g. locomotion) may be specific and fixed.

Alternatively, and especially in the context of motor learning and adaptation to new tasks, the synergies may be viewed as flexible structures, decoded by the interneurons of the spinal cord (similar to the concept of *spinal-like regulators* proposed by Raphael et al. (2010)). It has been shown by de Rugy (2010) that the process of visuomotor adaptation likely happens at the sensory level as well as the execution (muscle synergy) level. These observations may be linked to the gradual performance improvement observed during motor learning. One hypothesis regarding motor learning could be as follows: the nervous system initially tries to control a novel task (e.g. playing violin with a bow, which has very specific task requirements) with the available synergy sets. As the task is repeated, the nervous system explores the neighbouring solutions, and eventually learns a new synergy set (as well as a fine-tuned task space controller) for the specific task.

4.5.7 Other implications

The human musculoskeletal system is challenging to control due to the redundancies and non-linearities involved. As a result, prediction of the movements in new situations (when no measured data is available) is a difficult task. The motor control framework presented in this thesis is a viable tool in *predictive musculoskeletal simulations*, where a fast and biologically plausible motion controller is needed. The synergy-based motor control model can replace the current state-of-the-art (optimization-based control) to produce similar results in a fraction of the time. The example musculoskeletal simulations in this chapter showed that the proposed motor control model has high generalizability capabilities.

The results are even more interesting from an engineering perspective. It can facilitate the design and control of machines interacting with humans, such as prosthetic and orthotic devices, exoskeletons, and rehabilitation robots, by allowing fast prediction of the human behaviour. Furthermore, the motor control model has direct application to the feedback

control of real musculoskeletal systems with functional electrical stimulation (FES). In the next chapter, it will be shown how the same model can be used to produce upper extremity reaching movements by electrical stimulation of the muscles.

4.6 Chapter conclusions

This chapter presented the application of the proposed motor control framework to the movement control in musculoskeletal simulations. The examples ranged from single-DoF to redundant four-DoF arm models. Various aspects of the motor control framework were studied, including the high-level controller, synergy extraction methods, and handling of kinematic redundancy. Another important application of this motor control framework (feedback control of functional electrical stimulation devices) is presented in the next chapter.

Chapter 5

The Motor Control Framework for FES Control

This chapter presents the application of the proposed motor control framework to the feedback control of a functional electrical stimulation (FES) system to produce arbitrary goal-directed reaching movements.

5.1 The experimental setup

The experimental setup is shown in Figure 5.1. The stimulation device is RehaStim V.1 with Science Mode (Hasomed GmbH, Germany), which stimulates six muscles of the left arm (anterior and posterior deltoid, biceps and triceps brachii, pectoralis major, and the intermediate region of trapezius). The electrical pulses are delivered to the muscles via the electrode pads placed on the skin and over the muscle motor points (Behringer et al., 2014). The stimulation frequency and current are fixed at 33 Hz and 20 mA, respectively, and the stimulation pulse width is modulated using a computer running Matlab/Simulink.

The goal in this setup is to use the motor control framework as the FES controller, to control the position of the hand, and drive it to any arbitrary target in a 2D (table-top)

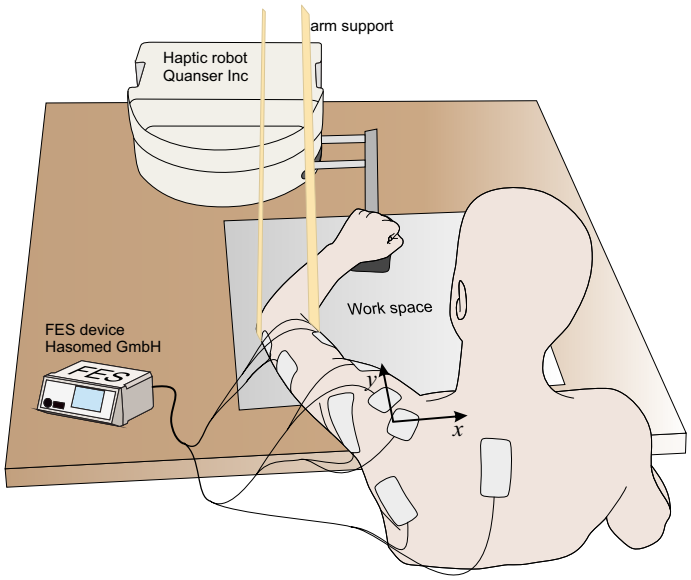

Figure 5.1: The experimental setup for testing the motor control framework as the feedback controller for an FES system

space. For this purpose, the hand position and the forces applied to the hand are measured using a 2D haptic robot (Quanser Inc. Canada). The robot can be programmed to be locked in place (for isometric trials), or move with/without applying resistance (during motion trials). The subject sits upright in front of the robot. A wrist brace is used to restrict wrist degrees of freedom, and also firmly connect the hand to the robot's end-effector. To reduce the arm-table friction and keep the arm in the horizontal plane, the arm is suspended using a sling. Since the arm always remains elevated by the sling at a certain height, the effective number of the arm's degrees of freedom is reduced to two; thus, only the (x, y) position of the hand is sufficient to describe the posture. For this argument to be valid, it is assumed that the torso movement is negligible, and there is no independent degree of freedom for the scapula; i.e. the scapula motion is linked to the shoulder elevation/flexion angles (through *scapulohumeral rhythm*, Grewal and Dickerson, 2013).

This FES controller was tested on the left arm of a healthy subject (28 year old male).

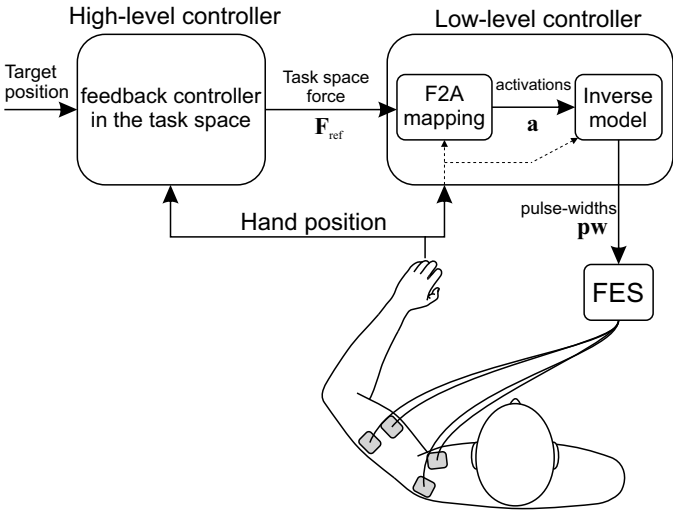

Figure 5.2: The overview of the motor control model as the FES feedback controller

To make sure that the subject's voluntary actions are minimized, he was asked to relax, and no information about the target positions were visible to him.

5.2 FES controller architecture

The feedback FES controller is the real-time implementation of the synergy-based motor control framework. The advantage of this motor control model is in its task space representation, which simplifies the calculations and allows for efficient control of the movements in the task space. The task space in this context is defined as a 2D Cartesian space, specified by the (x, y) position of the hand (i.e. the task space is $\mathcal{T}_2 = \{(x, y)\}$). Alternatively, for example, if the objective were to control the elbow flexion angle only, the task space would be a 1-dimensional space defined by elbow angle (the hand position would be irrelevant in this case).

The schematic of the motor control framework as the FES feedback controller is shown in Figure 5.2. The high-level controller in this implementation is a PID controller, whose

input is the position error in the task space. This task space controller defines a 2D reference *force* that is required to reach to the specified target. This force command should be fulfilled by activating the muscles. Thus, the role of the low-level controller is to translate the task space force command to muscle activations and consequently to stimulation pulse width (pw), which is fed to the FES device. This force-to-activation (F2A) mapping is essentially the same as the A2A mapping in the original motor control framework, where basis vectors are force vectors produced by the synergies (instead of acceleration vectors). Force vectors are used here, because they are easier to measure and implement in the FES feedback controller. The F2A mapping is briefly explained here.

In a given posture, defined by the hand's (x, y) position in the task space, the activation of a single synergy would result in a certain isometric hand force. The collection of all the force vectors produced by individual synergies is considered as the basis set for the task space.

The known basis vectors can be used to solve for the muscle activations in real-time, instead of the time-consuming optimization process (e.g. in Schearer et al. (2014, 2015)). The force command defined by the task space controller can be decomposed into the basis set to calculate the coefficient of each basis vector (Figure 5.3). Then, the synergies are combined using the calculated coefficients to obtain the muscle activations that produce the reference force. The schematic and block diagram of this process is shown in Figure 5.3.

5.3 Implementation of the FES controller

To implement this motor control framework as the FES controller, *models* of the stimulated muscles are needed. Because of the task-dependent architecture of the motor control framework, it is only required to identify a mapping that transforms the muscle stimulation intensity (pw) to the task space force vector. This feature is an important advantage of the proposed motor control model as no explicit information about the kinematics of the body (e.g. segment lengths and joint angles) and the joint moments is necessary.

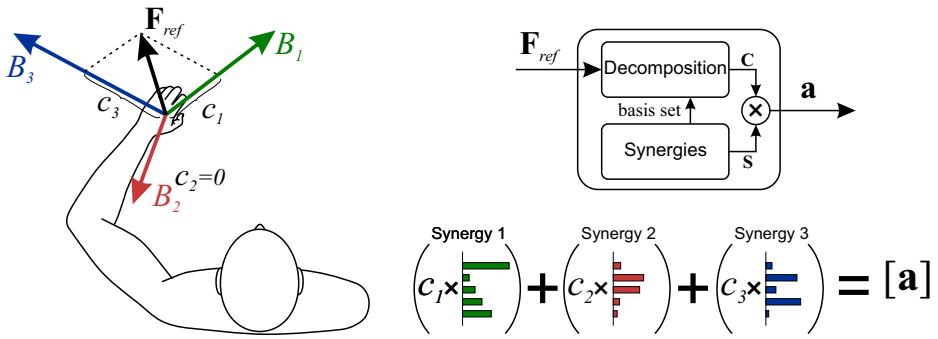

Figure 5.3: The schematic of the force-to-activation mapping. Each synergy produces a certain force in the task space that can be considered as a basis vector. An arbitrary reference force, $\mathbf{F}_{ref}$, can be decomposed into this basis set, to calculate the coefficient of each synergy, c_i. Combining the synergies with the corresponding coefficients gives the vector of muscle activations that produces the reference force.

5.3.1 Identifying pulse-width-to-force mappings

The muscle models used in this work are static input-output functions that estimate the 2D task space force from the stimulation intensity, pw, and the hand position:

$$\begin{aligned} \mathbf{F}_{est}: \quad & \mathbb{R}^3 \rightarrow \mathbb{R}^2 \\ & (pw, x, y) \mapsto (F_x, F_y) \end{aligned} \tag{5.1}$$

To obtain the muscle mappings of this form, in every point shown in Figure 5.4a, individual muscles are isometrically stimulated (the robot is locked in place) one by one with the patterns shown in Figure 5.4b, and the hand force/position is measured by the robot. Using these patterns, only one muscle is active in each instant of time; therefore, the measured force contains the contribution of a single muscle only. The stimulations are repeated at multiple positions in the task space to account for the posture-dependence of the produced forces.

The mapping in (5.1) is constructed by training three separate functions. The first

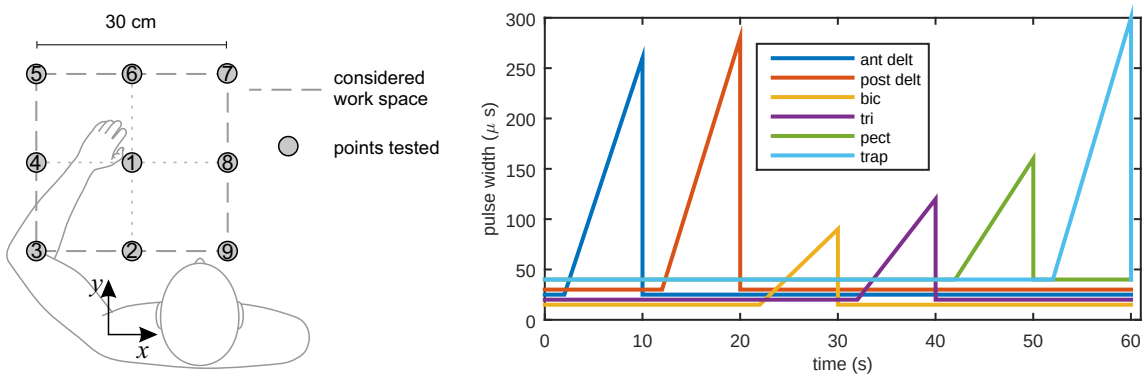

(a) (b)

Figure 5.4: (a) The workspace and the points at which the stimulation profiles are applied. The numbers inside the circles indicate the *posture ID* that are referred to in Figure 5.9. (b) The stimulation profiles used to train the muscle mappings. For each muscle, the maximum pulse width is the threshold where the stimulation becomes uncomfortable for the subject, and the base value is the onset of feeling the stimulations on the skin (no force is produced at this level of stimulation). These thresholds are the same for all the tested points.

function is trained to estimate the direction of the hand force as a function of posture. The second function estimates the maximum hand force, also as a function of posture. Finally, the third function is the pulse-width-to-activation mapping, which is used to scale the maximum hand force as a function of stimulation pulse width. The reason for the separation of the force direction from its magnitude is to ensure that the direction of the estimated force remains the same for all intensity levels (ideally this direction should only depend on the geometry of the musculoskeletal system). Therefore, the force direction mapping is trained despite the changing stimulation intensity and is only a function of posture.

The direction mapping is trained using the *best line of action* of the measured hand forces at various postures. This line of action is obtained by fitting a line (zero y-intercept)

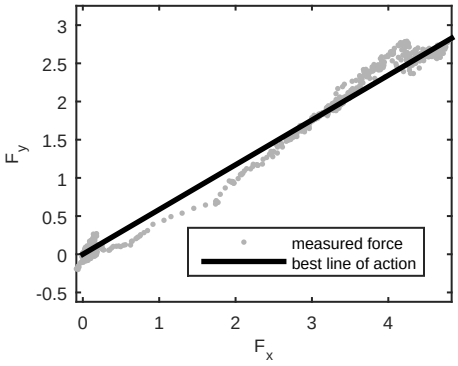

Figure 5.5: An example for the best line of action (pectoralis major muscle in the centre of the workspace). The dots represent the measured force as the pulse-width increases.

to the measured force (as seen in Figure 5.5). Next, the unit vector, $\hat{\mathbf{u}}_F$, representing this direction is found, and second-order polynomial surfaces ($\mathcal{P}(x, y)$) are used to fit its u_x and u_y components as functions of the hand position.

$$\hat{\mathbf{u}}_F = \begin{bmatrix} u_x \\ u_y \end{bmatrix} = \begin{bmatrix} \mathcal{P}_1(x, y) \\ \mathcal{P}_2(x, y) \end{bmatrix} \tag{5.2}$$

Figure 5.6 shows the estimated force directions of the stimulated muscles in the 2D task space. In these plots, the origin of the coordinate system is at the left shoulder, x is the transverse direction with positive pointing to the right, and y is forward. The goodness of the polynomial fit for the direction mapping is given in Table 5.1.

The amplitude mapping contains two fitted functions. The estimation of the posture-dependent maximum muscle force is obtained using a second-order polynomial surface, which is fitted to the maximum of the measured force amplitudes (at maximum pulse-width) in various postures. This mapping gives the maximum hand force production capacity of the muscle as a function of posture as:

$$F_{max} = \mathcal{P}(x, y) \tag{5.3}$$

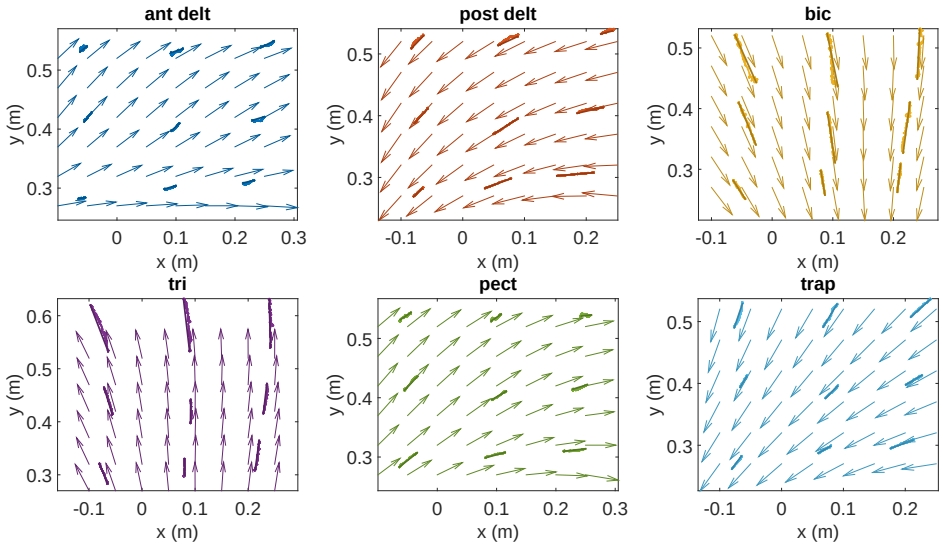

Figure 5.6: The trained mappings for the direction of the force in the entire workspace. The arrows show the direction of the force estimated by the mapping. The thick lines represent the measured data, and the best line of action are shown with thin lines. The force measurements are shown with 1N = 0.005m scale in this plot. The hand position is given in the coordinate system located at the left shoulder, $+x$ is to the right, and $+y$ is forward.

Figure 5.7 shows the estimated maximum task space forces of the stimulated muscles. The goodness of the fit is given in Table 5.1.

The last mapping is used to estimate the *muscle activation*, a. Muscle activation in this context is defined as the linear scaling of the maximum force, between 0 and 1:

$$a(pw) := \frac{|F(pw)|}{|F(pw_{max})|} \tag{5.4}$$

The muscle activation is a non-linear function of the stimulation pulse width, which is modelled as a sigmoid function with four parameters c_i. During the experiments, it was

Table 5.1: The goodness of fit for the direction, amplitude, and activation mappings. *Adjusted R-squared* is given as the measure.

	Ant. deltoid	Post. deltoid	Biceps	Triceps	Pectoralis Major	Trapezius
u_x	0.202	0.949	0.987	0.995	0.633	0.929
u_y	0.126	0.945	0.784	0.886	0.727	0.918
F_{max}	0.227	0.940	0.921	0.828	0.884	0.639
a	0.900	0.909	0.906	0.965	0.918	0.950

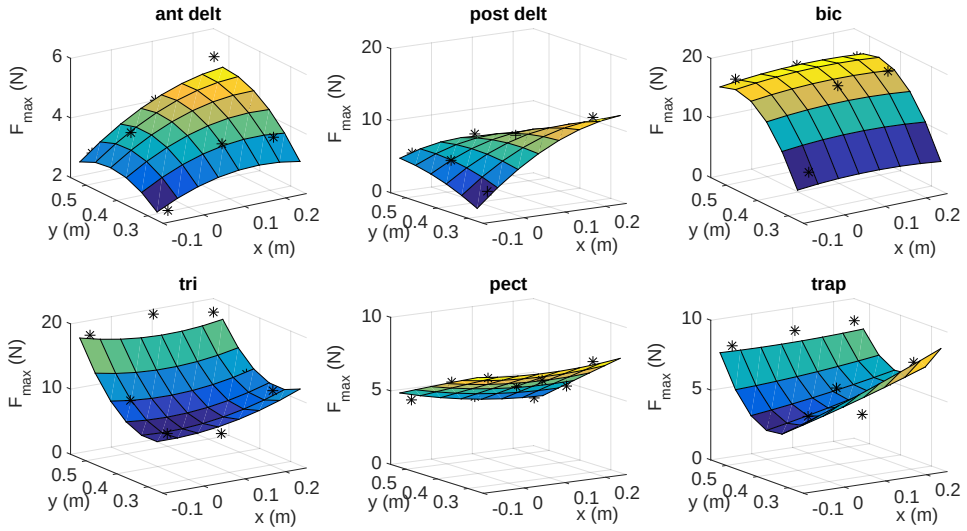

Figure 5.7: The fitted polynomial surfaces to estimate the maximum capacity of the muscles as functions of posture. The measured data are shown with black asterisks.

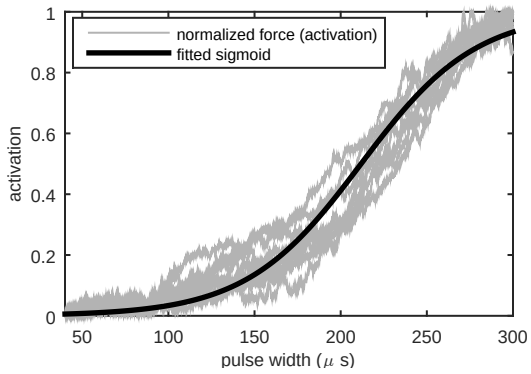

Figure 5.8: The sigmoid function fitted to the measured data collected at 9 different positions in the workspace (the example belongs to the pectoralis major muscle)

observed that the activation-pw relation is not significantly affected by the posture (only the maximum force changes by posture, see Figure 5.8). Therefore, the following mapping is trained using the collection of the data obtained in all the postures.

$$a = f(pw) = c_1 + \frac{c_2 - c_1}{1 + 10^{(c_3 - pw)c_4}} \tag{5.5}$$

The trained amplitude mappings (The combination of the activation and F_{max} mappings) for the stimulated muscles are shown in Figure 5.9. The quality of the sigmoid fit (adjusted R-squared) is also given in Table 5.1 for all the muscles.

Finally, the three functions are combined to obtain the *posture-dependent pulse-width-to-force mappings* for individual muscles:

$$\mathbf{F}_{est}(pw, x, y) = \hat{\mathbf{u}}_F(x, y) F_{max}(x, y) a(pw) \tag{5.6}$$

where $\hat{\mathbf{u}}_F$, F_{max} and a are the functions that estimate the force unit vector, maximum muscle capacity, and activation level, respectively. The first two functions are the polynomial surfaces, and the last one is a sigmoid function.

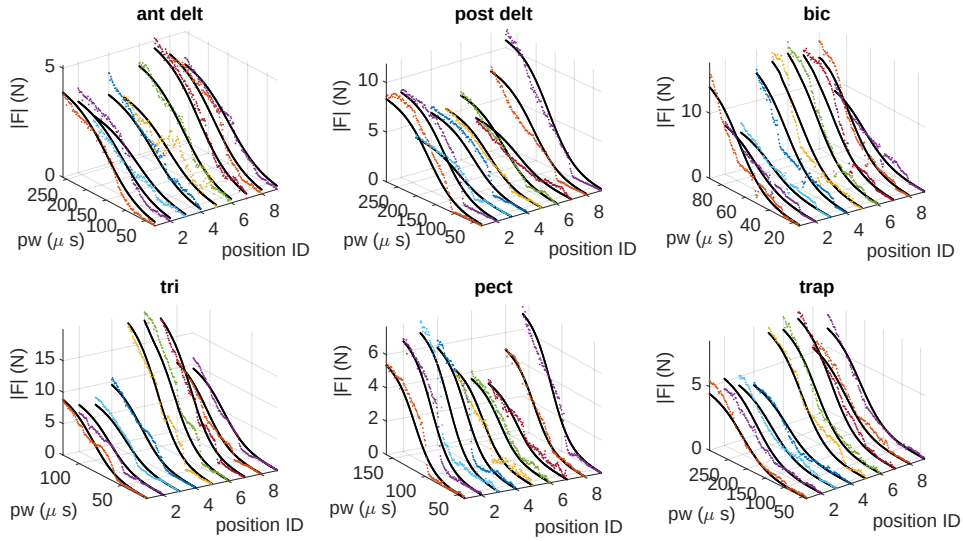

Figure 5.9: The estimated force amplitudes as functions of stimulation pulse width in various postures (identified by *position ID* in the plots). The amplitude estimations (black lines) are compared against the measured force amplitudes (coloured dots).

Defining muscle activation is important in the synergy framework, as its relationship with muscle force is linear—a feature that is necessary for the superposition principle that is the basis of the synergy framework. Stimulation pulse width, unfortunately, does not exhibit such a relationship. Once the required muscle activations are calculated through the processes in the F2A mapping, an *inverse mapping* is required to calculate the needed stimulation pulse widths. The inverse mapping $pw = f^{-1}(a)$ can be easily obtained by taking the inverse of the sigmoid function in (5.5) as:

$$pw = f^{-1}(a) = c_3 - \frac{1}{c_4} \log\left(\frac{c_2 - a}{a - c_1}\right) \tag{5.7}$$

5.3.2 Obtaining the synergies

For the muscle synergies to be useful in the motor control framework, they need to have an important feature: their basis vectors must span the task space in such a way that any force vector can be a linear combination of the basis vectors with *positive coefficients* (muscles are pull-only elements). This requirement implies that: 1) at least three synergies are required to control the motion in the 2D task space, and 2) their basis vectors cannot all be in one half-plane. Furthermore, the structure of the synergies can have a significant effect on the efficiency and performance of the control loop. As a result, proper identification of the synergies is a critical step in this motor control model.

Three methods are studied to obtain the synergies; one is a heuristic method, and the other two use non-negative matrix factorization of optimal muscle activation data (once with the CNNMF, which gives shared bases, and once with the normal NNMF, which results in posture-dependent bases).

In the heuristic method, the muscles with similar functions are grouped together and stimulated with fixed relative activation levels. In this context, the direction of the hand force produced by a muscle defines its function. Therefore, the synergy 1 includes anterior deltoid and pectoralis major muscles; synergy 2 includes posterior deltoid and trapezius muscles; synergy 3 includes biceps brachii; finally, synergy 4 includes only triceps brachii.

The direction of forces produced by each synergy varies with posture, but as a general rule, synergy 1 moves the hand medially, synergy 2 moves the hand laterally, synergy 3 moves the hand posteriorly, and synergy 4 moves the hand anteriorly. The synergies and the associated basis vectors are shown in Figure 5.10.

The basis vectors that the heuristic synergies produce can successfully span the task space (see Figure 5.10b). However, it should be noted that this property may not necessarily hold in general. For instance, muscles may change function drastically across larger or more complex task spaces. More importantly, the inclusion of more muscles makes it harder to identify such synergies. For example, the trapezius muscle is placed in the

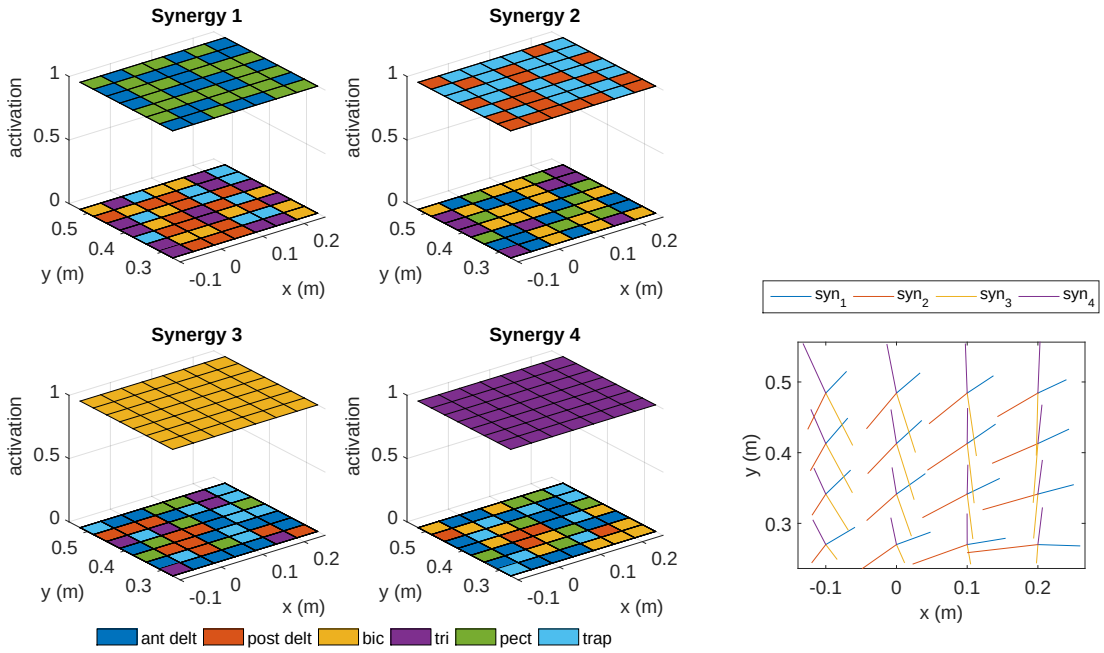

(a) (b)

Figure 5.10: The synergies and the basis sets obtained from the heuristic method. (a) The muscle synergies, and (b) the corresponding basis sets in the 2D task space.

synergy #2 alongside the posterior deltoid, but its function is to retract the scapula and consequently move the hand laterally and back, which is neither the same as posterior deltoid nor biceps brachii. Therefore, considering more systematic methods to obtain useful synergies is highly beneficial.

The factorization algorithms are used to calculate the synergies more systematically. To start the process, a large number of optimization problems are solved. In a particular posture, the best set of muscle activations that results in a target hand force is found. For this purpose, the muscle mappings are used to find the estimates for the hand forces. The target hand forces in the optimizations are 15 equally-spread vectors (with 24° differences) at a given point in the horizontal plane. The optimization algorithm tries to minimize the

objective function J:

$$\mathbf{a}^*_{6\times 1} = \underset{0<a_i<1}{\arg\min}\{J\} \tag{5.8}$$

where

$$J = w_1 \left| \left(\sum_{i=1}^{6} \mathbf{F}^i_{est} \right) - \mathbf{F}_{target} \right|^2 + w_2 \sum_{i=1}^{6} pw_i + w_3 \sum_{i=1}^{6} \left| F^i_{est} \right|^2 \tag{5.9}$$

where the index i represents the i^{th} muscle, and w's are weighting factors to balance and non-dimensionalize the terms (values given in Appendix E). In this cost function, the first term is the constraint forcing the estimated total force being close to the target force, the second term penalizes high stimulation intensities, and the last one has the effect of sharing the load among similar-function muscles.

The optimal activations that produce the 15 target forces can be gathered in the matrix:

$$\mathbf{A}_{6\times 15} = [\mathbf{a}^*_1, \mathbf{a}^*_2, \ldots, \mathbf{a}^*_{15}] \tag{5.10}$$

The usual practice of using NNMF is applied to this data matrix to obtain the synergy matrix $\mathbf{S}$ and the coefficient matrix $\mathbf{C}$ as:

$$\mathbf{A}_{6\times 15} \simeq \mathbf{S}_{6\times k}\mathbf{C}_{k\times 15} \tag{5.11}$$

where k is the number of synergies (represented by the columns of $\mathbf{S}$).

In the normal NNMF method, this process is repeated at P different postures to obtain the posture-dependent synergies with posture-dependent bases. Figure 5.11 shows the results when $P = 16$ (a 4×4 grid in the task space).

Alternatively, the optimal activation matrices in all the P postures can be stacked in a larger matrix and fed to the CNNMF algorithm to get the posture-dependent synergies with shared bases:

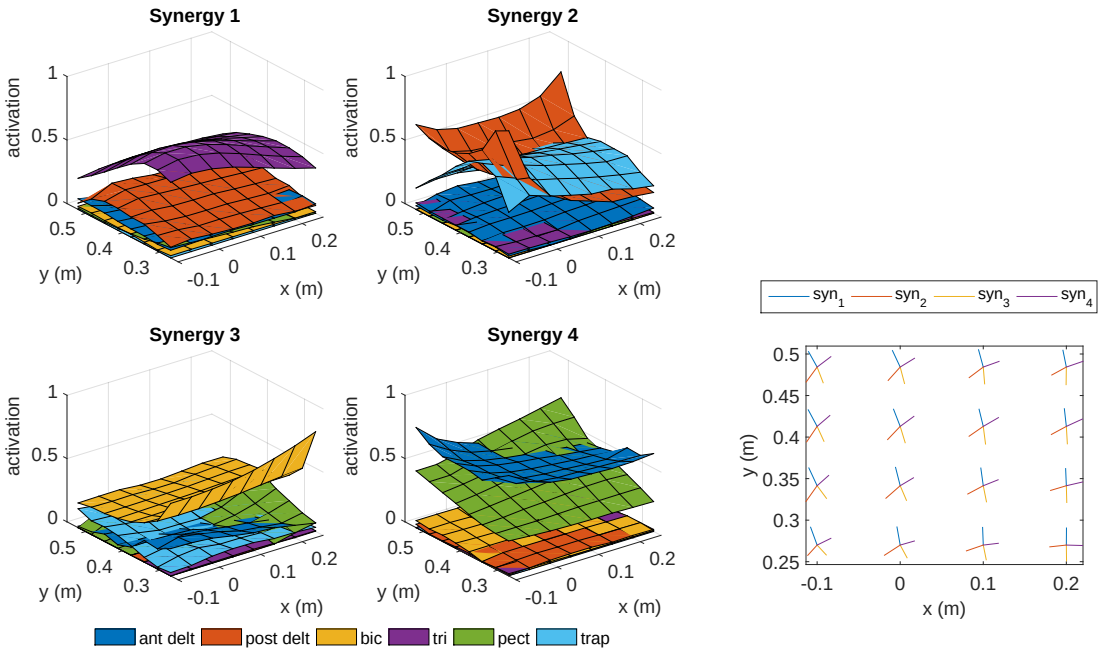

(a) (b)

Figure 5.11: The synergies and the basis sets obtained from the normal NNMF. (a) The muscle synergies, and (b) the resulting *posture-dependent* basis sets in the 2D task space.

$$\mathbf{A}_{6P\times 15} = \begin{bmatrix} \mathbf{A}^1_{6\times 15} \\ \mathbf{A}^2_{6\times 15} \\ \vdots \\ \mathbf{A}^P_{6\times 15} \end{bmatrix} = \begin{bmatrix} \mathbf{S}^1_{6\times k} \\ \mathbf{S}^2_{6\times k} \\ \vdots \\ \mathbf{S}^P_{6\times k} \end{bmatrix} \mathbf{C}_{k\times 15} \tag{5.12}$$

The concatenated NNMF method has the advantage of giving synergies that are readily consistent across posture (i.e. the transition of synergies from one posture to a neighbouring one is always smooth). This is a feature that is hard to achieve using the normal NNMF method (see section 3.3.1. Furthermore, as can be observed in equation (5.12), the coefficient matrix is shared between all postures, implying that the basis vectors are approximately posture-invariant—another feature that speeds the calculations in the F2A

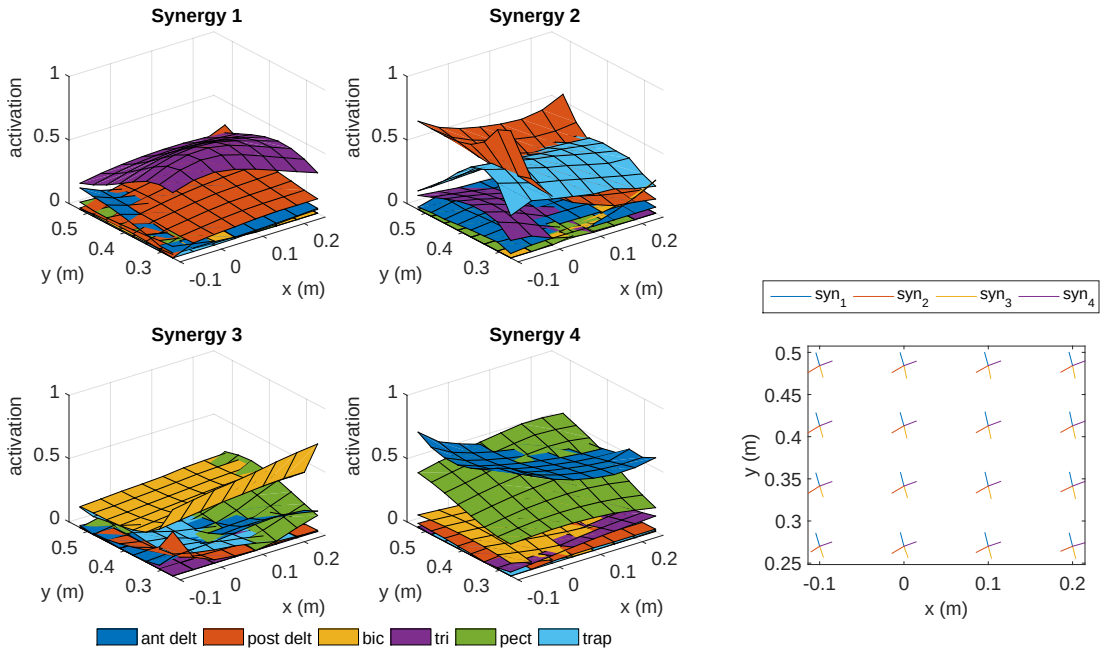

(a) (b)

Figure 5.12: The synergies and the basis sets obtained from the concatenated-NNMF (CNNMF). (a) The muscle synergies, and (b) the resulting *shared* (i.e. posture-invariant) basis sets in the 2D task space.

mapping. Figure 5.12 shows the synergies obtained from the CNNMF method and the corresponding basis vectors.

To get the estimate of the total hand force that each synergy produces (i.e. the basis vectors in Figures 5.10b, 5.11b and 5.12b), the synergies obtained from any of the three methods were fed to the muscle mappings. Therefore, one should note that the bases are estimates themselves, rather than the exactly measured response of the muscles.

During the real-time control of the movement, the hand position is measured by the robot, which is used to interpolate between the previously calculated synergy matrices and basis sets, to obtain the synergies/bases at the current posture. This information is then

used in the F2A mapping to get the muscle activations, which are finally converted by the inverse mapping to pulse-width commands that are sent to the FES device.

5.4 Results

In the first set of tests, isometric trials are performed. In these tests, the robot is locked in four different locations in the task space, and the F2A algorithm estimates the stimulation pulse widths that would generate the reference isometric hand force. Then the muscles are stimulated with the calculated pulse widths, and the actual hand force is measured. These trials assess the combined performance of two components of the framework: the first component is the muscle mapping, and the second one is the F2A. The existence of inaccuracies in each part will result in error in the force produced. Figure 5.13 shows the reference (big circles) and the resulting hand forces (small dots, which are color coded), as well as the root-mean-square (RMS) of the error between them. The three methods compared are: the heuristic synergies (denoted as *heuristic* in the plots), the factorized synergies with posture-dependent bases (denoted by NNMF), and the factorized synergies with shared bases (denoted by CNNMF). Four synergies are used in all these trials. Performing a one-way ANOVA test on the force error showed that no statistically significant difference exists between the three methods ($p = 0.096$).

Next, the motor control model is used as the feedback motion controller for the FES system. The closed-loop control performance is shown in Figure 5.14. To minimize the subject's voluntary compensations, random point-to-point movements (not visible to the subject) are chosen as the reference trajectories. The subject was also asked to relax as much as possible to further reduce the chance of voluntary actions. The reference and the resulting motions are shown in Figure 5.14, with the tracking error visualized in Figure 5.15 (mean and standard deviation of the error are also reported in this figure). The one-way ANOVA test on the target error (the distance between the reference target point and the actual hand position) showed no statistically significant difference between the three

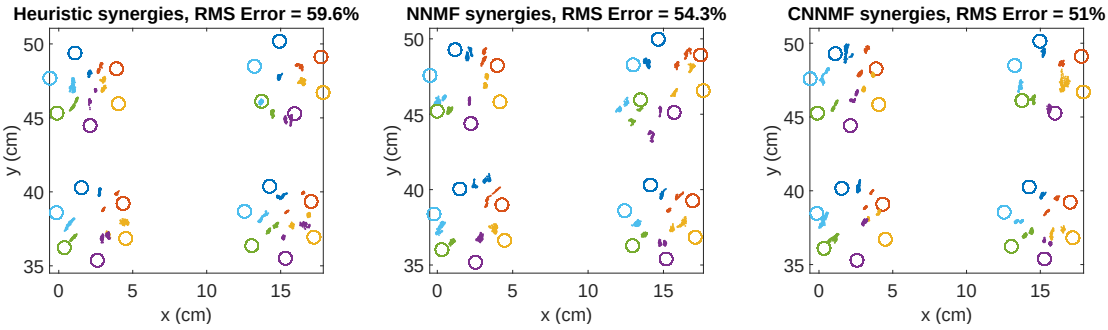

(a) (b) (c)

Figure 5.13: The results from the isometric force production trials. Three methods for synergy calculation are presented, all of which contain four synergies. In these tests, the reference hand forces are six equally spaced vectors of amplitudes 5 N. To visualize the force vectors in the 2D plane, the forces are plotted with 0.5 cm/N scale. The root mean square (RMS) of the error is calculated as RMS $= \frac{\sqrt{\sum |F_{fes} - F_{ref}|^2}}{|F_{ref}|}$.

methods ($p = 0.118$).

5.5 Discussion

The motor controller presented in this thesis takes advantage of the known muscle actions in the task space, to reduce the computational time and improve control performance. Successful implementation of the proposed motor control framework as the feedback FES controller proved its real-time capabilities.

The experimental results showed that the choice of the synergy extraction method has no significant effect on the isometric force production accuracy and tracking performance of the FES controller. Comparing the mean and standard deviation of the target and path error in Figure 5.15 further suggests that all three methods have similar performances. The tracking performance seems to be more affected by the quality of the muscle mappings (which is affected by various uncertainties such as fatigue and skin conditions) than by the

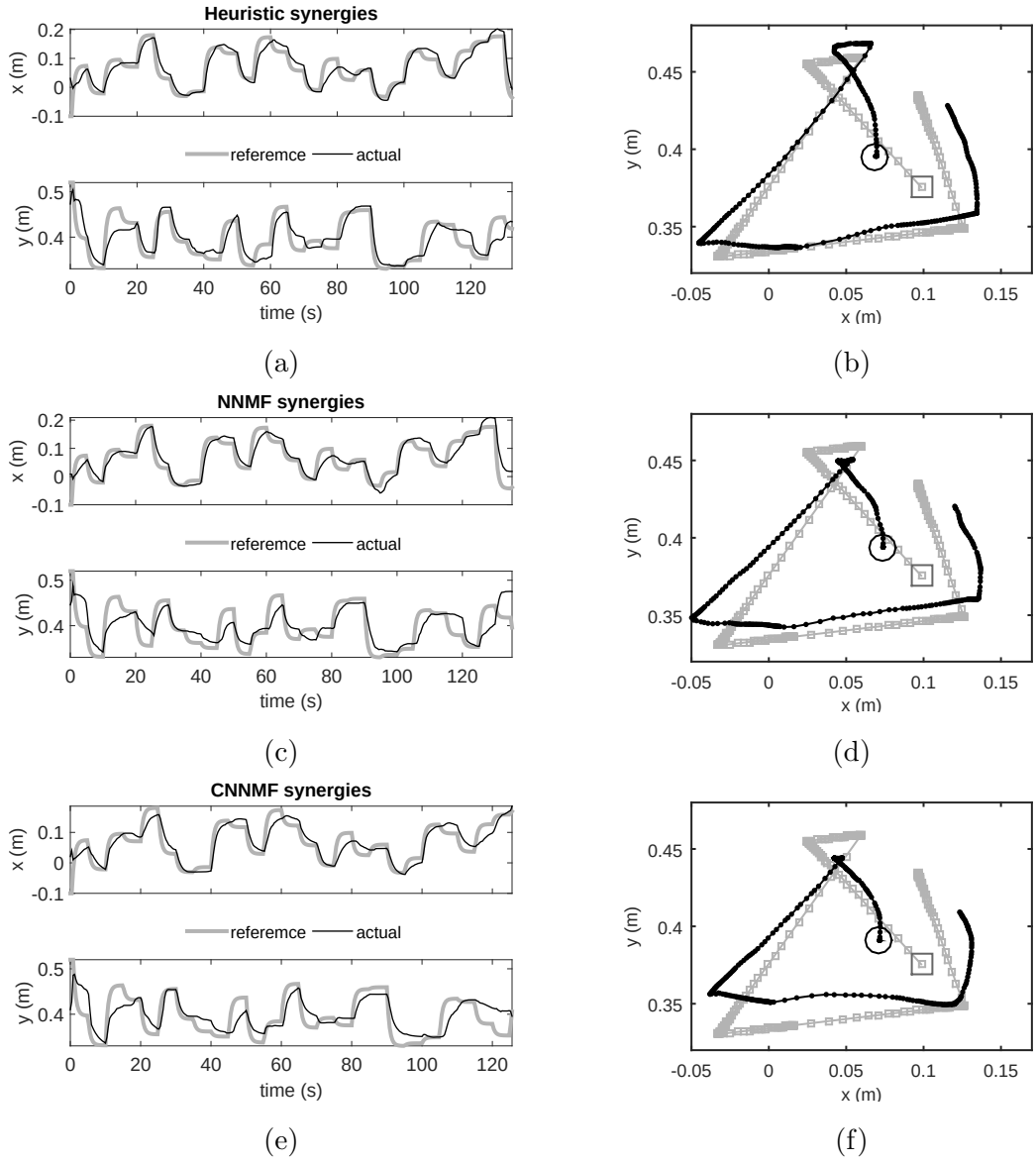

Figure 5.14: The feedback control performance resulting from the three synergy calculation methods. The plots on the left show the reference trajectories (thick grey lines) and the actual movements (thin black lines) of the hand versus time. The plots on the right show episodes of the randomly generated paths (grey) and the produced motion (black) in the experiments. The starting position is indicated by the a large circle and square.

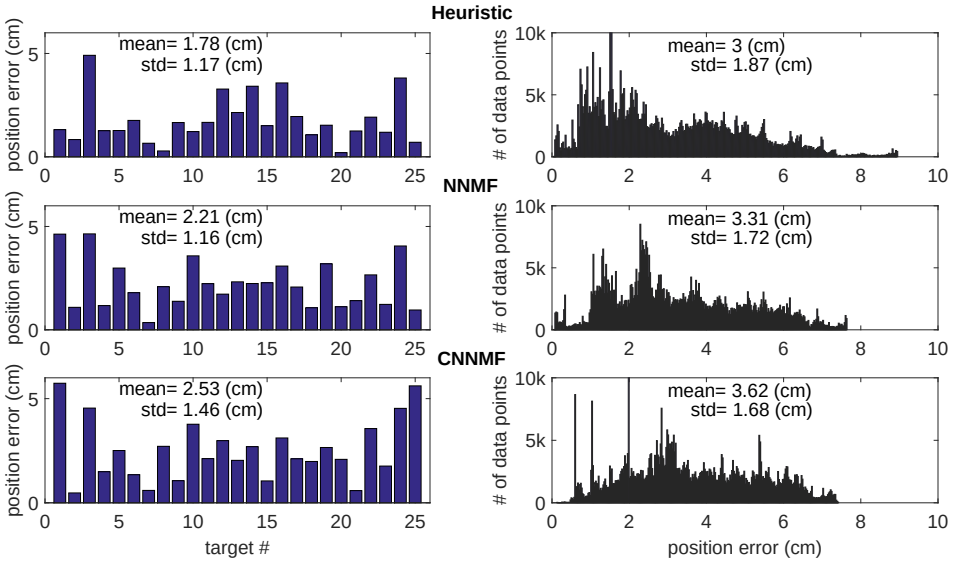

Figure 5.15: Left column (target error): the position error between the target and the actual hand position at the end of each reaching movement. Right column (path error): the histogram of the error in the entire duration of the movements. These plots show the number of sample times with the amount of error indicated by the horizontal axis. The mean and standard deviation of the error are also reported.

choice of the synergies.

No formal study was done on the effect of muscle fatigue on the performance of the FES controller. However, the informal observations revealed that the isometric force production accuracy and the tracking error worsens during the course of the experiment. The quality of the electrode pads also seemed to affect the reliability of the results. To compensate for these uncertainties, an on-line method can be used to re-train the muscle mappings, based on the inputs and the measurements. The development of such methods is beyond the scope of this thesis.

To improve the proposed controller performance, it is also possible to include the system dynamics in the calculations. As mentioned before, the hand and robot dynamics may

affect the results when F2A is used instead of A2A. Furthermore, all the information stored in the controller (in the form of the synergies and the basis set) belongs to isometric conditions. As a result, the controller performance further degrades when the velocities are not negligible. To account for the velocity dependent accelerations and inertia effects, the arm's equations of motion, as well as its model parameters are needed. Unfortunately, obtaining such information is time-consuming. In a clinical setting where therapy time is limited, one should weight the benefit of the improved control performance over the cost of the time spent on parameter identification.

The controller was tested on one healthy subject. Therefore, more trials are needed to comment on the generalizability of the results. Moreover, it is unclear how the controller will perform on clinical populations. Stroke patients, for example, may suffer from spastic muscles, which may adversely affect the FES controller performance.

5.6 Chapter conclusions

The application of the proposed motor control model to the feedback controller of functional electrical stimulation devices was presented. As an advantage, this control method only required information in a task space, which disentangles the control task from many of the complexities of the musculoskeletal system, allowing for fast feedback control of the motions. As a result, the proposed FES controller is the first of its kind that can be used to generate and control arbitrary movements in a task space. The experimental results showed that the synergy-based motor control model could be used to produce movement in the 2D task space.

Chapter 6

Concluding Remarks

6.1 Conclusion

In this thesis, I presented a novel motor control framework for the fast and efficient control of complex musculoskeletal systems. The proposed framework includes a hierarchical structure, with a high-level feedback controller in the task space, and a low-level controller to translate the task space commands to muscle activations.

An important feature of this motor control framework was its task space representation. The control loop was based on the *task space variables*—the kinematic variables that are controlled in a task, e.g. hand position in reaching movements. Since the task space controller was separated from the complex dynamics of the system, its structure could be very simple, and for most of the examples an error-driven PID controller was employed. The output of the task space controller was the acceleration (force in the experimental studies) that the hand had to have in order to finish the task.

The task space acceleration command was then translated into the needed muscle activations using a complex mapping (called acceleration-to-activation, A2A, mapping in this text). The A2A mapping could quickly estimate the required muscle activations by decomposing the reference acceleration vector onto a basis set of the task space. The basis

vectors themselves are the actions of a number of *muscle synergies* on the task space; i.e. the activation of each synergy produces a certain acceleration in the task space, which can be considered as a basis vector. Decomposition of the reference acceleration onto the basis set then defines how the synergies should be combined to calculate the muscle activations.

The two main assumptions in this motor control model are 1) dependency of the control structure (high-level controller, and the underlying muscle synergies) on the task; and 2) dependency of the muscle synergies on the posture. These two assumptions allowed for efficient control of movements in a variety of examples.

The musculoskeletal simulations showed the potential of the proposed motor control framework as a biologically plausible motion controller for predictive simulations. Another important application of this framework was shown to be the novel feedback controller for functional electrical stimulation devices.

6.2 Summary of contributions

In summary, this research has made the following contributions to the field of motor control modelling and rehabilitation:

Motor control modelling

- Developed a biologically plausible motor control framework based on muscle synergy
- Showed the potential of muscle synergies to control movements
- Implemented the real-time near-optimal controller for musculoskeletal systems
- Showed the potential of the motor control framework for subject-specific applications
- Introduced the task-based motor control architecture

Muscle synergy

- Introduced and implemented two methods to identify task-specific synergies (concatenated-NNMF and optimization-based)
- Implemented a constrained-NNMF algorithm to impose linear constraints on muscle synergy extraction methods
- Proposed the concept of posture-dependent synergies
- Introduced the importance of task on the definition of muscle synergies
- Introduced the concept of *orthogonal synergies* for kinematically redundant systems
- Presented an alternate method to choose the number of synergies based on the closed-loop control performance

Neuromuscular systems

- Provided insight into the possible mechanisms of human motor control through mathematical modelling
- Introduced constraints on the number of synergies based on the dimensions of the task space

Rehabilitation

- Developed the first of its kind feedback controller for FES devices
- Proposed a novel approach for subject-specific tuning of the FES controller

6.3 Recommendations for future research

Although the experimental trials evaluated the performance of the A2A mapping as a predictive tool, they were not conclusive whether the same principles are responsible in the human motor control system. More advanced experiments are required to reshape the proposed framework as a *motor control theory*.

Another interesting extension to the proposed framework is its application to rhythmic motions (i.e. gait). In the presented framework, the synergies were defined based on the task variables, which only included some kinematic variables (i.e. positions/angles). In rhythmic motions, time (or perhaps the phase in the rhythm cycle) is another important dimension that may influence the *best solution for muscle activations* (i.e. the synergies). Synergies as time-dependent patterns have been introduced before (e.g. by D'Avella and Tresch, 2001; D'Avella et al., 2008; Bizzi et al., 2008); this idea can be extended to define synergies not as fixed functions of time, but rather as flexible structures that change based on the phase of the cycle, as well as posture.

On the FES side, the logical next step is to test the proposed method on more subjects (possibly include clinical populations) to evaluate the sensitivity of the results to subject variability and other uncertainties that may arise in impaired patients.

The inclusion of an adaptive method to re-train the muscle mapping during the exercise (to account for muscle fatigue, the changes to the properties of electrode/skin interface, and other uncertainties) seems to be another important future step.

The presented FES controller worked well for the reaching movements in a 2D space. However, the activities of daily living mostly require reaching to points in the 3D space (e.g. bringing the hand to mouth). The proposed motor control framework is capable of handling another dimension in the task space; however, the presence of gravity (which destabilizes the arm) may challenge the controller.

FES seems to be an effective rehabilitation program for stroke and incomplete spinal cord injury patients, because it activates natural sensory and motor pathways in the peripheral nervous system (which is thought to expedite neuroplasticity). Concurrent activities in the peripheral and central nervous systems also seem to improve recovery. Thus, brain-computer interface devices (e.g. electroencephalogram, EEG) that monitor patients' cortical activities have gained attention in rehabilitation. The goal is to match the patient's *intentions* with the artificially produced movements to stimulate neuro-recovery. A third promising paradigm is the robotic rehabilitation, which targets an increased number

of repetitions (also a stimulant of neuroplasticity). Therefore, the combination of these three programs (FES, EEG, and robot) may be a game-changer in rehabilitation.

References

Abbas, J. J. and Chizeck, H. J. (1995). Neural network control of functional neuromuscular stimulation systems: computer simulation studies. *IEEE Transactions on Biomedical Engineering*, 42(11):1117–27.

Ajoudani, A. and Erfanian, A. (2009). A Neuro-Sliding Mode Control With Adaptive Modeling of Uncertainty for Control of Movement in Paralyzed Limbs Using Functional Electrical Stimulation. *IEEE Transactions on Biomedical Engineering*, 56(7):1771–1780.

Allen, J. L. and Neptune, R. R. (2012). Three-dimensional modular control of human walking. *Journal of biomechanics*, 45(12):2157–63.

Anderson, F. C. and Pandy, M. G. (2001). Dynamic Optimization of Human Walking. *Journal of Biomechanical Engineering*, 123(5):381.

Ashe, J. and Georgopoulos, A. P. (1994). Movement Parameters and Neural Activity in Motor Cortex and Area 5. *Cerebral Cortex*, 4(6):590–600.

Bauman, M. J., Bruns, T. M., Wagenaar, J. B., Gaunt, R. A., and Weber, D. J. (2011). Online feedback control of functional electrical stimulation using dorsal root ganglia recordings. *Conference proceedings : ... Annual International Conference of the IEEE Engineering in Medicine and Biology Society. IEEE Engineering in Medicine and Biology Society. Conference*, 2011:7246–9.

Behringer, M., Franz, A., McCourt, M., and Mester, J. (2014). Motor point map of upper body muscles. *European Journal of Applied Physiology*, 114(8):1605–1617.

Berger, D. J. and D'Avella, A. (2014). Effective force control by muscle synergies. *Frontiers in computational neuroscience*, 8(April):46.

Berniker, M., Jarc, A., Bizzi, E., and Tresch, M. C. (2009). Simplified and effective motor control based on muscle synergies to exploit musculoskeletal dynamics. *Proceedings of the National Academy of Sciences of the United States of America*, 106(18):7601–6.

Bernstein, M. (1967). *The co-ordination and regulation of movements.* Pergamon Press, Oxford, New York, 1st edition.

Bizzi, E., Cheung, V. C. K., D'Avella, A., Saltiel, P., and Tresch, M. C. (2008). Combining modules for movement. *Brain Research Reviews*, 57(1):125–33.

Bizzi, E., Mussa-Ivaldi, F. A., and Giszter, S. (1991). Computations underlying the execution of movement: a biological perspective. *Science*, 253(5017):287–291.

Blana, D., Kirsch, R. F., and Chadwick, E. K. (2009). Combined feedforward and feedback control of a redundant, nonlinear, dynamic musculoskeletal system. *Medical & Biological Engineering & Computing*, 47(5):533–542.

Boettcher, C. E., Ginn, K. A., and Cathers, I. (2008). Standard maximum isometric voluntary contraction tests for normalizing shoulder muscle EMG. *Journal of Orthopaedic Research*, 26(12):1591–1597.

Boline, J. and Ashe, J. (2005). On the relations between single cell activity in the motor cortex and the direction and magnitude of three-dimensional dynamic isometric force. *Experimental Brain Research*, 167(2):148–159.

Cheung, V. C. K., D'Avella, A., Tresch, M. C., and Bizzi, E. (2005). Central and sensory contributions to the activation and organization of muscle synergies during natural

motor behaviors. *The Journal of Neuroscience : the Official Journal of the Society for Neuroscience*, 25(27):6419–34.

Crago, P. E., Memberg, W. D., Usey, M. K., Keith, M. W., Kirsch, R. F., Chapman, G. J., Katorgi, M. A., and Perreault, E. J. (1998). An elbow extension neuroprosthesis for individuals with tetraplegia. *IEEE Transactions on Rehabilitation Engineering*, 6(1):1–6.

D'Avella, A., Fernandez, L., Portone, A., and Lacquaniti, F. (2008). Modulation of phasic and tonic muscle synergies with reaching direction and speed. *Journal of neurophysiology*, 100(3):1433–54.

D'Avella, A. and Tresch, M. C. (2001). Modularity in the motor system: decomposition of muscle patterns as combinations of time-varying synergies. In *Advances in Neural Information Processing Systems 14: Proceedings of the 2001 Conference*, volume 14, Vancouver, British Columbia, Canada.

de Rugy, A. (2010). Generalization of visuomotor adaptation to different muscles is less efficient: Experiment and model. *Human Movement Science*, 29(5):684–700.

de Rugy, A., Loeb, G. E., and Carroll, T. J. (2012). Muscle Coordination Is Habitual Rather than Optimal. *Journal of Neuroscience*, 32(21):7384–7391.

de Rugy, A., Loeb, G. E., and Carroll, T. J. (2013). Are muscle synergies useful for neural control? *Frontiers in Computational Neuroscience*, 7(March):1–13.

Delis, I., Panzeri, S., Pozzo, T., and Berret, B. (2014). A unifying model of concurrent spatial and temporal modularity in muscle activity. *Journal of neurophysiology*, 111(3):675–93.

DeWolf, T. and Eliasmith, C. (2011). The neural optimal control hierarchy for motor control. *Journal of Neural Engineering*, 8(6):065009.

Emadi Andani, M., Bahrami, F., Jabehdar Maralani, P., and Ijspeert, A. J. (2009). MODEM: a multi-agent hierarchical structure to model the human motor control system. *Biological cybernetics*, 101(5-6):361–77.

Erdemir, A., McLean, S., Herzog, W., and van den Bogert, A. J. (2007). Model-based estimation of muscle forces exerted during movements. *Clinical Biomechanics (Bristol, Avon)*, 22(2):131–154.

Feldman, A. and Levin, M. (2009). The equilibrium-point hypothesispast, present and future. *Progress in Motor Control*, 629.

Freeman, C. T., Hughes, A.-M., Burridge, J. H., Chappell, P. H., Lewin, P. L., and Rogers, E. (2009). A model of the upper extremity using FES for stroke rehabilitation. *Journal of Biomechanical Engineering*, 131(3):031011.

Fu, K. C. D., Libera, F. D., and Ishiguro, H. (2015). Extracting motor synergies from random movements for low-dimensional task-space control of musculoskeletal robots. *Bioinspiration & Biomimetics*, 10(5):056016.

Garner, B. A. and Pandy, M. G. (2001). Musculoskeletal Model of the Upper Limb Based on the Visible Human Male Dataset. *Computer Methods in Biomechanics and Biomedical Engineering*, 4(2):93–126.

Gentner, R., Edmunds, T., Pai, D. K., and D'Avella, A. (2013). Robustness of muscle synergies during visuomotor adaptation. *Frontiers in Computational Neuroscience*, 7(September):120.

Georgopoulos, A. P., Kettner, R. E., and Schwartz, a. B. (1988). Primate motor cortex and free arm movements to visual targets in three-dimensional space. II. Coding of the direction of movement by a neuronal population. *Journal of Neuroscience*, 8(8):2928–2937.

Georgopoulos, A. P., Schwartz, A. B., and Kettner, R. E. (1986). Neuronal population coding of movement direction. *Science*, 233(1986):1416–1419.

Ghannadi, B., Mehrabi, N., and McPhee, J. (2015). Development of a Human-Robot Dynamic Model to Support Model-Based Control Design of an Upper Limb Rehabilitation Robot. In *ECCOMAS Thematic Conference on Multibody Dynamics*, Barcelona, Spain.

Gomi, H. and Kawato, M. (1993). Recognition of manipulated objects by motor learning with modular architecture networks. *Neural Networks*, 6:485–497.

Grewal, T. J. and Dickerson, C. R. (2013). A novel three-dimensional shoulder rhythm definition that includes overhead and axially rotated humeral postures. *Journal of Biomechanics*, 46(3):608–611.

Haruno, M., Wolpert, D. M., and Kawato, M. (2001). Mosaic model for sensorimotor learning and control. *Neural computation*, 13(10):2201–20.

Haruno, M., Wolpert, D. M., and Kawato, M. (2003). Hierarchical MOSAIC for movement generation. *International Congress Series*, 1250:575–590.

Ijspeert, A. J. (2008). Central pattern generators for locomotion control in animals and robots: a review. *Neural networks : the official journal of the International Neural Network Society*, 21(4):642–53.

Ivanenko, Y. P., Poppele, R. E., and Lacquaniti, F. (2006). Motor control programs and walking. *The Neuroscientist : a review journal bringing neurobiology, neurology and psychiatry*, 12(4):339–48.

Jagodnik, K. M., Blana, D., van den Bogert, A. J., and Kirsch, R. F. (2015). An optimized proportional-derivative controller for the human upper extremity with gravity. *Journal of Biomechanics*, 48(13):3701–3709.

Jagodnik, K. M. and van den Bogert, A. J. (2010). Optimization and evaluation of a proportional derivative controller for planar arm movement. *Journal of Biomechanics*, 43(6):1086–1091.

Kakei, S., Hoffman, D. S., and Strick, P. L. (1999). Muscle and movement representations in the primary motor cortex. *Science (New York, N.Y.)*, 285(5436):2136–2139.

Kapadia, N. M., Nagai, M. K., Zivanovic, V., Bernstein, J., Woodhouse, J., Rumney, P., and Popovic, M. R. (2014). Functional Electrical Stimulation Therapy for Recovery of Reaching and Grasping in Severe Chronic Pediatric Stroke Patients. *Journal of Child Neurology*, 29(4):493–499.

Kargo, W. J., Ramakrishnan, A., Hart, C. B., Rome, L. C., and Giszter, S. F. (2010). A simple experimentally based model using proprioceptive regulation of motor primitives captures adjusted trajectory formation in spinal frogs. *Journal of neurophysiology*, 103(1):573–90.

Kettner, R. E., Schwartz, a. B., and Georgopoulos, A. P. (1988). Primate motor cortex and free arm movements to visual targets in three-dimensional space. III. Positional gradients and population coding of movement direction from various movement origins. *Journal of Neuroscience*, 8(8):2938–2947.

Kirk, D. E. (2004). *Optimal Control Theory: An Introduction*. Dover Books on Electrical Engineering Series. Dover Publications, Mineola, New York.

Kirsch, N., Alibeji, N., and Sharma, N. (2015). Nonlinear Model Predictive Control of Functional Electrical Stimulation. In *Volume 2: Diagnostics and Detection; Drilling; Dynamics and Control of Wind Energy Systems; Energy Harvesting; Estimation and Identification; Flexible and Smart Structure Control; Fuels Cells/Energy Storage; Human Robot Interaction; HVAC Building Energy M*, page V002T27A005. ASME.

Kirsch, N., Alibeji, N., and Sharma, N. (2017). Nonlinear model predictive control of functional electrical stimulation. *Control Engineering Practice*, 58:319–331.

Kutch, J. J., Kuo, A. D., Bloch, A. M., and Rymer, W. Z. (2008). Endpoint Force Fluctuations Reveal Flexible Rather Than Synergistic Patterns of Muscle Cooperation. *Journal of Neurophysiology*, 100(5):2455–2471.

Kutch, J. J. and Valero-Cuevas, F. J. (2012). Challenges and new approaches to proving the existence of muscle synergies of neural origin. *PLoS computational biology*, 8(5):e1002434.

Latash, M., Levin, M., Scholz, J., and Schöner, G. (2010). Motor control theories and their applications. *Medicina (Kaunas, ...*, 46(6):382–392.

Lee, D. D. and Seung, H. S. (2000). Algorithms for non-negative matrix factorization. *Advances in Neural Information Processing Systems*, 13(1):556–562.

Lillicrap, T. P. and Scott, S. H. (2013). Preference Distributions of Primary Motor Cortex Neurons Reflect Control Solutions Optimized for Limb Biomechanics. *Neuron*, 77(1):168–179.

Liu, D. and Todorov, E. (2009). Hierarchical optimal control of a 7-DOF arm model. In *2009 IEEE Symposium on Adaptive Dynamic Programming and Reinforcement Learning*, number 2, pages 50–57. IEEE.

Lockhart, D. B. and Ting, L. H. (2007). Optimal sensorimotor transformations for balance. *Nature Neuroscience*, 10(10):1329–36.

Loeb, G. E. (2012). Optimal isn't good enough. *Biological cybernetics*, 106(11-12):757–65.

Lynch, C. L. and Popovic, M. R. (2008). Functional Electrical Stimulation. *IEEE Control Systems Magazine*, 28(2):40–50.

Lynch, C. L. and Popovic, M. R. (2012). A comparison of closed-loop control algorithms for regulating electrically stimulated knee movements in individuals with spinal cord injury. *IEEE transactions on neural systems and rehabilitation engineering : a publication of the IEEE Engineering in Medicine and Biology Society*, 20(4):539–48.

McKay, J. L. and Ting, L. H. (2008). Functional muscle synergies constrain force production during postural tasks. *Journal of biomechanics*, 41(2):299–306.

Mehrabi, N., Sharif Razavian, R., Ghannadi, B., and McPhee, J. (2017). Predictive Simulation of Reaching Moving Targets Using Nonlinear Model Predictive Control. *Frontiers in Computational Neuroscience*, 10(143).

Mehrabi, N., Sharif Razavian, R., and McPhee, J. (2013). A Three-Dimensional Musculoskeletal Driver Model to Study Steering Tasks. In *Proceedings of the ASME 2013 International Design Engineering Technical Conferences and Computers and Information in Engineering Conference IDETC/CIE 2013*, volume 7A, pages 1–8, Portland, Oregon, USA. ASME.

Mehrabi, N., Sharif Razavian, R., and McPhee, J. (2015a). A Physics-Based Musculoskeletal Driver Model to Study Steering Tasks. *Journal of Computational and Nonlinear Dynamics*, 10(2):021012.

Mehrabi, N., Sharif Razavian, R., and McPhee, J. (2015b). Steering disturbance rejection using a physics-based neuromusculoskeletal driver model. *Vehicle System Dynamics*, 53(10):1393–1415.

Meyer, A. J., Eskinazi, I., Jackson, J. N., Rao, A. V., Patten, C., and Fregly, B. J. (2016). Muscle Synergies Facilitate Computational Prediction of Subject-Specific Walking Motions. *Frontiers in Bioengineering and Biotechnology*, 4:77.

Moghadam, M. N., Aminian, K., Asghari, M., and Parnianpour, M. (2013). How well do the muscular synergies extracted via non-negative matrix factorisation explain the variation of torque at shoulder joint? *Computer methods in biomechanics and biomedical engineering*, 16(3):291–301.

Moran, D. and Schwartz, A. B. (1999). Motor Cortical Representation of Speed and Direction During Reaching. *Journal of Neurophysiology*, 82:2676–2692.

Morasso, P. (1981). Spatial control of arm movements. *Experimental Brain Research*, 42:223–227.

Neptune, R. R., Clark, D. J., and Kautz, S. A. (2009). Modular control of human walking: a simulation study. *Journal of Biomechanics*, 42(9):1282–7.

Park, H. and Durand, D. M. (2008). Motion control of musculoskeletal systems with redundancy. *Biological Cybernetics*, 99(6):503–16.

Perotto, A. and Delagi, E. F. (2011). *Anatomical guide for the electromyographer : the limbs and trunk*. Charles C Thomas, Springfield, Illinois, 5 edition.

Piazza, S., Torricelli, D., Brunetti, F., Del-Ama, a. J., Gil-Agudo, A., and Pons, J. L. (2012). A novel FES control paradigm based on muscle synergies for postural rehabilitation therapy with hybrid exoskeletons. *Conference proceedings : ... Annual International Conference of the IEEE Engineering in Medicine and Biology Society. IEEE Engineering in Medicine and Biology Society. Conference*, 2012:1868–71.

Popovic, D. and Popovic, M. (1998). Tuning of a nonanalytical hierarchical control system for reaching with FES. *IEEE Transactions on Biomedical Engineering*, 45(2):203–212.

Popovic, D. and Popovic, M. (2007). Control for therapeutic functional electrical stimulation. In *11th Mediterranean Conference on Medical and Biomedical Engineering and Computing*, pages 3–6.

Popovic, M. and Popovic, D. (2001). Cloning biological synergies improves control of elbow neuroprostheses: Simulating natural control of the extremities using inductive learning. *IEEE Engineering in Medicine and Biology Magazine*, 20(1):74–81.

Previdi, F. (2002). Identification of black-box nonlinear models for lower limb movement control using functional electrical stimulation. *Control Engineering Practice*, 10(1):91–99.

Raphael, G., Tsianos, G. a., and Loeb, G. E. (2010). Spinal-like regulator facilitates control of a two-degree-of-freedom wrist. *The Journal of neuroscience : the official journal of the Society for Neuroscience*, 30(28):9431–9444.

Roh, J., Cheung, V. C. K., and Bizzi, E. (2011). Modules in the brain stem and spinal cord underlying motor behaviors. *Journal of neurophysiology*, 106(3):1363–78.

Safavynia, S. A., Torres-Oviedo, G., and Ting, L. H. (2011). Muscle Synergies: Implications for Clinical Evaluation and Rehabilitation of Movement. *Topics in spinal cord injury rehabilitation*, 17(1):16–24.

Sartori, M., Gizzi, L., Lloyd, D. G., and Farina, D. (2013). A musculoskeletal model of human locomotion driven by a low dimensional set of impulsive excitation primitives. *Frontiers in computational neuroscience*, 7(June):79.

Schearer, E. M., Liao, Y.-W., Perreault, E. J., Tresch, M., Memberg, W. D., Kirsch, R. F., and Lynch, K. M. (2016). Semiparametric Identification of Human Arm Dynamics for Flexible Control of a Functional Electrical Stimulation Neuroprosthesis. *IEEE Transactions on Neural Systems and Rehabilitation Engineering*, 24(April):1–1.

Schearer, E. M., Liao, Y.-W., Perreault, E. J., Tresch, M. C., Memberg, W. D., Kirsch, R. F., and Lynch, K. M. (2014). Multi-Muscle FES Force Control of the Human Arm for Arbitrary Goals. *IEEE Transactions on Neural Systems and Rehabilitation Engineering*, 22(3):654–663.

Schearer, E. M., Liao, Y.-W., Perreault, E. J., Tresch, M. C., Memberg, W. D., Kirsch, R. F., and Lynch, K. M. (2015). Evaluation of a Semi-Parametric Model for High-Dimensional FES Control. *2015 7Th International Ieee/Embs Conference on Neural Engineering (Ner)*, pages 304–307.

Scholz, J. and Schöner, G. (1999). The uncontrolled manifold concept: identifying control variables for a functional task. *Experimental Brain Research. Experimentelle Hirnforschung. Expérimentation cérébrale*, 126(3):289–306.

Schwartz, A. B., Kettner, R. E., and Georgopoulos, A. P. (1988). Primate motor cortex and free arm movements to visual targets in three-dimensional space. I. Relations

between single cell discharge and direction of movement. *Journal of Neuroscience*, 8(August):2913–2927.

Sharif Razavian, R. and McPhee, J. (2015). Minimization of Muscle Fatigue as the Criterion to Solve Muscle Forces-Sharing Problem. In *Volume 1: Adaptive and Intelligent Systems Control; Advances in Control Design Methods; Advances in Non-Linear and Optimal Control; Advances in Robotics; Advances in Wind Energy Systems; Aerospace Applications; Aerospace Power Optimization; Assistive Robo*, page V001T15A001. ASME.

Sharif Razavian, R., Mehrabi, N., and McPhee, J. (2015). A Neuronal Model of Central Pattern Generator to Account for Natural Motion Variation. *Journal of Computational and Nonlinear Dynamics*, 11(2):021007.

Sharif Shourijeh, M. and McPhee, J. (2013). Optimal Control and Forward Dynamics of Human Periodic Motions Using Fourier Series for Muscle Excitation Patterns. *Journal of Computational and Nonlinear Dynamics*, 9(2):021005.

Sharif Shourijeh, M. and McPhee, J. (2014). Forward Dynamic Optimization of Human Gait Simulations: A Global Parameterization Approach. *Journal of Computational and Nonlinear Dynamics*, 9(3):031018.

Sharif Shourijeh, M., Mehrabi, N., and McPhee, J. (2015). Using Static Optimization in Forward Dynamic Simulation of Human Musculoskeletal Systems. In *In Proceedings of the ASME 2015 International Design Engineering Technical Conferences, 2015*, page 8 pages, Boston, MA. ASME.

Sharif Shourijeh, M., Mehrabi, N., and McPhee, J. (2017). Forward Static Optimization in Dynamic Simulation of Human Musculoskeletal Systems: A Proof-of-Concept Study. *Journal of Computational and Nonlinear Dynamics*, (c).

Sharif Shourijeh, M., Smale, K. B., Potvin, B. M., and Benoit, D. L. (2016). A forward-muscular inverse-skeletal dynamics framework for human musculoskeletal simulations. *Journal of Biomechanics*, 49(9):1718–1723.

Shourijeh, M. S., Flaxman, T. E., and Benoit, D. L. (2016). An approach for improving repeatability and reliability of non-negative matrix factorization for muscle synergy analysis. *Journal of Electromyography and Kinesiology*, 26:36–43.

Shourijeh, M. S., Sharif Razavian, R., and McPhee, J. (2017). Estimation of Maximum Finger Tapping Frequency Using Musculoskeletal Dynamic Simulations. *Journal of Computational and Nonlinear Dynamics*, 12(5):051009.

Smale, K. B., Shourijeh, M. S., and Benoit, D. L. (2016). Use of muscle synergies and wavelet transforms to identify fatigue during squatting. *Journal of Electromyography and Kinesiology*, 28:158–166.

Sohn, M. H. and Ting, L. H. (2016). Suboptimal muscle synergy activation patterns generalize their motor function across postures. *Frontiers in Computational Neuroscience*, 10(February):1–15.

Steele, K. M., Rozumalski, A., and Schwartz, M. H. (2015). Muscle synergies and complexity of neuromuscular control during gait in cerebral palsy. *Developmental Medicine & Child Neurology*, pages n/a–n/a.

Steele, K. M., Tresch, M. C., and Perreault, E. J. (2013). The number and choice of muscles impact the results of muscle synergy analyses. *Frontiers in computational neuroscience*, 7(August):105.

Thelen, D. G. (2003). Adjustment of Muscle Mechanics Model Parameters to Simulate Dynamic Contractions in Older Adults. *Journal of Biomechanical Engineering*, 125(1):70.

Thrasher, T. A., Zivanovic, V., McIlroy, W., and Popovic, M. R. (2008). Rehabilitation of Reaching and Grasping Function in Severe Hemiplegic Patients Using Functional Electrical Stimulation Therapy. *Neurorehabilitation and Neural Repair*, 22(6):706–14.

Ting, L. H. (2007). Dimensional reduction in sensorimotor systems: a framework for understanding muscle coordination of posture. *Progress in brain research*, 165:299–321.

Ting, L. H. and Macpherson, J. M. (2005). A limited set of muscle synergies for force control during a postural task. *Journal of neurophysiology*, 93(1):609–13.

Ting, L. H. and McKay, J. L. (2007). Neuromechanics of muscle synergies for posture and movement. *Current Opinion in Neurobiology*, 17(6):622–8.

Todorov, E. and Jordan, M. I. (2002a). A Minimal Intervention Principle for Coordinated Movement. In *Advances in Neural Information Processing Systems: Proceedings of the 2002 Conference*, pages 27–34.

Todorov, E. and Jordan, M. I. (2002b). Optimal feedback control as a theory of motor coordination. *Nature Neuroscience*, 5(11):1226–1235.

Todorov, E., Li, W., and Pan, X. (2005). From task parameters to motor synergies: A hierarchical framework for approximately optimal control of redundant manipulators. *Journal of robotic systems*, 22(11):691–710.

Torres-Oviedo, G. (2006). Muscle Synergy Organization Is Robust Across a Variety of Postural Perturbations. *Journal of Neurophysiology*, 96(3):1530–1546.

Tresch, M. C., Cheung, V. C. K., and D'Avella, A. (2006). Matrix factorization algorithms for the identification of muscle synergies: evaluation on simulated and experimental data sets. *Journal of Neurophysiology*, 95(4):2199–212.

Tresch, M. C. and Jarc, A. (2009). The case for and against muscle synergies. *Current Opinion in Neurobiology*, 19(6):601–607.

Valero-Cuevas, F. J., Hoffmann, H., Kurse, M. U., Kutch, J. J., and Theodorou, E. A. (2009a). Computational Models for Neuromuscular Function. *IEEE reviews in biomedical engineering*, 2:110–135.

Valero-Cuevas, F. J., Venkadesan, M., and Todorov, E. (2009b). Structured variability of muscle activations supports the minimal intervention principle of motor control. *Journal of neurophysiology*, 102(1):59–68.

Walter, J. P., Kinney, A. L., Banks, S. a., D'Lima, D. D., Besier, T. F., Lloyd, D. G., and Fregly, B. J. (2014). Muscle synergies may improve optimization prediction of knee contact forces during walking. *Journal of Biomechanical Engineering*, 136(2):021031.

Zariffa, J., Steeves, J., and Pai, D. K. (2012). Changes in hand muscle synergies in subjects with spinal cord injury: Characterization and functional implications. *Journal of Spinal Cord Medicine*, 35(5):310–318.

Zelik, K. E., La Scaleia, V., Ivanenko, Y. P., and Lacquaniti, F. (2014). Can modular strategies simplify neural control of multidirectional human locomotion? *Journal of neurophysiology*, 111(8):1686–702.

APPENDICES

Appendix A

Experiment 1 Results

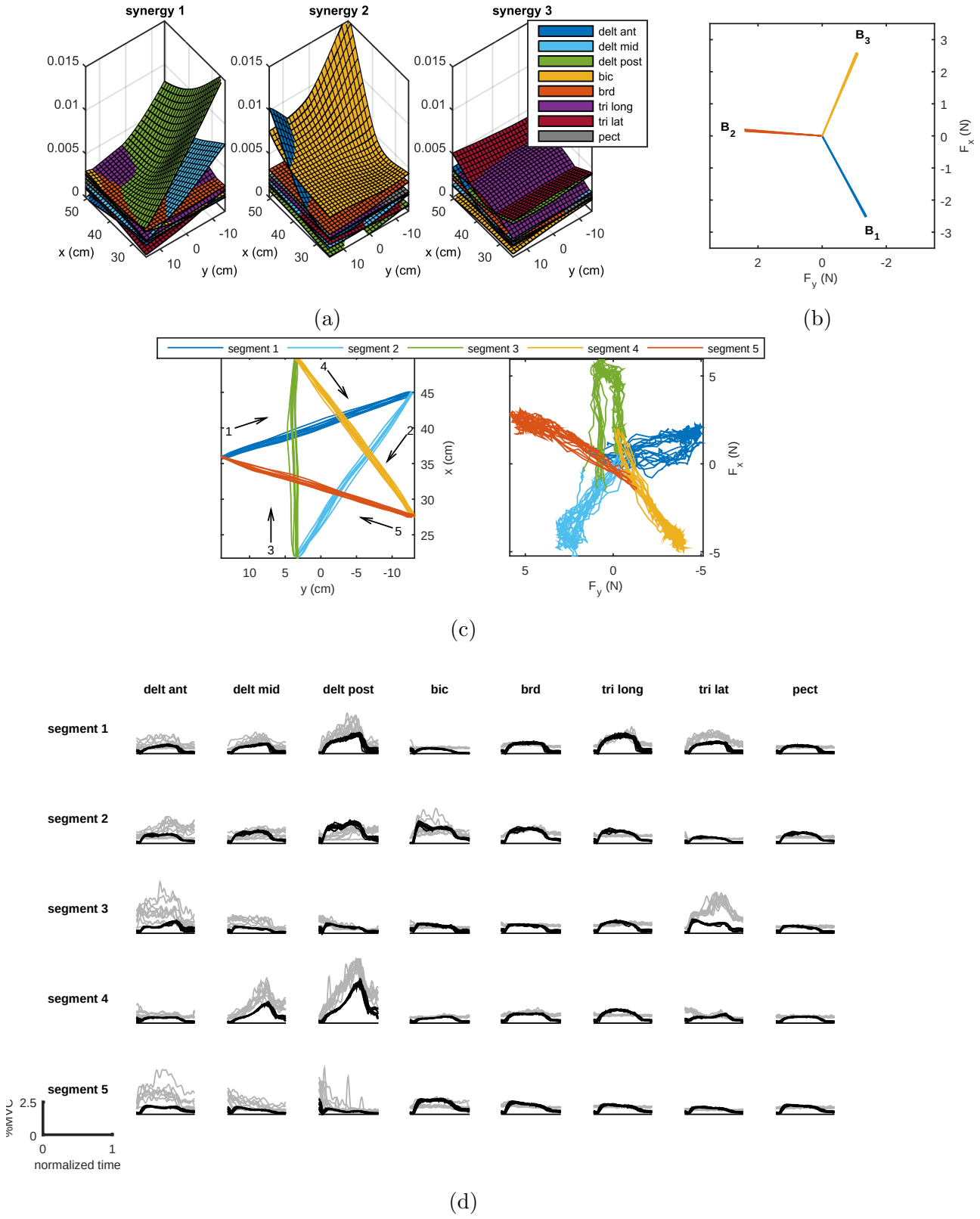

Figure A.1: The experiment #1 results, belonging to subject #1. For descriptions, see caption of Figure 3.10

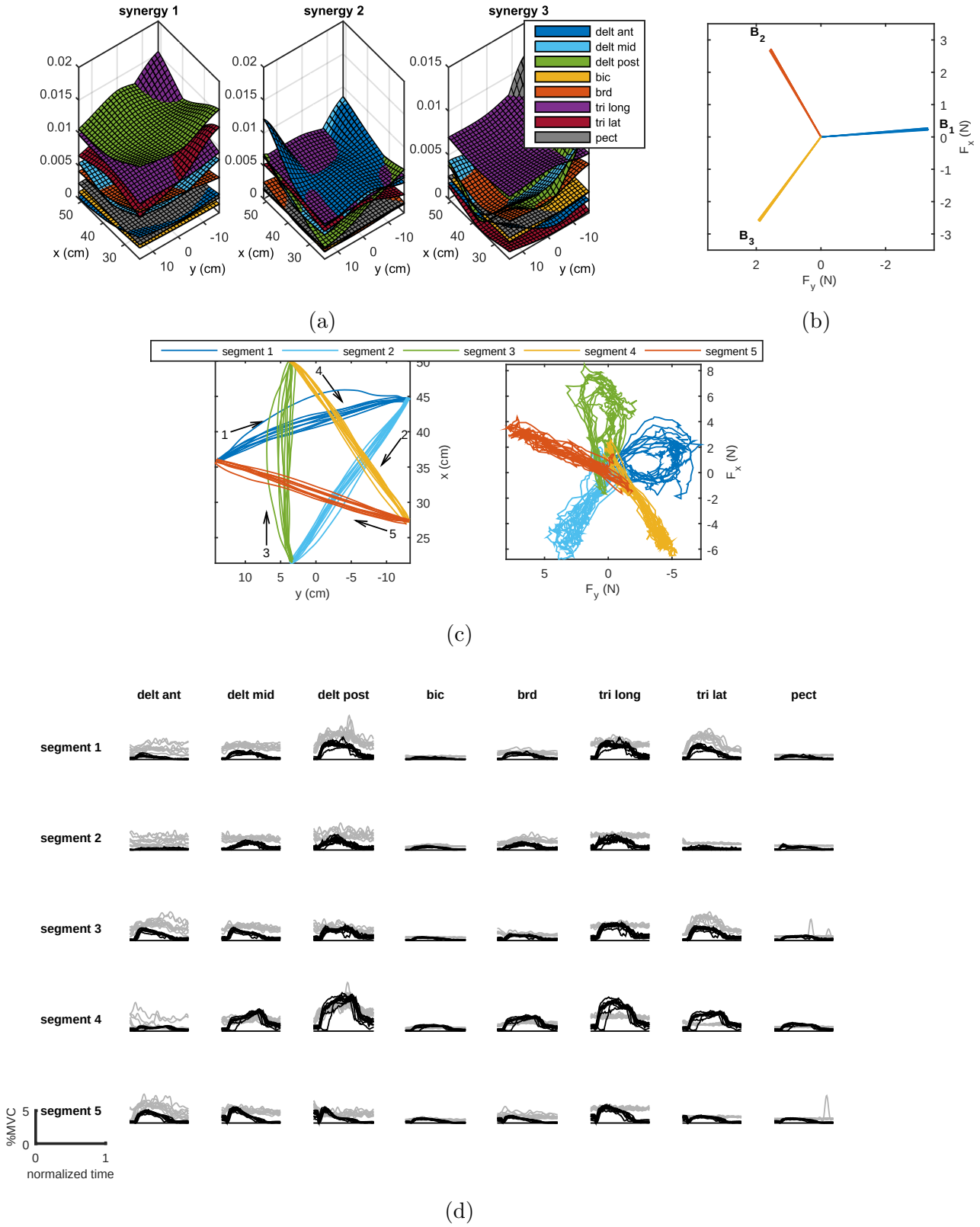

Figure A.2: The experiment #1 results, belonging to subject #2. For descriptions, see caption of Figure 3.10

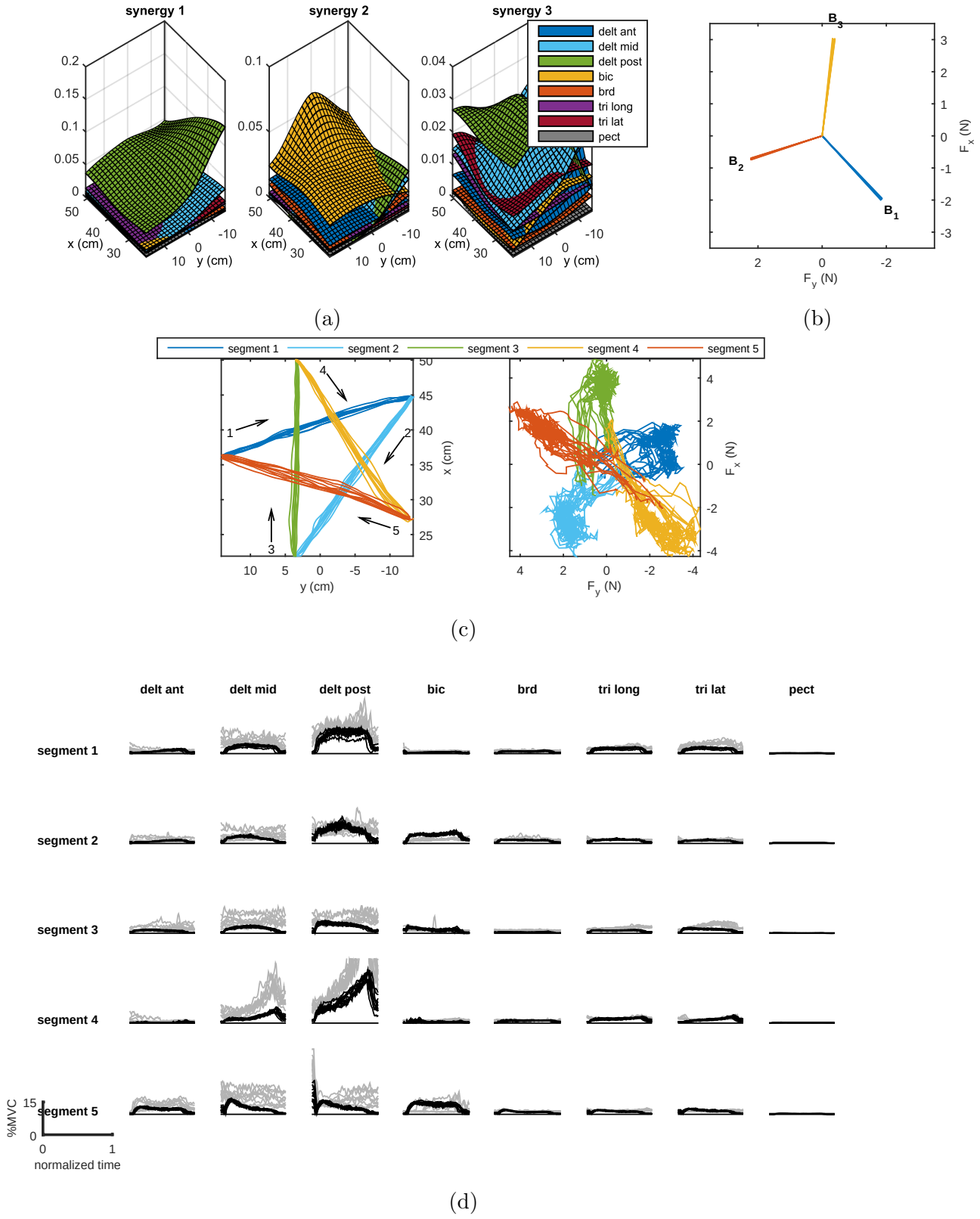

Figure A.3: The experiment #1 results, belonging to subject #3. For descriptions, see caption of Figure 3.10

Appendix B

Experiment 2 Results

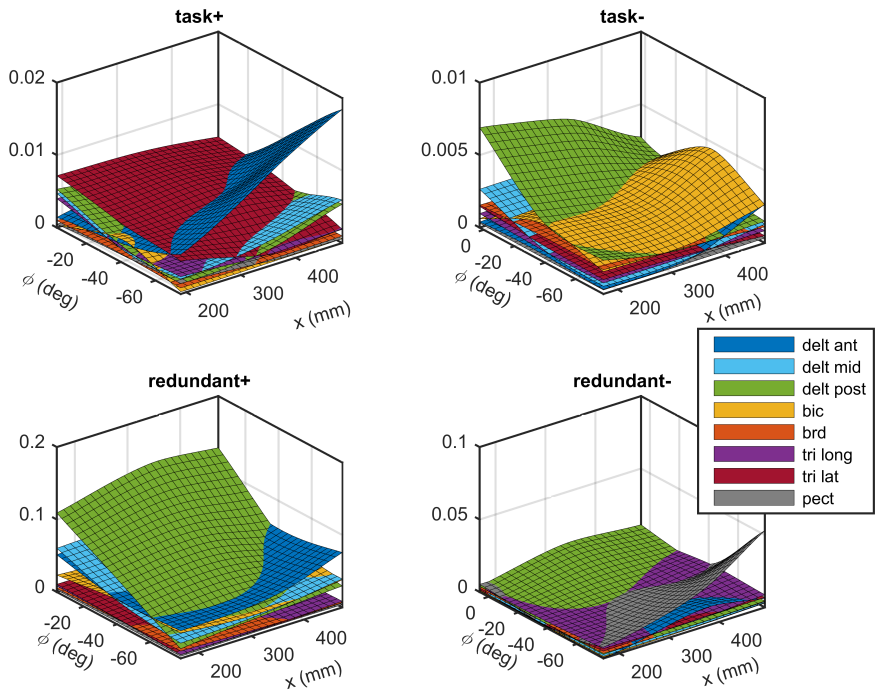

Figure B.1: The experiment #2 results, belonging to subject #1. For descriptions, see caption of Figure 3.14

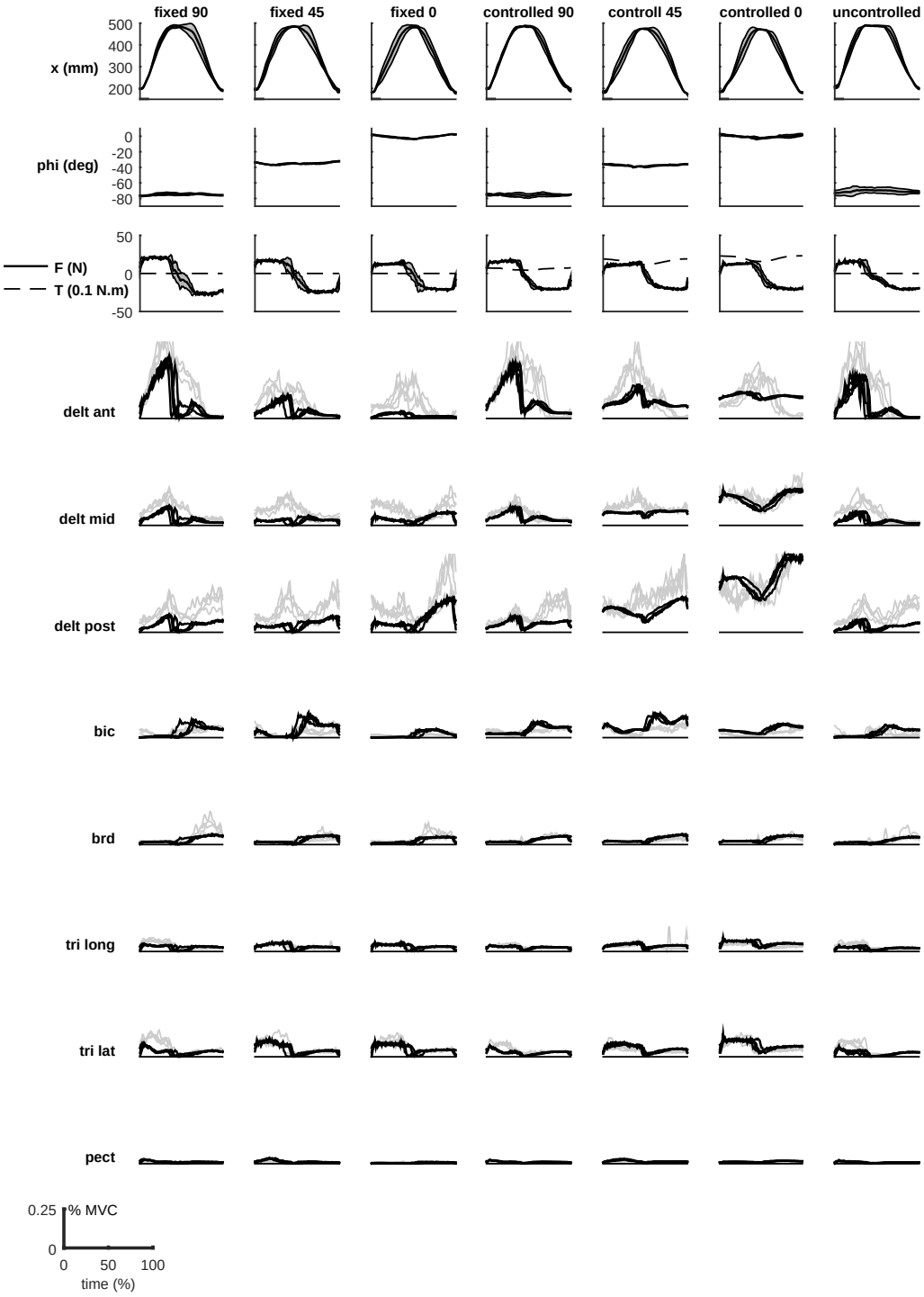

Figure B.2: The experiment #2 results, belonging to subject #1. For description, see caption of Figure 3.15

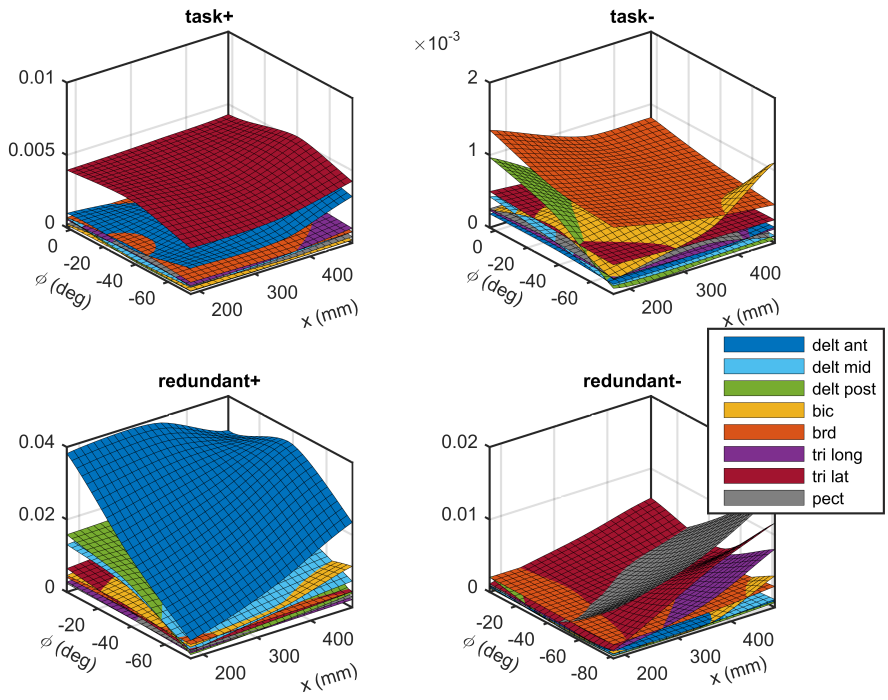

Figure B.3: The experiment #2 results, belonging to subject #2. For descriptions, see caption of Figure 3.14

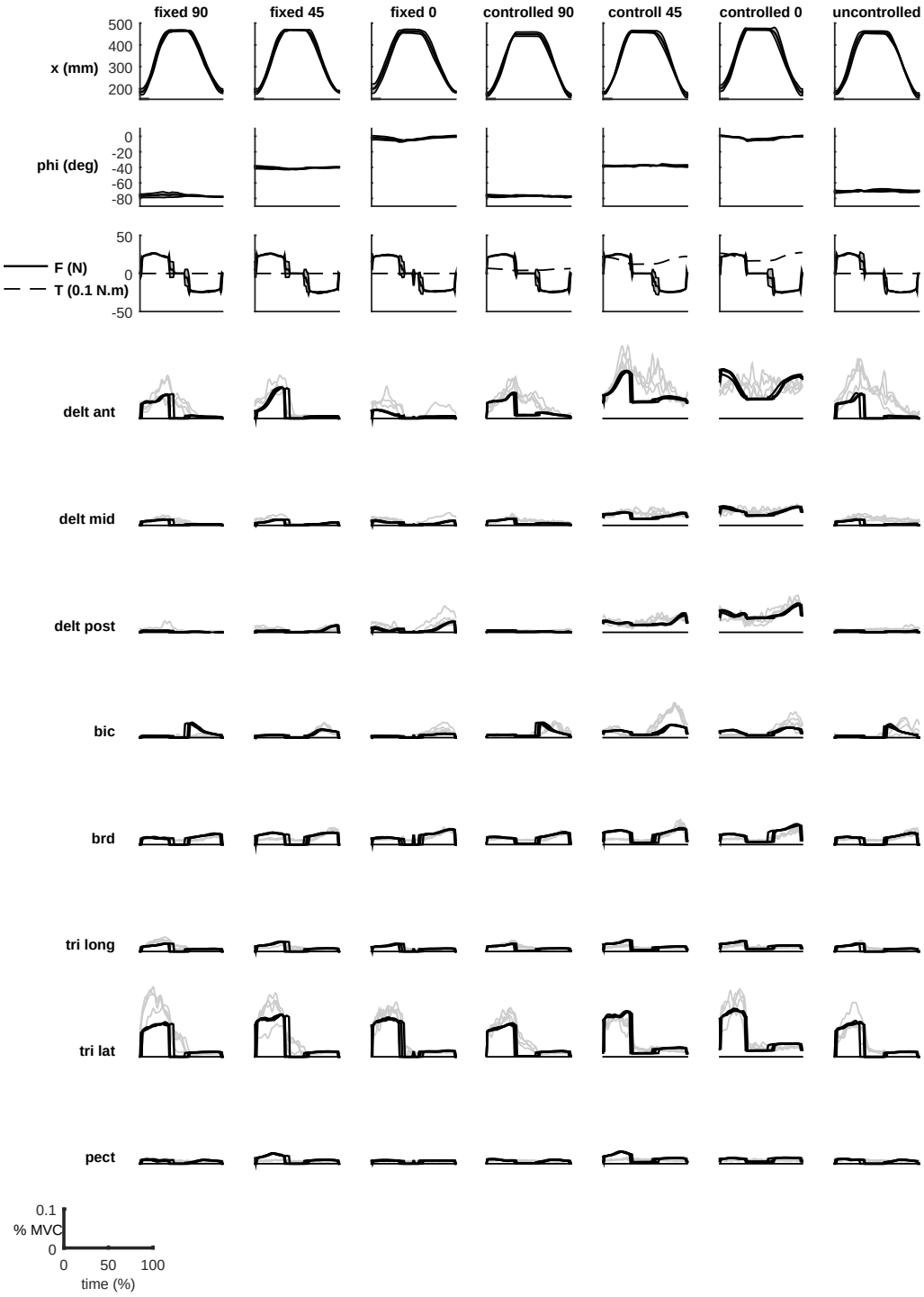

Figure B.4: The experiment #2 results, belonging to subject #2. For description, see caption of Figure 3.15

Appendix C

Experimental procedude details

C.1 Maximum voluntary contractions

To measure the EMG signals during the maximum voluntary contractions, the procedures described in Boettcher et al. (2008) are followed. The relevant information is restated in Table C.1. In these tests, the subject was asked to exert as much force as he/she can in the specified direction.

C.2 Surface EMG sensor locations

To place the surface EMG electrode, the locations recommended by SENIAM (Surface ElectroMyoGraphy for the Non-Invasive Assessment of Muscles, URL: http://www.seniam.org/) were used for anterior/middle/posterior deltoid, long/lateral heads of triceps brachii, and biceps brachii. For the brachiradialis and pectoralis major, the recommendations by Perotto and Delagi (2011) were used. Skin preparation includes shaving of the sensor area and cleaning with rubbing alcohol.

C.3 FES electrode locations

The FES electrode pads were placed on the muscle motor points, as recommended by Behringer et al. (2014). The electrodes might be moved to reduce discomfort during stimulations. The skin was cleaned with rubbing alcohol before attaching the electrodes.

Table C.1: The MVC test protocols used in the experiments

#	Muscle	MVC test
1	Anterior deltoid	"Empty can" (subject in upright position, arm abducted in scapular plane with 180° pronation, pushing anteriorly)
2	Middle deltoid	"Empty can" (subject in upright position, arm abducted in scapular plane with 180° pronation, pushing anteriorly)
3	Posterior deltoid	Prone elevation (subject in prone position, arm abducted in scapular plane with 180° pronation, pushing posteriorly)
4	Biceps brachii	Elbow flexion (subject in upright position, zero upper arm abduction/flexion, 90° forearm flexion, 90° supination, flexing the elbow)
5	Brachioradialis	Elbow flexion (subject in upright position, zero upper arm abduction/flexion, 90° forearm flexion, neutral forearm, flexing the elbow)
6	Triceps long	Elbow extension (subject in upright position, zero upper arm abduction/flexion, 90° forearm flexion, neutral forearm, extending the elbow)
7	Triceps Lateral	Elbow extension (subject in upright position, zero upper arm abduction/flexion, 90° forearm flexion, neutral forearm, extending the elbow)
8	Pectorialis major	Palm press (subject in upright position, 90° upper arm flexion, 45° elbow flexion, neutral forearm, pressing the hands against each other)

Appendix D

Matlab Implementation of Constrained NNMF

```
% calculate the projection matrix
NL = null(L); % null space of L
P = (NL/(NL'*NL))*NL'; % projection transformation

% initialize with random guess
w0 = rand(m,k);
h0 = rand(k,n);

% iterate until convergence reached
for i = maxiter
    h = max(0, w0\A);
    w = max(0, A/h);

    w = max(0, P*w);
```

```
    % checking if convergence criteria is met
    check = Check_Convergence(A,w,h);

    if check
        break; % finish the iteration
    else
        w0 = w; % update the matrices
        h0 = h;
    end
end
```

Appendix E

Simulation Parameters

Table E.1: Muscle parameters for the four muscle groups in the 2D forearm model

parameter	BRD	BIC*	BRA	TRI*
$F_{0_{max}}$ (N)	101	855	854	2518
L_0^{CE} (cm)	27	14	10	10
α_p (deg)	5	10	15	15
PCSA (cm^2)	3.08	26	26	76
r ** (cm)	3	3.7	5.4	-2

* the parameters for these muscles are averaged/summed across different heads of the muscles

** the constant moment arm is the average value over the range of motion

Table E.2: Forearm/hand properties in 2D forearm model

property	value
inertia*	0.265 kgm^2
mass	1.87 kg
COM location*	0.145 m

* with respect to elbow joint

Table E.3: List of muscle origin/insertion points used in the 3D arm model

#	muscle	max iso. force (N)	first connection (origin)	coordinate (mm)			second connection (insertion)	coordinates (mm)		
				x	y	z		x	y	z
1	Coracobrachialis (CORB)	63	torso	20	30	35	humerus	174	21	0
2	Deltoid (DELT1)*	240	torso	-30	40	15	humerus	106	-24	-11
3	Deltoid (DELT2)*	200	torso	-9	64	25	humerus	119	-9	9
4	Deltoid (DELT3)*	200	torso	-45	35	-10	humerus	95	-9	9
5	Latissimus dorsi (LAT)	360	torso	-35	90	-125	humerus	50	0	-13
6	Pectoralis major (PECM)	210	torso	45	95	-125	humerus	-14	1	2
7	Supraspinatus (SUPSP)	98	torso	-20	90	35	humerus	-14	17	27
8	Biceps brachii (BICshort)	47	torso	0	0	15	ulna	38	0	10
9	Biceps brachii (BIClong)	90	torso	0	15	10	ulna	38	0	10
10	Infraspinatus (INFRA)*	210	torso	-15	80	-40	humerus	28	-19	27
11	Anconeus (ANC)*	40	humerus	265	5	-19	humerus	42	12	-29
12	Triceps brachii (TRIlong)*	135	torso	-25	20	-20	radius	38	27	-20
13	Triceps brachii (TRImed)*	108	humerus	78	11	-10	ulna	38	27	-20
14	Brachialis (BRA)	167	humerus	176	-8	16	radius	33	5	10
15	Brachioradialis (BRD)	45	humerus	246	-27	0	radius	283	-12	0

* These muscles consider via-points to preserve the muscle path and functionality

Table E.4: The mass and inertia properties of 3D arm segments

Segment	Mass (kg)	Inertia $[I_{xx}\ I_{yy}\ I_{zz}]^*$ (g.mm^2)			Length (mm)	CoM from proximal (mm)
Humerus	0.945	[0.189	1.46	1.46]	280	140
Ulna	0.376	[0.03	0.417	0.417]	240	78
Radius	0.244	[0.054	0.312	0.312]	240	159
Hand	0.405	[0.220	0.377	0.377]	30	0

*around center of mass, the mechanical x-axis is assumed to be along the bone

Table E.5: One-DoF musculoskeletal simulation parameters

Parameter	value
PID coefficients in 2D forearm model	$K_P = 10\ (rad^{-1})$ $K_d = 2\ (s\ rad^{-1})$ $K_i = 10\ (s^{-1}rad^{-1})$
FSO weightings in 2D forearm model	$w_1 = 1$ $w_2 = 3 \times 10^6\ (rad^{-2})$ $w_3 = 5 \times 10^2\ (s^2rad^{-2})$
PID coefficients in 3D driver model	$K_P = 100\ (rad^{-1}))$ $K_d = 0\ (s\ rad^{-1}))$ $K_i = 100\ (s^{-1}rad^{-1})$
FSO weightings in 3D driver model	$w_1 = 1$ $w_2 = 3 \times 10^4\ (rad^{-2})$ $w_3 = 1 \times 10^2\ (s^2rad^{-2})$

Table E.6: 2D planar arm model simulation parameters

Parameter	value
MPC parameter	time step = 1×10^{-3} (s)
	prediction horizon length = 200
	control horizon length = 20
	look-ahead length = 50
	control variable weights = (0, 0)
	rate of control variables weights = (0.005, 0.005)
	tracking error weighs = (1, 1)
PID coefficients	$K_P = 40$ (m^{-1})
	$K_d = 20$ $(s\ m^{-1})$
	$K_i = 10$ $(s^{-1}m^{-1})$
NMPC weightings	$w_1 = 1(s^{-1})$
	$w_2 = 1 \times 10^7$ $(s^{-1}m^{-2})$
	$w_3 = 1 \times 10^3$ (sm^{-2})
	$w_4 = 1 \times 10^{-2}$ (s^3m^{-2})

Table E.7: Three-DoF musculoskeletal simulation parameters

Parameter	value
PID coefficients	$K_P = 3000$ (s^{-2})
	$K_d = 100$ (s^{-1})
	$K_i = 2000$ (s^{-3})
NMPC weightings	$w_1 = 1(s^{-1})$
	$w_2 = 1 \times 10^6$ $(s^{-1}m^{-2})$
	$w_3 = 1 \times 10^5$ (sm^{-2})
	$w_4 = 0$

Table E.8: Four-DoF musculoskeletal simulation parameters

Parameter	value
PID coefficients	$K_P = 3000\ (s^{-2})$ or $(rads^{-2}m^{-1})$
	$K_d = 100\ (s^{-1})$ or $(rads^{-1}m^{-1})$
	$K_i = 1500\ (s^{-3})$ or $(rads^{-3}m^{-1})$
NMPC weightings	$w_1 = 1(s^{-1})$
	$w_2 = 1 \times 10^5\ (s^{-1}m^{-2})$
	$w_3 = 1 \times 10^4\ (sm^{-2})$
	$w_4 = 1 \times 10^5\ (s^{-1}rad^{-2})$

Table E.9: FES experiment parameters

Parameter	value
PID coefficients	$K_P = 150\ (Nm^{-1})$
	$K_d = 30\ (Nsm^{-1})$
	$K_i = 30\ (Ns^{-1}m^{-1})$
Cost function weightings	$w_1 = 1000\ (N^{-2})$
	$w_2 = 1 \times 10^{-6}\ (\mu s^{-1})$
	$w_3 = 1\ (N^{-2})$